

PN. ACH-~~608~~
611

164821

FINAL REPORT

COVERING PERIOD: NOVEMBER 15, 1995 to JANUARY 31, 2000

SUBMITTED TO THE U.S. AGENCY FOR INTERNATIONAL DEVELOPMENT, BUREAU FOR GLOBAL PROGRAMS, FIELD SUPPORT AND RESEARCH, CENTER FOR ECONOMIC GROWTH

“ HIGHLY EFFICIENT METHODS FOR SEA-WATER DISTILLATION UTILIZING SOLAR ENERGY “

PRICIPAL INVESTIGATOR: DR. A.I. KUDISH

GRANTEE INSTITUTION: BEN-GURION UNIVERSITY OF THE NEGEV (BGU, ISRAEL)

COLLABORATOR: DR. G. MINK

INSTITUTION: THE HUNGARIAN ACADEMY OF SCIENCES (HUNGARY)

PROJECT NUMBER: C 15-050

GRANT NUMBER: TA-MOU-95C15-050

USAID GRANT PROJECT OFFICER: DR. DAVID MULENEX

PROJECT DURATION: NOVEMBER 15, 1995 to JANUARY 31, 2000

2) TABLE OF CONTENT

1.	TITLE PAGE	1
2.	TABLE OF CONTENTS	2
3.	EXECUTIVE SUMMARY	4
4.	RESEARCH OBJECTIVES	6
4.1	The problem addressed and its importance to development	6
4.2	On-going research by other scientists	6
4.3	Research objectives	9
4.4	The innovative aspects of the project	10
4.5	Support from other organizations during the implementation of the project	10
4.5.1	Hungarian research group:	10
	Support from RLIC-HAS (1995-97) and RLMEC-CRC-HAS (1998-2000)	
	Support from the National Science Foundation of Hungary (OTKA) (1998-2000)	
	Travel support from Israeli and Hungarian governmental offices (1999-2000)	
4.5.2	Israeli research group	11
	Support from BGU (1995-2000)	
	Travel support from Israeli and Hungarian governmental offices (1999-2000)	
5.	METHODS AND RESULTS	11
5.1	Methods and experimental procedures	11
5.2	Solar still prototypes	14
5.3	Results	17
6.	IMPACT, RELEVANCE AND TECHNOLOGY TRANSFER	32
6.1	Impact of findings on the developing country	32
6.2	The project's impact on individuals, laboratories, departments, and institutions.	32
6.3	Impact on laboratories, department, institutions	33
6.4	Possibilities of the use of the results	33
6.5	New capacity, equipment and expertise left behind in the developing country	33
7.	PROJECT ACTIVITIES/ OUTPUTS	34
8.	PROJECT PRODUCTIVITY	37
9.	FUTURE WORK	37
10.	LITERATURE CITED	38
11.	APPENDIX	41
	Publication reprints	
	a. Design parameters, performance testing and analysis of a double-glazed, air-blown solar still with thermal energy recycle. <i>Solar Energy</i> 64 , 265-277 (1998).	
	b. Performance studies on an air-blown, multiple-effect solar still operating on solar and/or waste energy. <i>Proc. Int'l. Congress Energy and the Environment</i> , 28-30 October, Opatija, Croatia, II , 57-69 (1998).	

- c. Performance of an air-blown solar still with internal multi-tubular heat exchanger for condensation heat recycle. *Proc. Int'l. Congress Energy and the Environment*, 28-30 October, Opatija, Croatia, **II**, 71-77 (1998).
- d. Performance and analysis of a multiple-effect solar still utilizing an internal multi-tubular heat exchanger for thermal energy recycle. *Proc. Int'l. Solar Energy Society Conference, Solar World Congress*, 4-9 July, 1999. Jerusalem, Israel, in press.
- e. Performance and analysis of a multiple-effect solar still utilizing solar and/or waste thermal energy. *Proc. Int'l. Solar Energy Society Conference, Solar World Congress*, 4-9 July, 1999, Jerusalem, Israel, in press.

3) EXECUTIVE SUMMARY

There exists today an estimated two billion people who go without fresh water on a daily basis. The consumption of water unfit for drinking, due to pathogens and salinity, is a major health hazard world-wide. In addition, the continuing growth of the world's population and the consequent increased food shortage, requires the expansion of agriculture into arid zones, i.e., the greening of the desert. Famines, both more or less publicized, in many regions on the globe provide ample evidence for the necessity of solving this problem by concerted efforts, both national and international. The significance of this research project is obvious in that potable water is a commodity that is becoming scarce and has been source of conflict between nations throughout history. If the latter part of the 20th Century can be characterized as one that the scarcity of oil was a casus belli than it is reasonable to state that the casus belli in the 21st Century will be the scarcity of water. In fact, the success of the peace treaties now in effect and in the making in the Middle East will depend to a significant degree on the availability of water for all countries concerned. Solar desalination can be an important source of water in this region, which is primarily composed of arid and desert lands and has an abundance of solar radiation.

Five different solar still modules were developed during the course of this project and are described in detail in the report. Though the prototypes developed, tested and optimized throughout this study may differ significantly both in their appearance and materials of construction, they all possess a common feature- the ability to execute the following processes in a thin and low cost rectangular box.

- Evaporation of the feedstock water by solar energy in an upper chamber, which is transported by an air stream to a lower chamber
- Condensation of the major fraction the water vapors transported by the air stream in the lower chamber.
- Recycle of the thermal energy of condensation of the distillate by both preheating the entering feedstock and directly heating the evaporation surface of the still and, thereby, significantly enhancing the still productivity.

The performance of prototype (I) has been discussed in detail by Mink et al. (1998)]. The performance of prototypes (I) and (III) has been analyzed and simulation models developed and verified, as reported upon by Kudish et al. (1997) and Mink et al. (1999), respectively. The performance analysis of prototype (IV) operating in the following modes: solar (normal mode), solar + waste thermal energy (hybrid mode) and waste thermal energy (nocturnal mode) have been reported upon by Kudish et al. (1999).

It was found that prototype (IV), which operates in a hybrid mode (using a combination of solar + waste thermal energy, when available on-site, as the driving forces), attained the highest maximum temperatures relative to the other four prototypes. Prototype (III) was somewhat superior to the remaining prototypes at lower air flow rates, whereas the three other prototypes exhibited somewhat similar behavior with regard to their measured maximum temperatures as a function of air flow rate, cf., Fig. 7 in text.

The results of the inter-comparison of the total productivity rates for the five prototypes indicated, quite conclusively, that prototype (IV) was the most productive solar still, viz., it produced $> 1.5 \text{ kgm}^{-2}\text{h}^{-1}$ under the operating conditions during performance testing. All

prototypes, with the exception of prototype (I), arrived at an essentially constant total productivity rate with increasing air flow rate (i.e., over the range of air flow rates investigated). The observed behavior of prototype (I), was in all likelihood, a consequence of the lower limit on the air flow rate achievable when it underwent performance testing. It is observed that prototypes (II), (III) and (V) exhibit somewhat similar behavior with regard to total productivity as a function of air flow rate. The relative performance rating for these three prototypes, based upon total productivity, is (II) > (III) > (V). It appears that prototype (I) may exhibit a behavior quite similar to (II) in the range of low air flow rates but, as explained above, there is no data available in the lower range of air flow rates. The measured maximum productivity rates for prototypes (I), (II), (III) and (V) were in the range between 0.8 to 1.1 kgm²h⁻¹ under the operating conditions during performance testing, cf., Fig. 8 in text.

The main design parameters, optimum operating conditions and an estimate of the fixed capital investment costs for a 365 m³/y capacity plant constructed for each of the five prototypes have also been summarized, cf., Table 4 in text. We conclude that when waste thermal energy is available at the site, prototype (IV) operating in the hybrid mode offers the highest productivity at the lowest fixed capital investment costs for a desalination plant of defined capacity. In addition, Kudish et al. (1999) showed that its daily productivity could be further enhanced by operating prototype (IV) during daytime hours in the hybrid mode and during non-solar or nighttime hours in the nocturnal mode, utilizing the available on-site waste thermal energy. In addition, the data reported in Table 4 indicate that prototype (V) may be the preferred design, based on economics, for sites not possessing a waste thermal energy source. Furthermore, prototype (V) has an advantage of possessing a very low mass and a relatively simple design. We believe, however, that prototype (V) may have higher maintenance and replacement costs relative to those for the other prototypes.

The project accomplished almost all its R&D goals with the exception of the construction and operation of a pilot-plant installation. The reason for this shortcoming was a result of the drastic change in the financial situation of the Hungarian group after the reorganization of RLIC to the RLMEC, CRC HAS. Consequently, the construction of a fully equipped 12 m² solar still area demonstration plant planned at RLIC was abandoned in early 1999. The construction of such a pilot plant will require the additional support from international funding sources. The construction of such a pilot is definitely warranted, based upon the results obtained during the present investigation.

The major impact of this joint research project on the Hungarian partner has been the development of a Hungarian research team with both experience and expertise in the field of solar energy conversion and utilization. As a result of this project a fully equipped solar laboratory has been established at the RLMEC and the staff of the laboratory has attained an international reputation in the field of solar-to thermal energy conversion systems. They are now capable, using both theoretical and experimental data analysis, of designing and scaling-up solar stills and evaporators for different applications. Their expertise may be applied to the design of solar to thermal energy conversion systems for agricultural, chemical and environmental protection purposes. These include such applications as solar desalination, solar drying of industrial or agricultural materials and thickening of dilute solutions of valuable or hazardous salts as an intermediate stage in their management/processing.

4) RESEARCH OBJECTIVES

4.1) The problem addressed and its importance to development

Today there exists an estimated two billion people who go without fresh water on a daily basis. The consumption of water unfit for drinking, due to pathogens and salinity, is a major health hazard world-wide. In addition, the continuing growth of the world's population and the consequent increased food shortage, requires the expansion of agriculture into arid zones, i.e., the greening of the desert. Famines, both more or less publicized, in many regions on the globe provide ample evidence for the necessity of solving this problem by concerted efforts, both national and international.

Arid and semiarid zones constitute approximately 60% of the earth's land area and they are, in general, characterized by both high levels of solar radiation and shortages of fresh water. In tropical regions, especially during the dry period, the shortage of quality water also creates serious health problems. Such regions often possess reservoirs of either brackish or saline water that may be used for both drinking and irrigation after suitable treatment.

The construction of reverse osmosis (RO) or conventional desalination plants utilizing fossil fuel sources to the supply fresh water may not be practical in many remote areas. This may be due to one or more of the following reasons: they require qualified technical staff for both maintenance and operation; conventional desalination plants are economic only for very large scale applications, viz., high-capacity plants; they both require high fixed capital investment; the availability of a reliable power source to operate the plant. Solar desalination systems, on the other hand, may be an ideal source of fresh water for both drinking and agriculture in such remote areas. This is especially true in that both the demand for fresh water and the intensity of solar radiation are, in general, cyclical in nature and in phase with each other.

The significance of this research project is obvious in that potable water is a commodity that is becoming scarce and has been source of conflict between nations throughout history. If the latter part of the 20th Century can be characterized as one that the scarcity of oil was a casus belli than it is reasonable to state that the casus belli in the 21st Century will be the scarcity of water. In fact, the success of the peace treaties now in effect and in the making in the Middle East will depend to a significant degree on the availability of water for all countries concerned. Solar desalination can be an important source of water in this region, which is primarily composed of arid and desert lands and has an abundance of solar radiation.

4.2) On-going research by other scientists

The utilization of solar energy for the distillation of brackish or saline water has been practiced for a very long time. Various types of solar stills and solar-assisted desalination units have been designed and investigated. The simplest and most widespread solar still is of the single-basin type design. It consists of a closed box with a tilted glass glazing a water basin with a black liner and a trough to collect the distillate. The distillate evaporates from the surface of the water in the still basin heated by the solar radiation, condenses on the inner surface of the relatively cooler glazing and flows down the tilted glazing, ideally as a thin water film, by gravity into the distillate collection trough. The main shortcoming of these stills is that their productivity per unit area of still basin is low, only about $1 \text{ m}^3 \text{ m}^{-2} \text{ yr}^{-1}$, and their investment costs are roughly proportional to

the still area. Consequently, they are not, in general, cost-competitive with the alternative conventional methods, except for special cases such as remote and non-electric grid connected sites.

The first large scale application of this solar still genre (4700 m² in area) was built in 1872 in Chile as a fresh water source for a copper mine in the Andes, Harding (1883). An abundance of manuscripts and some excellent monographs, e.g., Talbert et al. (1970), Malik et al. (1982) and Kudish (1991), have been published on this subject. A large number of innovative designs of solar stills and systems ranging from the minimal to the high-tech have been proposed, constructed and tested. As reported by Cooper (1973), Delyannis and Delyannis (1980) and Kudish et al. (1986), the overall efficiency of a typical basin-type solar still is only about 30% and over the past three decades many efforts have been devoted to enhancing this efficiency. The scientific and patent literature abound with different proposals to modify the design of the still components, but in most cases only few percent increase in efficiency has been achieved.

Another type of solar still, designed to operate with a very low thermal capacity, is the tilted-wick still, cf., Telkes (1955). This type of still has been found to have a somewhat higher distillation rate per unit area but it operates at relatively high temperatures. The latter feature negates to some extent its design advantage, viz., a low thermal capacity, by enhancing its temperature gradient relative to the ambient and, thus, increasing the thermal energy losses. In spite of their simple construction, low operation and maintenance costs both the basin- and tilted-wick type solar stills suffer from the same shortcoming, i.e., the condensation of the distillate vapor on the inner glazing surface and the consequent dumping of the latent heat of condensation to the ambient. In addition, even when neglecting their relatively low maintenance costs, the price of fresh water produced by both the basin- and tilted-wick type stills is estimated by Total Life Cycle Cost (TLCC) analysis to be in the range of 15 US\$/m³.

It is apparent from the thermodynamic analysis of the process, that if the latent heat of condensation and the sensible enthalpy of the warm distillate could be successfully recycled and used for both heating and evaporating the feedstock, a considerable enhancement in the process productivity and efficiency would be achieved. This is the case with regard to those conventional systems, such as vapor compression, multi-stage evaporation or multi-stage flash distillation, which are defined as multi-effect systems. In such systems the yields have been increased by a factor of 3-20, with the same energy input, relative to a simple, single-effect distillation systems.

Solar stills can also be designed to operate as multi-effect systems by utilizing, to some degree, the latent heat of condensation to preheat the feedstock. This may be accomplished, for example, by constructing the still with a double glazing and flowing the feedstock through the space between the glazing (a simple liquid in glass condenser) prior to entering the basin. Another approach is to use multiple-basin solar stills with transparent bases in the upper still(s), cf., Lobo and Araujo (1977), Sodha et al. (1980), Tiwari (1985), Fernandez and Chargoy (1990) and Tiwari and Sharma (1991). It is obvious that such innovative still designs offer no practical alternative, even with a 40% increase in productivity as was reported in the latter case, when the incremental costs and construction complications are taken into consideration.

A pilot plant for sea-water desalination by multi-effect humidification was constructed in 1992, Baumgartner et al. (1992). This plant consists of a flat plate solar collector fabricated from a

corrosion resistant titanic alloy and an external, well-insulated evaporator-condenser chamber. The heated feedstock, exiting the solar collector, partially evaporates and the vapors condense on a heat exchanger that, in turn, serves to preheat the feedstock before it enters solar collector. The heat recovery factor for this system, which is defined as the ratio of the thermal energy utilized for evaporation relative to that supplied, is high, between 3 and 4.5 on a daily average. Cost estimations provided by the technology developers have shown that the price of the fresh water produced is presently in the range of 50 US\$/m³ but they plan to reduce it to about 25 US\$/m³ by improving the system design with the addition of a high capacity thermal storage tank, Müller-Holst et al. (1997).

Air-blown solar still prototypes were developed at the RLIC, one of the partners of the present project, at about the same time, Mink et al. (1988) and Aboabboud et al. (1993). The absorption of solar radiation, evaporation, condensation and efficient recycle of the thermal energy of condensation of the distillate, both to preheat the feedstock and heat the backside of the evaporation surface, occurs within a thin, compact rectangular box. These stills are tilted towards to the sun to increase the flux density of the incident solar radiation and a double glass glazing is used to reduce the thermal energy losses from the still glazing to the ambient. This is a result of the fact that the glazing does not function as a condensing surface and need not be cooled by the ambient. In fact, condensation on the inner surface of the glazing should be avoided, since it reduces the system efficiency. Consequently, it is possible and highly recommended that the double glass glazing be replaced by non-wettable, transparent polymeric insulation materials (TIM's).

The thermal mass of these stills is very low and, therefore, steady state conditions, both in terms of temperatures and productivity, are achieved in less than an hour from start-up. Performance studies, under controlled conditions utilizing a solar simulator, showed that these stills are characterized by a broad productivity maximum as a function of increasing air flow rate. Operating such stills in the range of the optimum air flow rate results in a productivity that is about 2.5 times higher than that for both the basin and tilted-wick type solar stills, whereas the construction is only slightly more complicated. Consequently, these air-blown stills with their thermal energy recycle offer significant productivity gain at marginal incremental construction costs. The optimum air flow rate range is within the laminar flow regime, corresponding to a linear velocity < 1 m/s, and therefore, low cost, low pressure air pumps can be used. The parasitic electric energy requirements are not significant, about 0.5 W/m² still area, and in rural/remote applications it can be supplied by PV panels.

The state-of-the-art of such air-blown solar stills prior to the initiation of the present project was reported upon by Mink et al. (1998). The prototype air-blown solar still, to be referred throughout the following text as Module-1, was subjected to performance testing using a solar simulator with a constant irradiation flux density of 650 W/m². The productivity of this still, under steady-state conditions, was 1 kgm⁻²h⁻¹, viz., about 2.5 times greater than that for single basin-type stills. Module-1 consisted of an upper evaporation chamber and a lower condensation chamber separated by a metallic sheet, a serpentine copper tube for preheating the feedstock and a double glass glazing.

A TLCC analysis was performed on the solar still design and performance, at the time of the initiation of the project, to determine possible design changes that would enhance both

productivity and reduce costs, Kudish et al. (1995). These calculations lead to the following conclusions:

- perform in-depth theoretical analysis of the heat and mass transfer processes occurring within the still in order to optimize them and thereby increase productivity;

- utilize corrosion resistant materials, e.g., solar grade plastics which are produced in large quantities for solar architecture, to decrease the fixed capital investment of the still and increase its life time;

- design the solar still so as to utilize waste thermal energy, when available at the site, to enhance the productivity by operating the system during the day using both solar and waste thermal energy, hybrid mode, and during the night using waste thermal energy, i.e., nocturnal distillation.

Several new solar still prototypes were designed, tested and analyzed during the course of the project, each offering a step-by-step cost reduction with respect to Module-1. The results of these studies have been reported by Kudish et al. (1997) Mink et al. (1998) and Mink et al. (1999). The economics of the use of waste thermal energy, both in the hybrid and the nocturnal distillation modes, have been reported upon by Kudish et al. (1999).

During the course of the study, we have kept abreast of the on-going research efforts by other scientists by both following that reported in the scientific literature and by attending scientific conferences. We did not encounter any reported breakthroughs with regard to the economics of solar distillation. As previously discussed, the multi-effect humidification technique of Baumgartner et al. (1992) is much too costly. Also, the system design changes reported by Müller-Holst et al. (1997 and 1999) have not reduced the costs to an acceptable level. El-Bahi and Inan (1997 and 1999) recently reported upon the performance of basin-type solar stills, which were modified with the aim of productivity enhancement. In their design a metallic compartment is attached to a basin-type still. The vapors enter this compartment by self-diffusion, condense and the heat of condensation of the distillate is recycled to some extent. We believe that the productivity gain achieved in this system is marginal, especially, when it is compared with the additional costs of construction. A second modification applied by the authors, the use of a low cost metallic mirror attached to the upper extremity of the low angle tilted glazing, can provide a significant contribution to the system performance. It can achieve a significant enhancement of the solar radiation incident on the still glazing that can result in an estimated 10-30 % higher productivity relative to the simple basin-type stills, depending on the incident angle of the solar radiation.

4.3) Research objectives

The enhanced and relatively high productivity at marginal incremental costs, modular construction and, therefore, ease of scale-up made the air-blown solar still design a very attractive alternative to the conventional solar still design. Furthermore, a TLCC analysis of such a system indicated its ultimate advantages relative to the traditional solar still designs. Therefore, it was decided that the joint research program of the two institutions would concentrate on performance optimization of these stills in terms of both productivity and cost. The research objectives were formulated as follows:

The overall aim of the project was to arrive at a solar still design that was capable of producing fresh water at a cost competitive with the local alternative and the specific research objectives were:

- To optimize the heat and mass transfer processes of the thermal energy recycle process and thereby improving the system efficiency and productivity, viz., enhance the fresh water yield per unit area;
- To develop hybrid systems which utilize external on-site waste thermal energy for day and night heating (nocturnal distillation) and thereby approaching a 24 hour per day operating system;
- To simplify the system design(s) in order to minimize the level of technical skill required for system maintenance;
- To arrive at a design(s) that is (are) amenable to the construction of a high-capacity solar desalination plant, viz., a modular solar still design.

The successful achievement of the project goals promised a rapid propagation of the technology, since not only the production of potable water in remote areas, but also the irrigation of greenhouses that produce high-cash crops would be a viable market for such technology.

4.4) The innovative aspects of the project

The innovative aspects of this joint research program were the following:

- To perform a detailed theoretical analysis of the heat and mass transfer processes occurring in air-blown solar still to determine the bottlenecks that prevent the further enhancement of the productivity. During the planning stage of this project only qualitative information was available regarding the operation of the whole system, due to the complexity of the heat and mass transfer processes occurring within the system and the fact that they are mutually interrelated.
- To develop simulation models, utilizing experimental data to validate them, and then applying them to predict the effect of structural modifications on the productivity. Due to the complex and design specific nature of the processes involved, it was foreseen that such models should be developed on an individual basis, i.e., module specific.
- To perform TLCC analysis of the modules to determine the economic bottlenecks preventing cost reduction. Such information was not available at the beginning of the project, regarding their economics of operation and maintenance.
- Based on the results of the above theoretical analysis, to develop directives for designing new solar still modules utilizing new, low cost and corrosion resistant construction materials to decrease the investment costs and increase the lifetime of the stills.
- To carry out performance testing, analysis and optimization of the new modules to determine the guiding principles and main directives for designing a pilot scale plant module. No such information concerning the design parameters of such a plant module existed at the time of project planning.

4.5) Support from other organizations during the implementation of the project

4.5.1) Support to the Hungarian research group

- Support from RLIC-HAS (1995-97) and RLMEC-CRC-HAS (1998-2000)-
During the whole period of the project, space and infrastructure from RLIC-HAS and RLMEC-CRC-HAS was made available for the Hungarian group participating in the project.

Due to a reorganization program of the Hungarian Academy of Sciences (HAS), the Research Laboratory of Inorganic Chemistry (RLIC-HAS), the Hungarian contractor of the project became a member institute of the Chemical Research Center, HAS in 1998, under the new name of Research Laboratory of Materials and Environmental Chemistry (RLMEC-CRC-HAS).

- Support from the National Science Foundation of Hungary (OTKA) (1998-2000)-
Based on the scientific achievements of the project, Mr. László Horváth, MSc., received, effective January 1, 1998, a three-year grant with an annual stipend of 300,000 HUF from the National Science Foundation of Hungary for young researchers below the age of 35, in the field of solar distillation. (Project No OTKA F-025342).
- Travel support from Israeli and Hungarian governmental offices (1999-2000)
Drs. Mink and Kudish applied for and were awarded travel grants under the Exchange of Researchers in the Framework of Israeli-Hungarian Scientific Cooperation 1999-2000, funded by the State of Israel, Ministry of Science, Jerusalem and the Republic of Hungary OMFB, Budapest. This grant provides for a 10 day visit by each PI and a 1 month visit by a researcher from each country during each year of the two year grant period.

4.5.2) Support to the Israeli research group

Support from the Ben-Gurion University of the Negev (1995-2000)-

During the whole period of the project, space and infrastructure from BGU was made available for the Israeli group participating in the project.

- Travel support from Israeli and Hungarian governmental offices (1999-2000)
See above.

5) METHODS AND RESULTS

5.1) Methods and experimental procedures

A number of variations on the original solar still prototype, Module-1 were designed, constructed, tested, analyzed and optimized during the R & D phase of this project.

The approach for achieving the stated objectives of this project was a combination of experimental measurements and theoretical analysis, which both complemented and feed upon each other. Thus, experimental data from the performance testing of the solar still prototypes were utilized to validate the simulation models and these, in turn, were used to perform parametric sensitivity studies and suggest design changes. These changes also included the utilization of polymers in the still construction, which provided corrosion resistance and, thereby, longer life time. The influence of the proposed design changes on the economics, viz., the cost per unit water produced, was closely monitored throughout the study.

The experimental research aspect of the project involved both performance testing and optimization of the different solar still prototypes. The experimental measurements were performed using on-line data monitoring and analysis of the pertinent parameters by software packages developed specifically for the tasks. The monitored experimental parameters included the temperatures at various critical points within the system, the ambient conditions such as

irradiation and ambient temperature, and the differential and cumulative yields during the experiments.

The theoretical analysis aspect of the project included the development of simulation models of the different solar still modules that were designed throughout this study. These models were based upon the appropriate energy and mass balances describing the distillation process. This approach resulted in a set of nonlinear energy transfer equations, which were solved by numerical integration, using an explicit predictor-corrector difference scheme. We were able to assume "steady-state" conditions by choosing sufficiently small integration time intervals.

Schematic diagrams of prototypes (I) and (II), variations of Module-1, and the experimental set-up used in their performance testing are shown Figs. 1 and 2. The experimental set-up consists of the following components: solar still module, solar simulator, two vapor/liquid separators for collecting the product, heat exchanger, peristaltic pump to transport the feedstock, low pressure adjustable flow rate air pump, electric balance to measure distillate, gas flow meter, magnetic valves (Mv) to drain the separators periodically and temperature sensors. The system is connected on-line to a personal computer for data collection and analysis. The air pump is positioned such as to ensure that the system operates at a pressure somewhat below ambient.

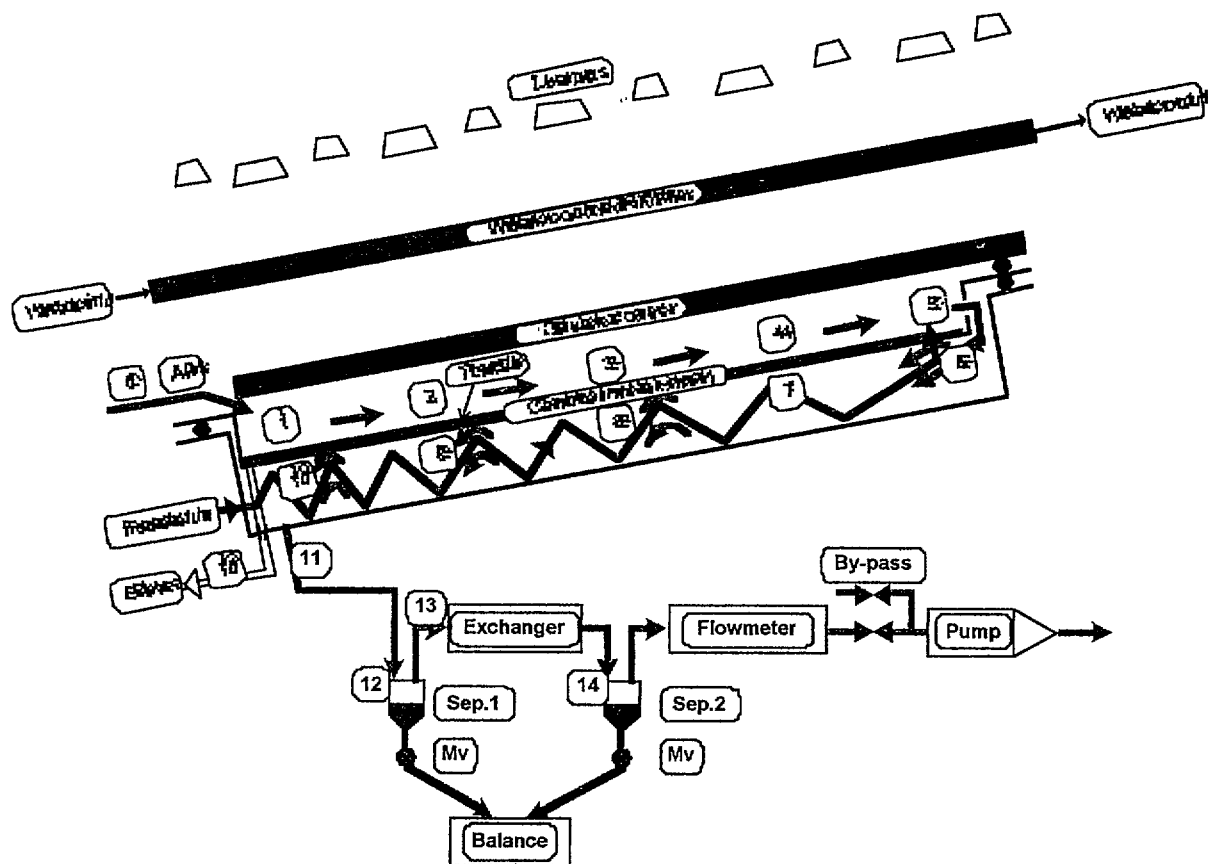


Fig. 1 A schematic diagram of the experimental set-up used for performance testing of solar still prototypes (I) and (II). The locations of the thermistors temperature probes are indicated by numbers 0 to 15.

Solar simulator- The solar simulator consists of 16 halogen lamps (12 x 500 W and 4 x 300 W lamps), each fitted with a radiating screen of the same geometry, which direct the radiation downward to the still. The simulator is positioned parallel to the solar still and the lamp arrangement provided an essentially homogeneous radiation intensity on the still outer glazing surface, which was verified experimentally. A 10 mm thick double-walled polycarbonate sheet is positioned parallel between the simulator and still. A stream of water flows through the sheet channels, in order to filter any radiation above 2.5 nm that is emitted by the solar simulator. The water absorbs the radiation in the range of 2.6 to 3 nm; whereas the polycarbonate absorbs all the radiation above 3 nm. The temperature of the filter, viz., the polycarbonate sheet, is 18^oC at the lower end where the water enters and 30^oC at the upper water exit. Consequently, the average sheet temperature is below the average room temperature, which is between 25 and 29 ^oC. The filter insures that the radiation incident on the solar still is in the range between 0.4 to 2.6 nm, since the lamp filament temperature is approx. 2500 K and its UV component negligible.

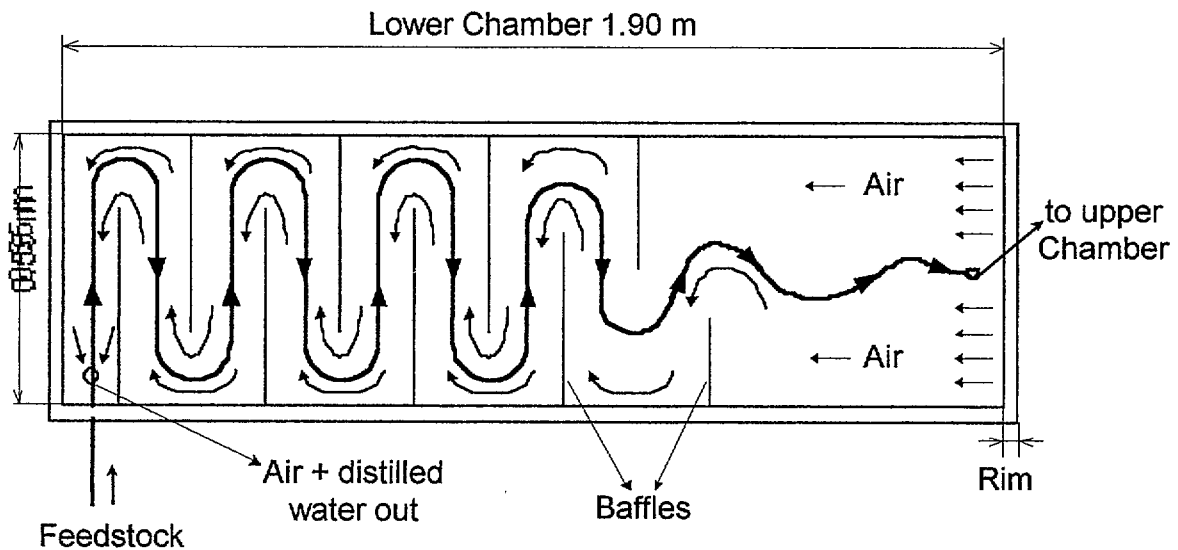


Fig. 2 A schematic diagram of the lower condenser chamber for prototype (I) and (II) solar stills, showing the serpentine tube through which the feedstock flows and the baffles.

External heat exchanger- The external heat exchanger was a standard laboratory glass condenser having a heat exchanger surface area of about 0.07 m². The heat exchange medium was mains water, entering with a temperature in the range of 15-18 ^oC and flowing countercurrently to the air stream exiting from the solar still's lower chamber. The heat exchanger was sized for the estimated optimum operating conditions and, therefore, was unable to cool the air stream vented to the ambient room temperature of about 26 ^oC for air mass flow rates in excess of 1 kgm⁻²h⁻¹.

Experimental conditions and procedure- The tilt angle of the solar still module and solar simulator was set at 20^o throughout the experiments. The solar radiation intensity, provided by the solar simulator, incident on the outer glazing surface was 650±39 Wm⁻². The differential and cumulative yields collected in Separators I and II were measured automatically with an accuracy of ±1 g by a type PT 6 Satorius electric balance. The temperatures were measured with an accuracy of ±1 ^oC by means of calibrated temperature sensors of the silicon base type KTY 11-

2A. The absolute humidity of air in the vicinity of the slot, at the upper extremity of metal plated separating the two chambers, was calculated from mass and energy balances on the still. A data acquisition system served to both monitor and store the temperature data from the sixteen thermistors and to calculate differential and cumulative yields at variable time intervals. It consisted of a PC with an A/D-D/A converter card, electronic measuring and magnetic valve control unit, temperature sensors and a digital balance with a RS232C serial interface. The data acquisition, control and analysis software was developed especially for this study.

The operating conditions during the performance testing were based upon previous studies performed on such systems, which found that the effect of feedstock flow rate on still performance was negligible cf., Aboabboud et al (1993). Consequently, in most cases the solar still performance was monitored using a constant feedstock flow rate of $2.96 \text{ kgm}^{-2}\text{h}^{-1}$ and investigated as a function of air flow rate, which varied in the range of 0 to $10 \text{ kgm}^{-2}\text{h}^{-1}$.

The experimental procedure for the performance testing was as follows:

- (1) the air and feedstock flow rates are defined and held constant;
- (2) the temperatures at the following locations are monitored:

air stream-

- upper chamber: inlet, equally spaced probes in the direction of flow and above the slot
- lower chamber: below the slot, equally spaced probes in the direction of flow and at the outlet
- saturated air stream exiting the still to the external condenser

feedstock-

- lower chamber: inlet
 - upper chamber: overflow weir and brine drain-off outlet
- (3) the distillation rate is determined by measuring the cumulative distillate during a specified time interval.

5.2) Solar still prototypes

Though the prototypes developed, tested and optimized throughout this study may differ significantly both in their appearance and materials of construction, they all possess a common feature- the ability to execute the following processes in a thin and low cost rectangular box.

- Evaporation of the feedstock water by solar energy in an upper chamber, which is transported by an air stream to a lower chamber.
- Condensation of the major fraction the water vapors transported by the air stream in the lower chamber.
- Recycle of the thermal energy of condensation of the distillate by both preheating the entering feedstock and directly heating the evaporation surface of the still and thereby significantly enhancing the still productivity.

5.2.1) Prototypes (I) and (II)

These two still prototypes differ from each other only in that (I) has a double-glass glazing with a 20 mm gap between glazings and (II) has a double-walled polycarbonate glazing with a 10 mm gap. The stills consist of two shallow trays of slightly different dimension, supplied with perimeter rims, such that the upper tray can be inserted into the lower tray. A rubber gasket tape

was inserted between the perimeter rims of the two trays and between the upper tray perimeter rim and glazing. The two trays and glazing were then clamped together by screws to insure air tightness of the solar still. The upper and lower trays were fabricated from a 1 mm thick copper sheet and the bottom and perimeter of the lower tray was externally insulated with a 50 mm thick polyurethane foam (not shown in Fig. 1). This arrangement separates the solar still into two chambers, which are connected by a slot at the upper extremity, viz., when the solar still is in its tilted position, of the upper chamber. A brine drain-off tube was soldered to the bottom of the tilted upper tray and passes through the lower tray via a stuffing box. The evaporation plate, i.e., the upper tray, was covered by a thin, black porous fabric, the wick. The serpentine tube, which transports the feedstock in the lower chamber, was attached to the bottom of the upper tray. The serpentine tube enters the upper chamber via the slot and the feedstock exits onto the upper tray, cf. Figs. 1 and 2. The exiting feedstock is then evenly distributed over the width of the wick by means of an overflow weir located near the top of the upper tray.

The air-blown, multiple-effect solar stills, cf., Fig. 1, consist of an upper evaporation and a lower condensation chamber and are of the tilted-wick genre. The slot at the top of the central metal sheet (viz., it, the bottom of the upper tray, does not extend across the full length of the tray but leaves a slot of 10 mm between its and the still's upper extremities) and allows flow between the two chambers. This metal sheet also functions as (i.) the support for the wick, which covers it on the upper chamber side; (ii.) the surface to which a serpentine tube, on the lower chamber side, is attached. The serpentine tube functions, in addition to being a conduit for the feedstock, as a heat exchanger for preheating the feedstock prior to entering the upper chamber. The spacing between the central metal plate and the upper chamber still glazing and the lower chamber backside are both < 15 mm.

The testing of the solar stills was carried out in the following manner:

1. Ambient air pumped into the upper chamber at the bottom of the tilted still, sweeps the water vapor evaporated from the tilted wick into the lower chamber via the slot at the top of the tilted still. The maximum temperature of the air stream is observed to occur at this point, i.e., above the slot, prior to entering to the lower chamber. The air stream functions as the hot fluid in the lower chamber, which is essentially an air-liquid heat exchanger.

2. The major fraction of the water vapor transported by the air stream condenses either on the backside of the central metal sheet supporting the wick or on the serpentine tube, which transports the cold feedstock entering at the bottom of lower chamber.

3. The feedstock enters the serpentine tube at a flow rate in excess of the rate of evaporation from the wick in the upper chamber and is preheated during its passage through the serpentine tube. The feedstock exits the serpentine tube at the top edge of the central plate and passes over a weir, which maintains an even flow and wetting across the width of the wick, and flows by gravity down the wick.

4. The distillate exits the lower chamber and is collected in separator 1 (primary distillate, I), whereas the saturated air stream exiting the lower chamber enters an external condenser via separator 1. The saturated air stream undergoes further condensation and is collected in separator 2 (secondary distillate, II) prior to venting to the ambient.

The air stream flows countercurrently to the direction of feedstock flowing down the wick in the upper chamber, whereas in the lower chamber the air stream flows both countercurrently and perpendicular to the direction of the feedstock flowing through the serpentine tube. Due to the

nature of this solar still, viz., the upper chamber glazing does not serve as a condensation surface, we utilize a double glazing to reduce thermal energy losses via the glazing to the ambient. In fact, it is possible to use non-wetting polymeric glazings such as the polycarbonate sheet used in prototype II.

5.2.2) Prototype (III)

This prototype, also referred to as a multi-tubular solar still, was constructed from corrosion resistant materials. It consists of a solar grade plastic tray and glass tubes arranged in the longitudinal direction. A black wick covers the glass tubes. The evaporation occurs on the wetted surface of wick covering the glass tubes and the condensation occurs inside the tubes. The feedstock flows through a plastic serpentine tube entering at the lower extremity of the still where the air stream exits the glass tubes. The glazing is a double-walled polycarbonate sheet.

The design changes in prototype (III) were not done to enhance the productivity of the previously described prototype (II) but to simplify its construction and, thereby, make it a more economically viable alternative by reducing the fixed capital investment cost per unit area. This was achieved by utilizing relatively inexpensive and corrosion resistant materials in the construction of the solar still. The new solar still design, though significantly different in appearance from the original, utilizes the same energy and mass transfer processes to obtain the final distillate product. Consequently, in spite of its simple construction, the energy and mass transfer processes occurring within the still are numerous and mutually interrelated. Another aim of this work was to develop a mathematical model, utilizing nonlinear differential equations capable of simulating still performance under both transitional and steady-state conditions.

Schematic diagrams of the prototype (III) solar still module are shown in Figs. 3 and 4. The solar still consists of a bottom and edge insulated, thin, rectangular plastic tray ($L = 1.84$ m; $W = 0.54$ m; $d = 12$ mm; area = 1 m²), 40 glass tubes ($D_{od} = 7$ mm; $D_{id} = 5$ mm; $L = 1.8$ m) covered with a black wick and a plastic serpentine tube ($D_{od} = 4$ mm; $D_{id} = 3$ mm; $L = 20$ m). The still glazing is a solar grade double-walled polycarbonate sheet (10 mm thick). A low pressure variable speed air pump was used to provide the air stream, the mass and thermal energy carrier, and a peristaltic pump for the feedstock.

The still operates in the following manner:

1. Ambient air at temperature T_0 enters at the lower extremity of the still.
2. Evaporation occurs from the wick, which is also wetting the external, upper surface of the glass tubes.
3. The air stream achieves, once again, both its highest temperature and vapor content at the upper extremity of the still.
4. The air stream is directed into the longitudinal glass tubes at the top of the still and reverses its direction of flow, i.e., it now flows down the tilted still. The major fraction of its vapor content condenses on the inner surface of the glass tubes and the thermal energy of condensation is conducted via the tube wall to the wet wick to enhance the rate of evaporation from the wick.
5. The enthalpy of air stream, at temperature T_6 , entering the lower compartment at the extremity of the still, which unifies the air streams exiting the 40 glass tubes, is utilized to preheat the feedstock, prior to entering the evaporation chamber. The feedstock flows through a 5 m long black tube packed within this compartment to facilitate the heat exchange process.

6. The feedstock is further heated as it flows through another 15 m of the black serpentine tube positioned above the glass tubes, in the evaporation chamber, prior to exiting the serpentine tube onto the black wick at the upper extremity of the evaporation chamber.

7. The air stream and distillate exiting the solar still enter a gas-liquid separator (Sep. 1) to collect the primary distillate, in order to determine the amount of distillate which condenses within the still. This is a measure of the efficiency of the thermal energy recycle process.

8. The saturated air stream exiting Sep. 1 enters an external heat exchanger and a second separator (Sep. 2), where the secondary distillate is collected.

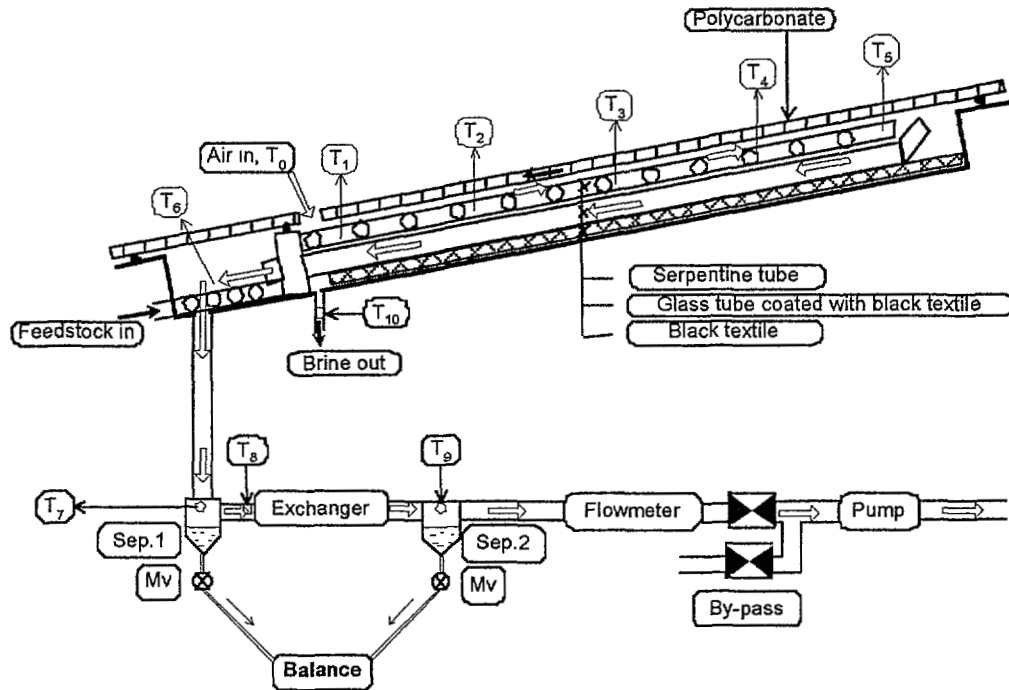


Fig. 3 Schematic diagram of the multi-tubular prototype (III) solar still and the experimental set-up. The locations of the temperature probes are indicated by numbers 0 to 10.

5.2.3) Prototype (IV)

This prototype is similar in design to that of prototype (II) but modified to operate with waste thermal energy, when available on-site, both with (hybrid mode) and without (nocturnal mode) solar radiation.

5.2.4) Prototype (V)

This solar still module is constructed entirely from solar grade polymer materials. In contrast to the above described modules, this prototype has not yet been reported upon in the scientific literature and, therefore, a patent is still under consideration by the collaborating Israeli and Hungarian groups.

5.3) Results

The solar still modules reported upon in this report were designed on the basis of the available state-of-the-art scientific literature, energy and mass transfer calculations, fluid mechanics and

economic analysis. We believe that one of the more important achievements of this joint research project is the determination of the design parameters for these prototypes. Another important achievement of this project is that the performance of these solar still prototypes has been tested, analyzed and optimized. The design of a high-capacity and cost-efficient solar desalination plant can now be formulated as a result of the accumulation of both sufficient information and experience during the course of this investigation.

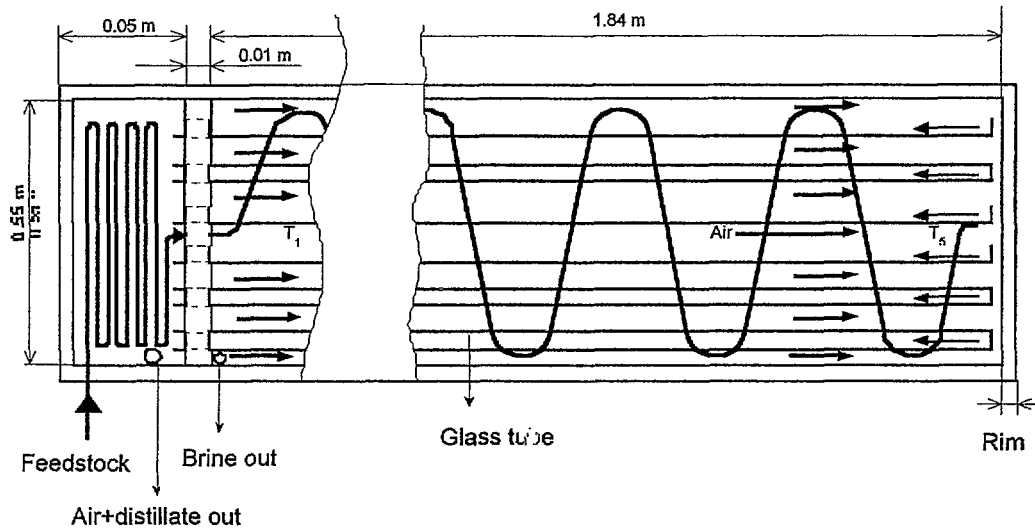


Fig. 4 A simplified top view of the multi-tubular solar still. The actual number of glass tubes is 40.

The experimental set-ups used in this study for all the prototypes tested, enabled us to either measure or calculate the following types of information:

- The approach to and development of steady state operating conditions.
- Determine the temperature profiles within the still.
- Determine the differential and cumulative yields as a function of time and air flow rate.
- Perform material and energy balances on the still when operating under steady state conditions.
- Verify the optimum operating conditions both experimentally and by mathematical simulation models.

Due to space limitations, we will discuss in detail the design parameters and the analysis of the results of the performance tests for prototype (II), whereas for the other prototypes we will present only the main results summarized in both tabulated and graphical formats.

5.3.1) Determination of the system design parameters for prototype (II)

1. Feedstock and air flow rates-

Previous investigations by Mink et al. (1993 and 1997) have shown that a feedstock flow rate $m_f = 2 \text{ kgm}^{-2}\text{h}^{-1}$ was sufficient to completely wet the wick. They also found that increasing the feedstock flow rate from 2.28 to $4.07 \text{ kgm}^{-2}\text{h}^{-1}$ had only a negligible effect on still productivity. Consequently, a constant feedstock flow rate of $2.96 \text{ kgm}^{-2}\text{h}^{-1}$ was applied, in this study, to a solar still of 1 m^2 still area, tilted at an angle of 20° . In the previous investigations the double glazing consisted of two 3 mm glass plates with a 20 mm air gap, whereas in the present study a

double-walled polycarbonate sheet with a 10 mm gap was used as the double glazing. A solar simulator provided a constant incident radiation intensity of $650 \pm 39 \text{ Wm}^{-2}$. In addition, Mink et al. (1993 and 1997) observed that the highest productivity was obtained for air flow rates in the range between 1.8 and $3.5 \text{ kgm}^{-2}\text{h}^{-1}$. The air flow rate of $1.8 \text{ kgm}^{-2}\text{h}^{-1}$ was the lowest air flow rate that could be maintained constant using the then available experimental set-up. In the present study, the air flow rates were varied between 0.32 and $4.51 \text{ kgm}^{-2}\text{h}^{-1}$ after the problem of maintaining stabilized air flow rates in the range below $1.8 \text{ kgm}^{-2}\text{h}^{-1}$ was corrected.

2. Utilization of the vapor content of the air stream exiting the solar still-

The primary distillate obtained via condensation in the lower chamber was estimated to be approx. $0.7 \text{ kgm}^{-2}\text{h}^{-1}$. In view of the fact that the rate of evaporation in the upper chamber was calculated to be of the order of $1.1 \text{ kgm}^{-2}\text{h}^{-1}$, it was apparent that the saturated air stream exiting the lower chamber was also a potential source of fresh water. This secondary distillate, of the order of $0.4 \text{ kgm}^{-2}\text{h}^{-1}$, could be recovered from the exiting air stream provided that it was cooled further by an external heat exchanger, viz., a condenser, to the ambient temperature.

If $H_{1,\text{out}}$ denotes the enthalpy of the saturated air exiting the lower chamber in $\text{J kg}^{-1}_{\text{BDA}}$ and m_a , the mass flow rate of the air stream expressed in units of $\text{kgm}^{-2}\text{s}^{-1}$, the rate of thermal energy exiting with the air stream $q_{1,\text{out}}$ is given by

$$q_{1,\text{out}} = m_a H_{1,\text{out}}. \quad (1)$$

It is obvious that the temperatures within such a still vary inversely with the mass flow rate of the air stream. Consequently, it would be advantageous to operate the solar still at even lower air stream flow rates, since higher exiting air stream enthalpy values translate into both higher temperatures and partial pressures of the water vapor (or vapor content) in the exiting air stream. Also, the overall heat transfer coefficient for condensation from the air stream decreases rapidly with decreasing temperature (see below). The lower air stream flow rates will result in an increase in both the air stream temperatures in the two chambers and the external condenser efficiency (i.e., the amount of secondary distillate obtained) as a result of the greater temperature gradient. An increase in the condenser efficiency will allow a reduction in condenser size and/or cooling energy requirements and a resultant decrease in construction and/or operating costs.

As suggested above, an optimum air stream flow rate must exist in the range of relatively low flow rates, since for this solar still design no distillate will be produced for an air flow rate of zero. Mink et al. (1993 and 1997) hypothesized that the optimum air flow rate was below the range they studied, viz., less than $1.8 \text{ kgm}^{-2}\text{h}^{-1}$. Consequently, in the present study the system was adapted to enable us to operate it under controllable and stable flow rates below $1.8 \text{ kgm}^{-2}\text{h}^{-1}$.

3. Vapor/liquid separator, heat exchanger-

During the performance testing of the solar still module in the laboratory it was important to measure the productivity rate within the module, primary distillation, i.e., the rate of condensation within the lower chamber, and that from the exiting air stream, the secondary distillation, separately. The former is a direct measure of the efficiency of the thermal energy recycle process. Therefore, the vapor/liquid mixture exiting the still module first entered a vapor/liquid separator 1 for the primary distillate, and then the vapor stream was passed through a heat exchanger/condenser prior to entering a second vapor/liquid separator 2 for the secondary

distillate. In a scaled-up version of this system it would be sufficient for the vapor/liquid mixture exiting the system to pass through a heat exchanger/condenser prior to entering a single vapor/liquid separator.

In the present study a simple water cooled condenser functioned as the heat exchanger but it would be very advantageous to utilize the non-negligible thermal energy present in this exiting stream to preheat the feedstock, viz., using the feedstock as the cooling medium. In such a design the temperature of feedstock entering the still would approach $T_{l,out}$ and, thereby, further increase the still operating temperatures. This method of operating the solar still was discussed in detail by Aboabboud et al. (1996).

4. Glazing-

The amount of solar radiation absorbed within the still is the difference between the incident solar radiation G_i and the radiation reflected from the still glazing G_r . The utilized solar energy Q_u is determined from the difference between the solar radiation absorbed and the thermal energy losses to the ambient through the glazing, $q_{loss,amb}$. Thus, the amount of utilized solar energy is

$$Q_u = G_i - G_r - q_{loss,amb} \quad (2)$$

The enthalpy of the air stream attains its maximum value at the top of the still, H_{max} , viz., in the vicinity of the slot connecting the upper and lower chambers, where it attains both its maximum temperature and water vapor content, and is equal to

$$m_a H_{max} = q_{max} = m_a H_{a,in} + Q_u + q_R + q_{released} \quad (3)$$

where $H_{a,in}$ is the enthalpy of the entering air + water vapor stream (in Joule per kg_{BDA}), q_R is the thermal energy recycled directly to the upper chamber and $q_{released}$ is the thermal energy transferred from the preheated feedstock to the air stream. It is apparent from Eqs. (2) and (3) that for a given incident solar radiation the still performance is determined mainly by the thermal energy losses to the ambient and the efficiency of the thermal energy recycle processes. The thermal energy losses to the ambient will increase with increasing temperature, since the system is designed to operate at low mass flow rates of air and at relatively high temperatures. It is obvious that the glazing should have good insulating properties, in order to minimize these thermal energy losses. This was accomplished by utilizing a double glazing. The disadvantage of a double glazing, viz., the enhanced reflection by about 8 % resulting from two glazing surfaces, is more than compensated for by the relatively higher temperature gradients, $\Delta T = T_w - T_a$, developed. In addition, since the glazing does not function as a condensation surface it was possible to use a non-wetting transparent insulating material such as the double-walled polycarbonate sheet as a glazing

5. Thermal energy recycle process and air velocity in the lower chamber-

The thermal energy recycle process occurs in the lower chamber via thermal energy transfer from the saturated air stream both to the central metal plate and the serpentine tube. The rate of condensation in the lower chamber and, thereby, the efficiency of the thermal energy recycle is directly related to these processes. The heat transfer processes include both condensation and convective heat transfer from the air stream. The combined heat transfer coefficient $h_{c,g}$ is strongly dependent on the air stream temperature, which determines the vapor content of

saturated air, and the fluid mechanical properties of the system constituents can be approximated by

$$h_{c,g} = 1/[(1/h_c) + q_g/(q h_g)], \quad (4)$$

where h_c is the heat transfer coefficient for the condensed water film (in the range of 5000 - 10000 $W m^{-2}K^{-1}$); h_g is the convective heat transfer coefficient of the gas film; q_g is the thermal energy of the gas stream (i.e., air + non-condensing vapor) and q is the total thermal energy.

The overall heat transfer coefficient U_{lw} for thermal energy recycle process from the lower chamber to the upper surface of the wet wick, where the evaporation process occurs, is given by

$$U_{lw} = 1/[(1/h_{c,g}) + (1/h_m) + (1/h_{sd}) + (1/h_f) + (1/h_w)] \quad (5)$$

where h_m is the heat transfer coefficient for the metal plate (260 000 $W m^{-2}K^{-1}$ for a 1 mm thick copper sheet); h_{sd} is the heat transfer coefficient for scale deposit (approximately 5000 $W m^{-2}K^{-1}$); h_f is the heat transfer coefficient for the feedstock film above the plate (about 3500 $W m^{-2}K^{-1}$) and h_w is the heat transfer coefficient for the wet wick (about 660 $W m^{-2}K^{-1}$ for a 1 mm thick water film).

The above equations for the heat transfer coefficients were solved by determining values for q_g/q from the Psychrometric Tables at temperature intervals of 5 °C and using the above values for the individual heat transfer coefficients. Heat transfer coefficients for the gas film h_g of 80, 20, 10 and 5 $W m^{-2}K^{-1}$ were considered and the results of this analysis are reported in Table 1. A value of $h_g = 80 W m^{-2}K^{-1}$ corresponds to turbulent flow, $Re > 10\ 000$, and a gas velocity of $\approx 10\ ms^{-1}$, for the case of an equivalent diameter of approximately 0.02 m. Applying the same value for the equivalent diameter, h_g values of 20, 10 and 5 $W m^{-2}K^{-1}$ correspond to approximately 2, 1 and 0.5 ms^{-1} gas velocities, respectively.

It is apparent from the results of the analysis as reported in Table 1 that the effectiveness of thermal energy recycle process and, consequently, the still performance depends mainly on U_{lw} . It would be possible to increase, to a limited extent, the value of U_{lw} by decreasing the thickness of the porous wick, cf., Table 1.

It is apparent from the results reported in Table 1 that the solar still performance can be optimized if operated under high temperatures and high values for the gas film heat transfer coefficient. In this system, high temperatures can be achieved only if sufficiently low mass flow rates are applied in the upper chamber, since at constant energy input the enthalpy gain of the air stream is inversely proportional to its mass flow rate. On the other hand, high linear air stream velocities are required in the lower chamber in order to achieve a high heat transfer coefficient, h_g . These apparently conflicting requirements can be resolved by decreasing the height of the lower chamber (viz., decreasing its cross-sectional flow area) and/or by accelerating the air stream velocity with the aid of baffles, thereby keeping the air mass flow rate low to optimize upper chamber performance.

In prototypes (I) and (II) the feedstock was preheated in the lower chamber and its height was fixed by the outer diameter of the serpentine tube. The gas velocity in the lower chamber was, therefore, accelerated by a factor of about three by means of baffles, which were concentrated in the lower temperature section of the chamber (cf., Fig. 2).

Table 1. Overall heat transfer coefficient for thermal energy recycle U_{Lw} as a function of both temperature and the heat transfer coefficient for the gas film h_g for a 1 mm thick wick.

$T_s, ^\circ\text{C}$	90	85	80	75	70	65	60	55	50	45	40	35
$h_g = 80 \text{ Wm}^{-2}\text{K}^{-1}$ $U_{Lw} (\text{Wm}^{-2}\text{K}^{-1})$	437	425	413	398	382	362	343	320	297	273	246	223
$h_g = 20 \text{ Wm}^{-2}\text{K}^{-1}$ $U_{Lw} (\text{Wm}^{-2}\text{K}^{-1})$	391 436*	358 393*	324 354*	290 315*	258 277*	225 240*	198 209*	169 177*	146 152*	124 128*	104 107*	88 90*
$h_g = 10 \text{ Wm}^{-2}\text{K}^{-1}$ $U_{Lw} (\text{Wm}^{-2}\text{K}^{-1})$	342	292	251	213	180	150	126	104	87	72	59	49
$h_g = 5 \text{ Wm}^{-2}\text{K}^{-1}$ $U_{Lw} (\text{Wm}^{-2}\text{K}^{-1})$	275	215	173	139	115	90	73	59	48	39	31	26

* for a 0.5 mm thick wick

6. Serpentine tube area vs. still area-

The ratio of the thermal energy transferred to the serpentine tube to that directly recycled to the central plate is estimated to be in the range of 0.3 to 0.6. This ratio is a function of the air stream flow rate, the temperature of the entering feedstock and the maximum temperature within the still. Ideally, the ratio of the tube to plate surface area should be identical to the thermal energy recycle ratio, since the nature of heat transfer process to the tube and the plate is essentially the same. Nevertheless, if it is assumed that the average temperature gradient between the central metal plate and tube is $T_{m,avg} - T_{t,avg} \approx 2 \text{ K}$, and considering that the overall heat transfer coefficient U_{Lw} is in the range between 200 - 300 $\text{Wm}^{-2}\text{K}^{-1}$, i.e., the still operates under nearly optimum condition, it is possible to reduce the tube to plate surface area ratio to about 0.2 m^2m^{-2} , in order to reduce material costs. This would be more than sufficient if the entering feedstock would be preheated close to $T_{1,out}$ by utilizing the enthalpy present in the air stream exiting the solar still.

7. Pressure drop in the system-

A possible disadvantage in increasing the air stream velocity in the lower chamber is that parasitic electric energy required by the air pump also increases. This may be a major problem in rural application where the electric energy may be supplied by PV panels. In addition, a system operating under high pressure drops requires a more robust and expensive construction than that operating at nearly atmospheric pressure. The present solar still system was designed for very low pressure drops ($< 100 \text{ Pa}$) and may be considered to operate under atmospheric conditions.

5.3.2) Results of the performance analysis of Prototype (II)

1. Temperature profiles-

The maximum air stream temperature was measured at the upper extremity of the solar still, in the vicinity of the slot, cf. Table 2 below. It was determined that thermal energy recycle begins to take effect about 30 minutes after start-up by comparing the continuously monitored air stream temperatures at the inlet to the upper chamber to that at the outlet from the lower chamber, viz., after about 30 minutes the latter exceeded the former. The steady-state distillation

rate was found to be of the order of $1 \text{ kgm}^{-2}\text{h}^{-1}$, except for relatively low air flow rate. It is of interest to note, that if the air pump remained in operation after the solar simulator was shut-off and the system was at steady-state that the still continued to produce distillate, albeit at a decreasing rate, for about another hour. In other words, in spite the solar still's relatively low thermal mass the thermal energy recycle is still capable of enhancing the yield after 'sunset', i.e., after the solar simulator is shut-off.

The steady-state temperatures, as measured by the 16 thermistors (cf., Fig. 1 for thermistor locations) are reported in Table 2 as a function of the air flow rate. As expected, the temperature measured at a specific location varies inversely with the air flow rate, viz., it increases with decreasing air flow rate or increasing residence time within the still.

Table 2. The temperature profile of prototype (II) under steady-state conditions as a function of air flow rate at a constant feedstock flow rate of $2.96 \text{ kgm}^{-2}\text{h}^{-1}$. The positions of the thermistors are as indicated in Fig. 1 (numbered 0 to 16).

Air Flow rate $\text{kgm}^{-2}\text{h}^{-1}$	T_a	Upper Chamber					Lower Chamber					$T_{1,\text{out}}$	$T_{\text{Sep. I}}$	$T_{X,\text{in}}$	$T_{X,\text{out}}$	T_{Brime}
	T_0 $^{\circ}\text{C}$	T_1 $^{\circ}\text{C}$	T_2 $^{\circ}\text{C}$	T_3 $^{\circ}\text{C}$	T_4 $^{\circ}\text{C}$	T_5 $^{\circ}\text{C}$	T_6 $^{\circ}\text{C}$	T_7 $^{\circ}\text{C}$	T_8 $^{\circ}\text{C}$	T_9 $^{\circ}\text{C}$	T_{10} $^{\circ}\text{C}$	T_{11} $^{\circ}\text{C}$	T_{12} $^{\circ}\text{C}$	T_{13} $^{\circ}\text{C}$	T_{14} $^{\circ}\text{C}$	T_{15} $^{\circ}\text{C}$
4.51	26.0	51.2	65.6	72.2	71.3	71.6	71.3	70.6	69.9	66.0	56.0	56.0	54.9	54.6	35.4	48.7
3.27	26.4	54.0	71.1	76.4	75.9	76.6	76.7	75.9	75.1	71.1	59.6	59.6	58.1	57.8	36.0	51.5
2.21	26.3	57.5	77.1	81.3	81.2	82.1	82.1	81.6	80.7	77.0	63.1	63.1	60.9	60.4	35.0	54.5
1.76	26.1	59.1	80.1	83.7	83.7	84.7	84.8	84.3	83.5	79.9	64.4	64.4	62.0	61.3	34.1	55.7
1.24	26.6	62.6	84.6	87.4	87.6	88.4	88.5	88.4	87.5	84.4	67.5	67.5	64.1	63.0	32.1	58.4
1.02	26.2	64.9	87.4	89.8	89.8	90.7	90.7	90.7	90.0	87.2	69.9	69.9	65.6	64.1	28.6	60.4
0.58	26.1	67.6	91.9	93.6	93.6	94.4	94.2	94.5	94.0	91.7	68.2	68.2	60.7	57.1	21.9	61.9
0.32	25.8	68.6	95.1	96.3	96.2	97.0	96.9	97.4	96.9	94.9	52.5	48.9	34.0	30.4	24.1	62.4

2. Productivity of prototype (II) as a function of air flow rate-

The productivity or distillation rate as a function of air flow rates is reported in Fig. 5 in terms of the primary (I), secondary (II), and total (Σ). The primary distillation rate refers to that condensed within the lower chamber during the thermal energy recycle process, but to be precise it is only an approximate measure of the efficiency of heat recycle. It contains marginal amounts of distillate resulting from both condensation on the inner surface of the lower chamber plate (i.e., due to the small but non-negligible thermal energy losses from the still bottom), and within the tubing connecting the lower chamber outlet to separator 1. These factors were taken into consideration when performing precise mass and energy balance calculations.

The secondary distillation rate is obtained by passing the saturated air stream exiting the solar still via separator 1 through an external condenser and into separator 2, prior to venting to the ambient. It is apparent from Table 3, presented in the following section, that with regard to still productivity there exists an optimum range of air flow rates for the system under consideration, approximately between 1 and $3 \text{ kgm}^{-2}\text{h}^{-1}$. It is also observed that the ratio of secondary to primary product increases with increasing flow rate, i.e., the primary decreases and the

secondary increases with increasing air flow rate (cf. Fig. 5). Nevertheless, the optimum air flow rate of the system is in the vicinity of $1.2 \text{ kgm}^{-2}\text{h}^{-1}$. At this flow rate both the parasitic electric energy required by the air pump and the load on the heat exchanger to condense the secondary distillate are lower, due to the higher temperature, lower mass flow and vapor content of the air.

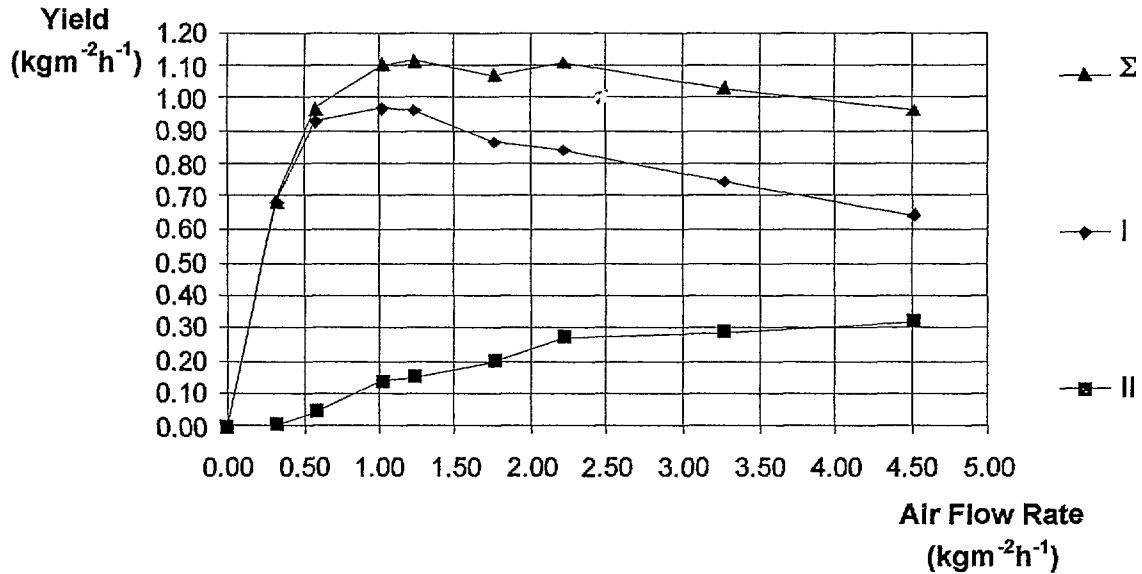


Fig. 5 The productivity (yield) as a function of air flow rate at a constant feedstock flow rate of $2.96 \text{ kgm}^{-2}\text{h}^{-1}$. Primary distillate (I), secondary distillate (I) and total distillate (Σ).

3. Mass and energy flows within Prototype (II) solar still-

Thermal energy analysis, using the appropriate mass and energy balances, of the solar still operating under steady-state conditions as a function of air flow rate and at a constant feedstock flow rate of 2.96 kg h^{-1} , were performed. This provided us with a means of determining the sensitivity of a number of still parameters to changes in the rate of air flow. The results of these analysis are reported in Table 3. They include the following (a) the mass flow rate of vapor through the system, (b) the mass and heat flow of both feedstock and brine drain-off, (c) the heat flow in the upper chamber and (d) the heat flow in the lower chamber. In this analysis the temperature of the entering air stream and feedstock were assumed to be $\approx 26 \text{ }^\circ\text{C}$, viz., room temperature, and the average relative humidity of the entering air stream was assumed to be 80%.

The precision of the mass and energy balances was refined by determining the primary distillate rate as the difference between that measured and the calculated condensation rate of saturated air stream in the tubing between the lower chamber outlet and separator 1. This corrects for the inherent error introduced into the measured primary distillation rate by the condensation that occurs within the tubing connecting the outlet from the lower chamber to the separator 1. The corrected/calculated flow rate of primary distillate exiting the lower chamber, m'_{PDR} , was determined in the following manner:

$$m'_{\text{PDR}} = I - m'_{\text{SDR}} = I - m_{\text{BDA}}[M_v(\text{at } T_{1,\text{out}}) - M_v(\text{at } T_{X,\text{in}})], \quad (6)$$

where m'_{SDR} is the condensation/distillation rate in the tubing and M_v is the vapor content of the air in units of kg vapor/kg BDA. The maximum mass flow rate of vapor carried by the air stream corresponds to that at maximum temperature and is given as

$$m_{v,max} = m'_{PDR} + m_{BDA}[M_v(\text{at } T_{l,out})]. \quad (7)$$

The maximum rate of thermal energy flow is also attained at T_{max} and if the flow rate of air and vapor is expressed in kgs^{-1} , q_{max} , in W per m^2 still area, is given by

$$q_{max} = c_a m_{BDA} T_{max} + m_{v,max} H_{v,max}, \quad (8)$$

where c_a is the heat capacity of air in $\text{Jkg}^{-1}\text{K}^{-1}$ and $H_{v,max}$ is the enthalpy of vapor (Jkg^{-1}) at T_{max} .

Table 3. Mass and energy analysis on prototype (II) solar still operating at steady-state as a function of air flow rate at a constant feedstock flow rate of $2.96 \text{ kgm}^{-2}\text{h}^{-1}$. The mass and heat flows were normalized to unit still area.

(a) Mass flow rates of the water vapor through the solar still.

m_a $\text{kgm}^{-2}\text{h}^{-1}$	Upper Chamber $m_{v,u,in}$ $\text{kgm}^{-2}\text{h}^{-1}$	Upper Chamber m_{evgp} $\text{kgm}^{-2}\text{h}^{-1}$	Upper Chamber $m_{v,max}$ $\text{kgm}^{-2}\text{h}^{-1}$	Lower Chamber m'_{PDR} $\text{kgm}^{-2}\text{h}^{-1}$	Lower Chamber $m_{v,l,gut}$ $\text{kgm}^{-2}\text{h}^{-1}$	Tubing. $m'_{SDR, \tau}$ $\text{kgm}^{-2}\text{h}^{-1}$	Exchange r $m_{v,x,in}$ $\text{kgm}^{-2}\text{h}^{-1}$	Exchange r $m_{v,x,out}$ $\text{kgm}^{-2}\text{h}^{-1}$
4.51	0.078	1.082	1.160	0.614	0.546	0.036	0.510	0.190
3.27	0.056	1.136	1.192	0.703	0.489	0.047	0.442	0.152
2.21	0.038	1.149	1.187	0.781	0.406	0.059	0.347	0.077
1.76	0.030	1.131	1.161	0.812	0.349	0.058	0.291	0.091
1.24	0.021	1.166	1.187	0.891	0.296	0.069	0.227	0.077
1.02	0.018	1.151	1.169	0.887	0.282	0.073	0.209	0.077
0.58	0.010	0.996	1.006	0.861	0.145	0.069	0.076	0.036
0.32	0.006	0.683	0.689	0.657	0.032	0.023	0.009	0

(b) Mass and thermal energy flow rates of feedstock through the solar still.

m_a $\text{kgm}^{-2}\text{h}^{-1}$	T_{max} $^{\circ}\text{C}$	$m_{f,in}$ $\text{kgm}^{-2}\text{h}^{-1}$	$q_{f1,in}$ at T_a Wm^{-2}	q_{PR} Wm^{-2}	$q_{f1,out}$ at T_{max} Wm^{-2}	$T_{\text{Brine drain}}$ $^{\circ}\text{C}$	$m_{\text{Brine drain}}$ $\text{kgm}^{-2}\text{h}^{-1}$	$q_{\text{Brine drain}}$ Wm^{-2}	q_{released} Wm^{-2}
4.51	71.6	2.96	90	156	246	48.7	1.878	106	139
3.27	76.7	2.96	90	174	264	51.5	1.824	109	155
2.21	82.1	2.96	90	193	283	54.5	1.811	115	168
1.76	84.8	2.96	90	202	292	55.7	1.829	118	174
1.24	88.5	2.96	90	215	305	58.4	1.794	122	183
1.02	90.7	2.96	90	222	312	60.4	1.809	127	185
0.58	94.2	2.96	90	234	324	61.9	1.964	141	183
0.32	96.9	2.96	90	245	334	62.4	2.277	164	170

It should be noted, that Kudish et al. (1997) have simulated both the observed temperature profiles and the productivity rates using mathematical model, which are in agreement with the experimentally measured data.

(c) Heat flows in upper evaporation chamber

m_a $\text{kgm}^{-2}\text{h}^{-1}$	$q_{a,u,in}$ Wm^{-2}	q_R Wm^{-2}	q_{released} Wm^{-2}	Q_U Wm^{-2}	q_{max} Wm^{-2}	T_{max} $^{\circ}\text{C}$	T_{dew} $^{\circ}\text{C}$
4.51	110	216	139	470	935	71.6	68.7
3.27	80	256	155	45 ¹	942	76.7	74.2
2.21	54	285	168	415	922	82.1	79.8
1.76	43	296	174	383	896	84.8	82.3
1.24	30	330	183	363	906	88.5	86.4
1.02	25	316	185	363	889	90.7	88.5
0.58	14	289	183	274	760	94.2	91.7
0.32	9	154	170	187	520	96.9	93.0

(d) Heat flows in lower condenser chamber

m_a $\text{kgm}^{-2}\text{h}^{-1}$	T_{max} $^{\circ}\text{C}$	T_{dew} $^{\circ}\text{C}$	$q_{\text{max, in}}$ Wm^{-2}	q_{out} Wm^{-2}	$q_{\text{Dist.out}}$ Wm^{-2}	$q_{B,loss}$ Wm^{-2}	q_{RT} Wm^{-2}	q_{PR} Wm^{-2}	q_R Wm^{-2}
4.51	71.6	68.7	935	491	40	33	371	156	215
3.27	76.7	74.2	942	426	50	36	430	174	256
2.21	82.1	79.8	922	345	58	41	478	193	285
1.76	84.8	82.3	896	294	61	43	498	202	296
1.24	88.5	86.4	906	245	70	46	545	215	330
1.02	90.7	88.5	889	231	72	48	538	222	354
0.58	94.2	91.7	760	119	74	50	571	234	316
0.32	96.9	93.0	520	60	42	50	417	245	152

Note: Refer to the nomenclature for definition of symbols.

It is apparent from Fig. 5 that the optimum performance of the solar still module is obtained for air flow rates in the range of 1 to 2.2 $\text{kgm}^{-2}\text{h}^{-1}$, which correspond to a total productivity rate of about 1.1 $\text{kgm}^{-2}\text{h}^{-1}$. It is observed from Table 3 (c) that within this range of air flow rates the amount of solar energy utilized, Q_u , decreases with decreasing air flow rate, whereas the average temperatures within the upper chamber increase with decreasing flow rate, cf. Table 1. It is also observed from Table 3, however, that maximum values for primary distillation rate, total thermal energy recycle, sum of thermal energy recycled directly to the upper chamber, and thermal energy released from the feedstock to the air stream in the upper chamber occur for air flow rates between 1.02 and 1.24 $\text{kgm}^{-2}\text{h}^{-1}$. We conclude that in this range of air flow rates the thermal energy recycle more than compensates for the decrease in solar energy utilization efficiency, i.e., the first effect or direct solar to thermal energy conversion.

As a consequence of the above, it follows that for air flow rates in the range between 1 and 2.2 $\text{kgm}^{-2}\text{h}^{-1}$, the mass flow rate of water vapor exiting the lower chamber will be a minimum in the range of air flow rates between 1.02 and 1.24 $\text{kgm}^{-2}\text{h}^{-1}$ and the air stream temperature, $T_{\text{l,out}}$, will be a maximum. Consequently, the cooling load for the external heat exchanger will be a minimum for this range of air flow rates.

To demonstrate the heat flow processes occurring in the solar still module in this range of optimum performance a thermal energy flow diagram is presented in Fig. 6 for an air flow rate of $1.24 \text{ kgm}^{-2}\text{h}^{-1}$. It is seen from this diagram that the main heat transfer processes determining the solar still performance are Q_u , q_R and q_{RT} .

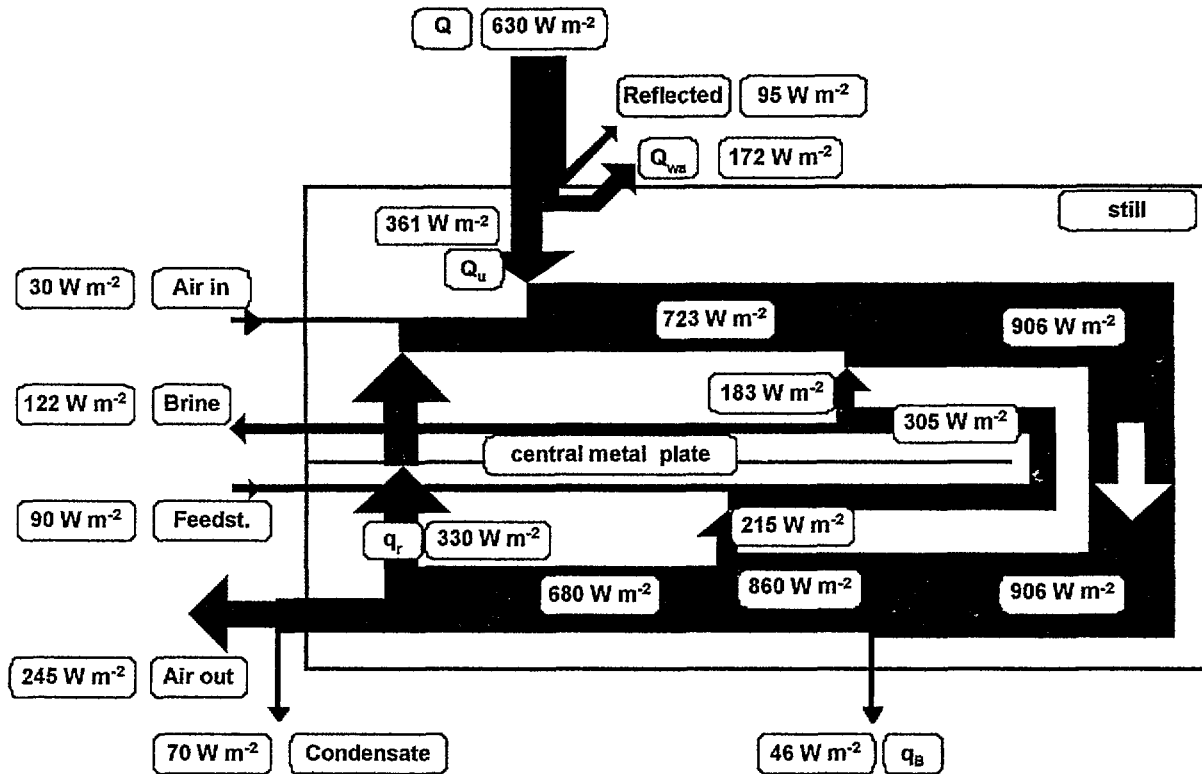


Fig. 6 Thermal energy flow diagram as calculated by means of the mass and energy balances on prototype (II) for an air flow rate = $1.24 \text{ kgm}^{-2}\text{h}^{-1}$ and feedstock flow rate = $2.96 \text{ kgm}^{-2}\text{h}^{-1}$.

The decrease in the solar still performance for air flow rates below $1 \text{ kgm}^{-2}\text{h}^{-1}$ is the result of two factors: (1) an increase in thermal energy losses from the upper chamber to the ambient and (2) the rapid decrease in the overall heat transfer coefficient for thermal energy with a decreasing heat gas film transfer coefficient. The latter is approximately proportional to the linear velocity of the air stream (i.e., the air and non-condensing water vapor) in the lower chamber. Consequently, a possible design change to enhance the solar still performance would be to attain higher linear air velocities in the lower chamber by decreasing its cross-sectional area. The downside of such a design change would be an increase in the pressure drop of the still system and a subsequent increase in parasitic energy consumption. There appears to be sufficient leeway for further reduction in the lower chamber cross-sectional area, since the present solar still design has a very low pressure drop, and we plan to study this effect in the future.

Further developments in the solar still design will be related to problems of scale-up, with the goal of arriving at a still design which is economically viable with regard to construction, operation and maintenance.

5.4) Inter-comparison of the performance and the estimated economics of prototypes (I) - (V)

The performance of prototype (I) has been discussed in detail by Mink et al. (1998). The performance of prototypes (I) and (III) has been analyzed and simulation models developed and verified, as reported upon by Kudish et al. (1997) and Mink et al. (1999), respectively. The performance analysis of prototype (IV) operating in the following modes: solar (normal mode), solar + waste thermal energy (hybrid mode) and waste thermal energy (nocturnal mode) have been reported upon by Kudish et al. (1999). Therefore, in this section contains only a brief inter-comparison of the results of the performance analysis of solar still prototypes (I) - (V). We will also present an estimate of the fixed capital investment costs for such systems.

The inter-comparison of the performance of the five prototype solar still investigated during the course of this joint research progress is summarized in Figs, 7 and 8. Fig. 7 contains an inter-comparison of the variation in the measured solar still maximum temperature, for the five prototypes, as a function of air flow rate. The inter-comparison of the variation in the measured total productivity rates (viz., the sum of the primary and secondary distillate rates), for the five prototypes, as a function of the air flow rate is presented in Fig. 8.

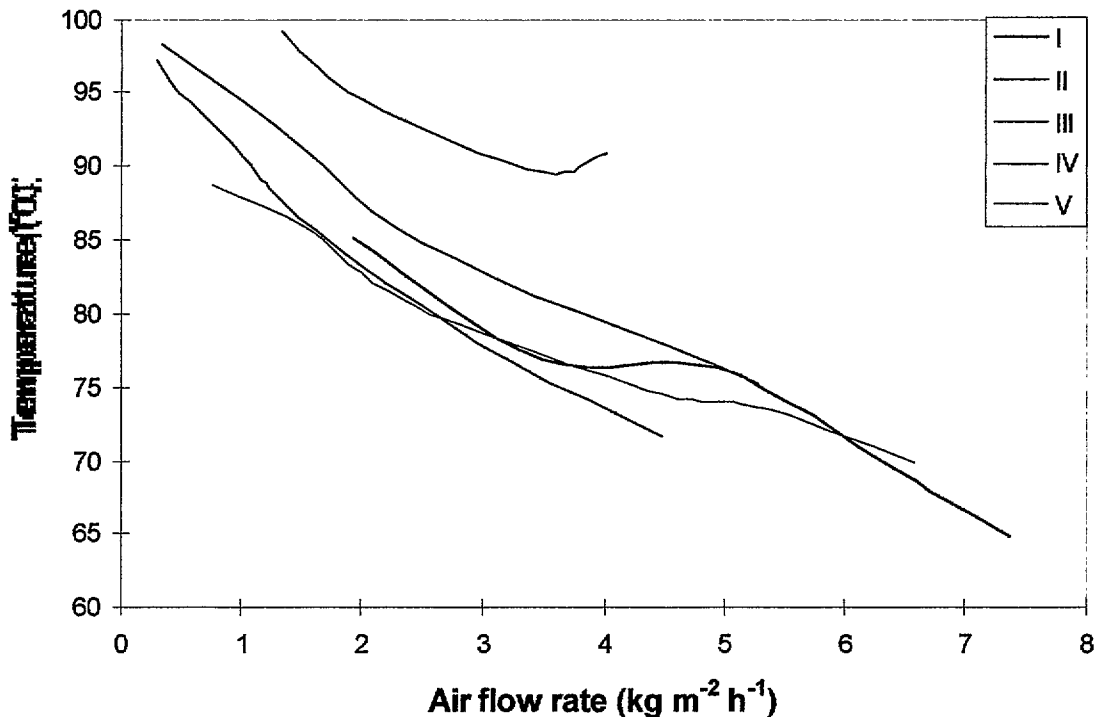


Fig. 7 An inter-comparison of the measured solar still maximum temperature, for the five prototypes, as a function of air flow rate.

It is observed from Fig. 7 that prototype (IV), which operates in a hybrid mode, attains the highest maximum temperatures relative to the other four prototypes. Prototype (III) is somewhat superior to the remaining prototypes at lower air flow rates, whereas the three other prototypes exhibit somewhat similar behavior with regard to their measured maximum temperatures as a function of air flow rate.

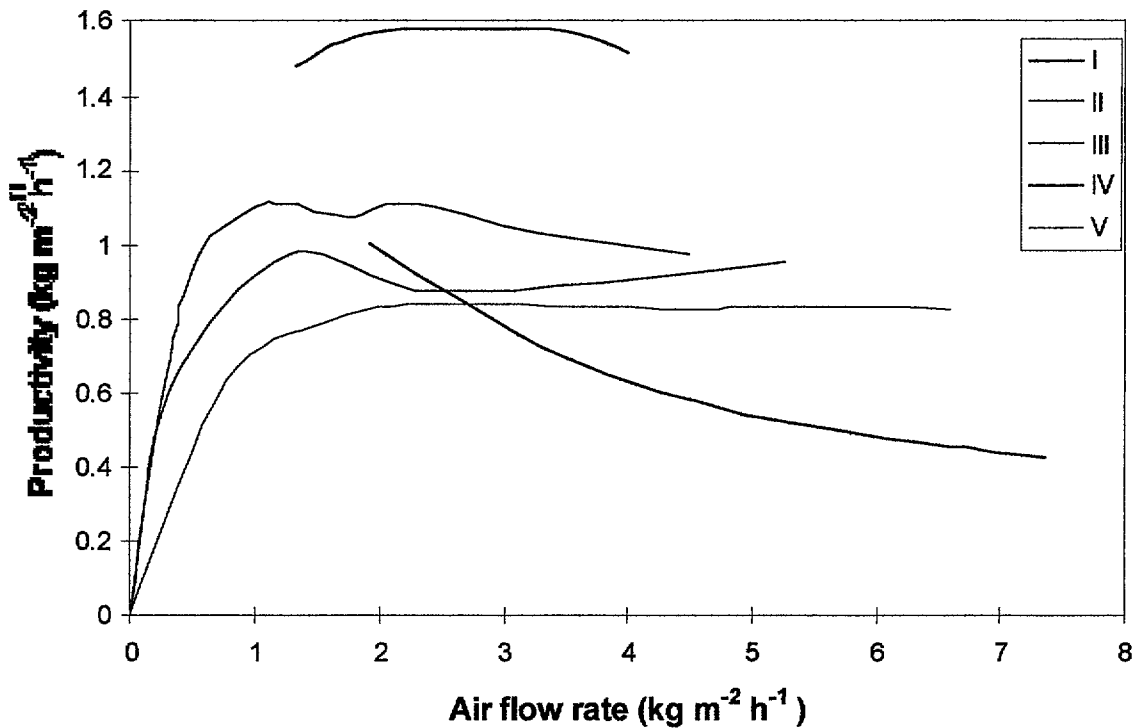


Fig. 8 An inter-comparison of the variation in the measured total productivity rates (viz., the sum of the primary and secondary distillate rates), for the five prototypes, as a function of the air flow rate.

The results of the inter-comparison of the total productivity rates for the five prototypes indicate, quite conclusively, that prototype (IV) is the most productive solar still. It is of interest to note, that all prototypes, with the exception of prototype (I), arrive at an essentially constant total productivity rate with increasing air flow rate (i.e., over the range of air flow rates investigated). The observed behavior of prototype (I), is in all likelihood, a consequence of the lower limit on the air flow rate achievable when it underwent performance testing. It is observed that prototypes (II), (III) and (V) exhibit somewhat similar behavior with regard to total productivity as a function of air flow rate. The relative performance rating for these three prototypes, based upon total productivity, is (II) > (III) > (V). It appears that prototype (I) may exhibit a behavior quite similar to (II) in the range of low air flow rates but, as explained above, there is no data available in the lower range of air flow rates.

The main design parameters, optimum operating conditions and an estimate of the fixed capital investment costs for a 365 m³/y capacity plant constructed for each of the five prototypes are summarized in Table 4. It is apparent from data reported in Table 4 that when waste thermal energy is available at the site, prototype (IV) operating in the hybrid mode offers the highest productivity at the lowest fixed capital investment costs for a desalination plant of defined capacity. In addition, Kudish et al. (1999) showed that the daily productivity could be further enhanced by operating prototype (IV) during daytime hours in the hybrid mode and during non-solar or nighttime hours in the nocturnal mode, utilizing available on-site waste thermal energy. In addition, the data in Table 4 indicate that prototype (V) may be the preferred design, based on

economics, for sites not possessing a waste thermal energy source. Furthermore, prototype (V) has an advantage of possessing a very low mass and a relatively simple design. We believe, however, that prototype (V) may have higher maintenance and replacement costs relative to those for the other prototypes.

Table 4. Summary of the main design parameters, optimum operating conditions for prototypes (I) - (V) and an estimate of the fixed capital investment costs for a 365 m³/y capacity plant.

	Prototype (I)	Prototype (II)	Prototype (III)	Prototype (IV)	Prototype (V)
Glazing	Double glass	Double-walled polymer	Double-walled polymer	Double-walled polymer	Double-walled polymer
Still body	2 Metal trays	2 Metal trays	Plastic tray & Glass tubes	2 Metal trays	Double-walled polymer
Serpentine tube	Metal tube	Metal tube	Plastic tube	Metal tube	Plastic tube
Mass (kg/m ²)	42	26	8	26	4
Height of still body ^A (mm)	45	35	25	35	35
Optimum air flow rate ^B (kg/m ² /h)	1.95	1.24	1.28	2.03	2.38
T _{max} ^C (°C)	84.1	88.4	92.8	94.3	80.7
Hourly yield ^C (kg/m ² /h)	0.99	1.10	0.97	1.57 ^D	0.84
Yearly yield ^E (kg/m ³ /y)	1,980	2,200	1,940	3,140	1,680
Still Area ^B of a 365 m ³ /y plant, (m ²)	185	166	187	116	217
Investment costs ^F (\$US/m ²)	145	130	110	135	80
Investment costs for a 365 m ³ /y plant (\$US)	26,688	21,528	20,695	15,692	17,381

^A Does not include the bottom insulation, 50 mm thick

^B At high productivity corresponding to a low air flow rate

^C At 650 Wm⁻² irradiation and optimum air flow rate

^D Operating in hybrid mode

^E Calculated on the basis of 2000 hours of operation per year at an average radiation intensity of 650 Wm⁻². E.g., Beer Sheva has 2009 hours per year with an average global solar radiation intensity of 704 Wm⁻².

^F Material & labor costs, including heat exchanger, pumps and tubing, based upon that calculated for a 100 m² plant

NOMENCLATURE

- A still area (m²)
 c heat capacity (Jkg⁻¹K⁻¹)
 d depth (mm)

G	solar radiation (Wm^{-2})
H	enthalpy (Jkg^{-1})
h	heat transfer coefficient ($Wm^{-2}K^{-1}$)
L	length (m)
M_v	vapor content of saturated air ($kgkg^{-1}_{BDA}$)
m	mass flow rate ($kgm^{-2}h^{-1}$)
m_{brine}	mass flow rate of brine drain-off ($kgm^{-2}h^{-1}$)
m'_{PDR}	calculated primary distillate rate ($kgm^{-2}h^{-1}$)
$m'_{SDR,T}$	calculated additional distillate rate in the tubing ($kgm^{-2}h^{-1}$)
Q_u	solar energy utilized (Wm^{-2})
q	thermal energy (Wm^{-2})
$q_{B,loss}$	backside thermal energy losses (Wm^{-2})
q_{brine}	thermal energy in brine drain-off (Wm^{-2})
$q_{loss,amb}$	thermal energy loss from upper chamber to ambient (Wm^{-2})
q_{PR}	thermal energy utilized to preheat the feedstock (Wm^{-2})
q_R	thermal energy recycled directly to upper chamber (Wm^{-2})
$q_{released}$	thermal energy released by the preheated feedstock to the air stream (Wm^{-2})
q_{RT}	total thermal energy recycled (Wm^{-2})
T	temperature ($^{\circ}C$)
T_{dew}	dew point temperature of air stream exiting upper chamber and entering lower chamber ($^{\circ}C$)
U_{lw}	overall heat transfer coefficient from lower chamber to wick ($Wm^{-2}K^{-1}$)
W	width (m)

Subscripts

a	air stream
abs	absorbed
amb	ambient
avg	average value
BDA	bone dry air
c	condensed water film
c,g	combined heat transfer coefficient
Dist,out	distillate exiting lower chamber
evap	evaporated
f	feedstock
g	gas film
I	primary distillate
II	secondary distillate
i	incident
id	inner diameter
in	stream entering chamber
l	lower chamber
m	central metal plate
max	maximum value
od	outer diameter
out	stream exiting chamber

r	reflected
sd	scale deposit
sep	vapor/liquid separator
t	serpentine tube
u	upper chamber
v	water vapor
w	wick
X	external heat exchanger/condense

6) IMPACT RELEVANCE AND TECHNOLOGY TRANSFER

6.1) Impact of findings on the developing country

The major impact of this joint research project has been the development of a Hungarian research team with both experience and expertise in the field of solar energy conversion and utilization. They are now capable, using both theoretical and experimental data analysis, of designing and scaling-up solar stills and evaporators for different applications. This expertise can now be applied to the design of solar to thermal energy conversion systems for agricultural, chemical and environmental protection purposes. These include such applications as solar desalination, solar drying of industrial or agricultural materials and thickening of dilute solutions of valuable or hazardous salts as an intermediate stage in their management/processing.

6.2) The project's impact on individuals, laboratories, departments, and institutions.

6.2.1) Mr. M.M. Aboabboud, a PhD. student of RLIC

During the latter part of his PhD. studies, which overlapped with the first 18 months of the project, he was in constant contact with the Israeli PI, Dr. Kudish, regarding questions concerning both the theoretical and practical aspects of solar distillation. This assistance from the Israeli PI was highly appreciated by Mr. Aboabboud. He returned to his own country, after his defense of his PhD. dissertation, and now occupies an important position where he continues his R&D work on the utilization of renewable energy

6.2.2) Mr. L. Horváth, MSc., a former diploma worker, now a researcher at RLIC/RLMEC

Through his full-time association with this project, which included participation in scientific conferences/exhibitions and training courses that was supported by the project budget, he gradually became a specialist in the solar thermal area. He was awarded a special, three-year grant, intended for young researchers below the age of 35, from the National Science Foundation of Hungary (OTKA) in the field of solar distillation based upon the joint publications resulting from the project. This is, to the best of our knowledge, the first such award from OTKA for research work in the solar thermal area. This emphasizes that the importance of renewable energy is now being recognized by OTKA. In fact, effective from 2000, the rational use of renewable energy has become a part of the Hungarian Governmental Energy Policy.

6.2.3) Dr. G. Mink, Head Environmental Technology group of RLIC-RLMEC, Hungarian PI

The project provided him with the ultimate possibility to continue his R&D work on solar distillation, which had never been formally supported in Hungary. The strong theoretical background of the Israeli group made it possible to continue this work on an advanced level. His participation in this joint research program gave Dr. Mink the opportunity to present his scientific achievements at major international conferences. He has been invited to present lectures on the application of solar energy at different academic institutions, industrial plants and military bases within Hungary. Dr. Mink has also been invited by one of the Hungarian colleges to present a special course (weekly two-hour lectures) on renewable energy beginning February 2000.

6.3) Impact on laboratories, departments, institutions

A growing scientific interest in Hungary towards the use of renewable energy has resulted from both the scientific lectures on the achievements of this project and the educational lectures presented and has led to a kind of restructuring of RLMEC. A new Environmental Chemistry Department focused mainly on the rational use of renewable energy was created at RLMEC in 1999. This department consists of the Environmental Chemistry group, headed by Dr. G. Várhegyi, involved with both the utilization of bio-mass and the recycle of plastic wastes, and the Environmental Technology group, headed by Dr. Mink, involved with solar thermal technologies. The latter group also deals with pollution surveillance and control through industrial contracts.

6.4) Possibilities of the use of the results

The collaborating partners, based upon the achievements of this project, are now able to design high-capacity, low cost and corrosion resistant prototype solar desalination plants that offer high productivity and cost-efficiency. The construction of a fully equipped 12 m² solar still area demonstration plant was planned at RLIC but was abandoned in early 1999, due to the drastic change in the financial situation of the group after the reorganization of RLIC to the RLMEC, CRC, HAS. The construction of such a pilot plant is definitely warranted, based upon the results obtained during the present investigation, but will require the additional support from international funding organisations.

6.5) New capacity, equipment and expertise left behind in the developing country

6.5.1 New capacity

As a result of this project a well-equipped solar energy laboratory has been established at the RLMEC and the staff of the laboratory has attained an international reputation in the field of solar-to-thermal energy conversion systems.

6.5.2 Equipment

A solar energy research facility has been established at the RLMEC and it is outfitted with a 1 m² solar simulator, automated data acquisition and measurement control system. A list of the instrumentation that was purchased through the project budget consists of the following:

1. Two Compaq PC's with 14" Compaq color monitor Windows 95 and graphic (Excel) software packages
2. A third and less expensive PC for data acquisition and measurement control
3. Two Hewlett-Packard color deskjets

4. A solarimeter with a RS232 serial interface for data processing of the radiation measurements
5. A variable speed peristaltic pump outfitted with a four channel pump head from Cole-Parmer, to ensure the regulation of the feedstock flow rate and the simultaneous distribution of the feedstock to more than one prototype if desired
6. Two gas flow meters and 6 solenoid valves from Cole-Parmer for measurement control
7. A conductivity meter with a RS232 interface for water quality control
8. A pH meter with a RS232 interface for water quality control
9. An ion analyzer with electrodes for different ions with a RS232 interface for water quality control
10. A solar simulator with a 1 m² area using GE lamps and a water-cooled IR filter to filter out the infrared radiation and, thereby insure that the incident radiation is in the 0.4 - 2.5 micrometer wavelength range.

6.5.3) Improvement of the scientific capabilities of the collaborating country

As a result of their close collaboration with the Israeli group, which has extensive experience in the design, analysis and simulation of solar to thermal energy conversion systems, the Hungarian group has developed an internationally recognized team in this area of research.

7) PROJECT ACTIVITIES/OUTPUTS

7.1) Training

7.1.1) Mr. M.M. Aboabboud

He submitted his PhD. dissertation (146 pp. including table and figures with 101 references) entitled "Design and Investigation of a new, Air-Blown Solar Still with Internal Energy Recycle". Mr. Aboabboud expressed his gratitude to Dr. Kudish for his support, ideas and advice during the course of his dissertation work, which overlapped with the first 18 months of this USAID program. On May 25, 1998 Mr. M.M. Aboabboud successfully defended his PhD. dissertation. The two referees were Prof. E. Bekassy, DSc. and Prof. I. Farkas, DSc. He received six grades of 3 (excellent) and a single grade of 2 (good) from the seven-member jury, i.e., his thesis work was awarded 20 points out of a possible maximum of 21 points.

7.1.2) Mr. L. Horváth

He received, effective January 1, 1998, a three-year grant with an annual stipend of 300 000 HUF from the National Science Foundation of Hungary for young researchers below the age of 35, in the field of solar thermal.

7.1.3) Drs. Mink and Kudish

Applied for and were awarded travel grants under the Exchange of Researchers in the Framework of Israeli-Hungarian Scientific Cooperation 1999-2000, funded by the State of Israel Ministry of Science, Jerusalem and the Republic of Hungary OMF, Budapest. This grant provides for a 7-14 day visit by each PI and a 1-2 month visit by a junior researcher from each country during each year of the two year grant period.

7.1.4) Dr. E.G. Evseev

He spent a month working at the Chemical Research Center in the RLMEC, from April 11 until May 12, 1999. He utilized this visit to become acquainted with the experimental set-up and to validate his simulation model for the RLMEC prototype module. He devoted his efforts, during this visit, to the study and development of a simulation model to describe an air-blown solar still with an internal multi-tubular heat exchanger for recycle of the thermal energy of condensation. He also developed a simulation model to describe a new type of multi-pass compact solar still, with thermal energy recycle, fabricated from a 4-walled polycarbonate sheet being developed.

7.1.5) Mr. L. Horváth

His visit to Israel, from July 4 through August 2, 1999, coincided with the International Solar Energy Society 1999 Solar World Congress,, which took place in Jerusalem from July 4-9, 1999. The remainder of his visit was spent at the Solar Energy Laboratory, BGU. During this time, he installed and programmed a new analog-to-digital card into the laboratory PC for on-line data collection and monitoring of the experimental set-ups. He then validated the program.

7.1.6) Dr. G. Mink

He utilized his 1999 travel grant to coincide with the International Solar Energy Society 1999 Solar World Congress, in Jerusalem, Israel from July 4-11, 1999. Dr. Mink then visited the BGU Solar Energy Laboratory after the Congress from July 11 through the 14. During this time he worked with Dr. Kudish on the preparation of a proposal to the EC-Mediterranean Partner Programme on the topic of solar desalination. The multi-national consortium involved in this proposal consists of Hungary, Italy, Israel, Palestine Authority and Turkey.

7.1.7) Dr. A.I. Kudish

He visited Budapest, using his travel grant, from August 1 through 10, 1999. During this time, he and Dr. Mink completed the scientific portion of the proposal to the EC-Mediterranean Partner Programme on the topic of solar desalination.

7.2) Lectures

1. Dr. Mink presented a lecture entitled "Energy Saving Solar Stills: Israeli-Hungarian USAID Project" on February 28, 1997 at a regular session of the Committee of Environment Protection of the Hungarian Academy of Sciences. The paper was co-authored by G. Mink, M.M. Aboabboud, L. Horváth and A.I. Kudish.
2. Dr. Mink presented a lecture entitled "Achievement and Trends in Solar technologies" on May 7, 1997 for a retraining course for army officers at the Regional Environmental Safety Center for the Army in Budapest.
3. Two lectures were presented by the Hungarian group at the regular scientific seminar of the RLIC: Dr. Mink- "Solar Desalination: Israeli-Hungarian USAID Project"; co-authored by G. Mink, L. Horváth, M.M. Aboabboud, E.G. Evseev and A.I. Kudish.
Mr. Horváth- "A New Type Solar Concentrator to Achieve Industrial Temperatures"; co-authored by L. Horváth and G. Mink.

4. Mr. Horváth presented a lecture at the Annual Meeting of the Doctoral School of the Chemical Research Center entitled "Experimental Studies on a Modern Solar Still" in Matrahaza, Hungary, March 1998.
5. Dr. Mink presented a lecture on November 18, 1998 at the scientific session of the Chemical research Center, Hungarian Academy of Science, entitled "Research & Development Work at the RLIC in the Area of Solar Thermal".
6. Dr. Kudish presented a mini-course entitled "Solar Energy Applications" at the Technical University Bergakademie, Freiberg, Germany on November 15-16, 1999.
7. Dr. Mink presented a lecture on February 22, 2000 at the Polytechnic of Dunaujvaros, Hungary, entitled "Is the Future Solar?"
8. Dr. Kudish will present a lecture on March 29, 2000 at the Faculty of Chemical Engineering of the Technical University of Budapest, Hungary entitled "A Short Historical Review of Solar Energy Usage".

7.3) Meetings Attended

1. EuroSun 96, September 16-19, 1996, Freiburg Germany.
2. International Solar Energy Society 1997 Solar World Congress, August 24-29, 1997, Taejon, Korea
3. International Congress Energy and the Environment, 16th Scientific Conference on Energy and the Environment, October 28-30, Opatija, Croatia,
4. International Solar Energy Society 1999 Solar World Congress, July 4-9, 1999, Jerusalem, Israel.

7.4) Publications

1. M.M. Aboabboud, L. Horváth, G. Mink, M. Yasin, and A.I. Kudish (1996) An energy saving atmospheric evaporator utilizing low grade thermal or waste energy, *Energy* **21**, 1107-1117.
2. M.M. Aboabboud, L. Horváth, J. Szépvölgyi, G. Mink, E. Radhika, and A.I. Kudish (1997) The use of a thermal energy recycle device in conjunction with a basin-type solar still for enhanced productivity, *Energy* **22**, 83-91.
3. G. Mink, M.M. Aboabboud, L. Horváth, E.G. Evseev and A.I. Kudish (1997) Design and performance of an air-blown, multiple-effect solar still with thermal energy recycle. *Proc. Int'l. Solar Energy Society Conference, Solar World Congress, 24-29 August, Taejon, Korea*, **6**, 135-144..
4. A.I. Kudish, E.G. Evseev, M.M. Aboabboud, L. Horváth and G. Mink (1997) Heat transfer processes in an air-blown, multiple-effect solar still with thermal energy recycle. *Proc. Int'l. Solar Energy Society Conference, Solar World Congress, 24-29 August, Taejon, Korea*, **6**, 158-167.
5. G. Mink, L. Horváth, E.G. Evseev and A.I. Kudish (1998) Design parameters, performance testing and analysis of a double-glazed, air-blown solar still with thermal energy recycle. *Solar Energy* **64**, 265-277.
6. A.I. Kudish, E.G. Evseev, L. Horváth and G. Mink (1998) Performance studies on an air-blown, multiple-effect solar still operating on solar and/or waste energy. *Proc. Int'l. Congress Energy and the Environment, 28-30 October, Opatija, Croatia*, **II**, 57-69
7. G. Mink, M.M. Aboabboud, L. Horváth, E.G. Evseev and A.I. Kudish (1998) Performance of an air-blown solar still with internal multi-tubular heat exchanger for

- condensation heat recycle. *Proc. Int'l. Congress Energy and the Environment*, 28-30 October, Opatija, Croatia, **II**, 71-77.
8. G. Mink, L. Horváth, E.G. Evseev and A.I. Kudish (1999) Performance and analysis of a multiple-effect solar still utilizing an internal multi-tubular heat exchanger for thermal energy recycle. *Proc. Int'l. Solar Energy Society Conference, Solar World Congress*, 4-9 July, Jerusalem, Israel, in press.
 9. A.I. Kudish, E.G. Evseev, L. Horváth and G. Mink (1999) Performance and analysis of a multiple-effect solar still utilizing solar and/or waste thermal energy. *Proc. Int'l. Solar Energy Society Conference, Solar World Congress*, 4-9 July, Jerusalem, Israel, in press.

8) PROJECT PRODUCTIVITY

The project accomplished almost all its R&D goals with the exception of the construction and operation of a pilot-plant installation. The reason for this shortcoming, as explained previously, was a result of the drastic change in the financial situation of the Hungarian group after the reorganization of RLIC to the RLMEC, CRC, HAS. Consequently, the construction of a fully equipped 12 m² solar still area demonstration plant planned at RLIC was abandoned in early 1999. The construction of such a pilot plant is definitely warranted, based upon the results obtained during the present investigation, but will require the additional support from international funding organisations.

9) FUTURE WORK

The two research groups are fully committed to continue their collaborative research efforts in the development of multi-effect solar desalination systems. They intend to place an emphasis on the utilization of non-corrosive materials in the construction of the solar still.

They were informed, in September 1998, that they had been awarded travel grants under the Exchange of Researchers in the Framework of Israeli-Hungarian Scientific Cooperation 1999-2000, which is funded by the State of Israel Ministry of Science, Jerusalem and the Republic of Hungary OMFB, Budapest. This grant provides for short-term visits (7-14 days) by the senior scientists and long-term visits (1-2 months) by the junior scientists to the collaborating institution each year, during the 2-year grant period. Their visits during the first year, 1999, of this grant have been described in section 7. These visits were, needless to say, very helpful in the planning and discussion of their collaborative research program. The visits during the year 2000 are now in the planning stages.

The two PI's have worked together in the preparation of a proposal to the EC-Mediterranean Partner Programme on the topic of solar desalination. The multi-national consortium involved in this proposal consists of Hungary, Israel, Italy, Palestine Authority and Turkey. The title of the proposal is: Development of Efficient and Cost-Competitive Plant Module for Sea-Water Desalination. The proposal was submitted in September 1999 to the EC for shared-cost under the "RTD actions: research, technology development projects, demonstration projects and combined projects". The proposal is presently under review and the decision is expected during early part of 2000. The two PI's fully intend to continue to collaborate on the development of multi-effect solar desalination systems, irrespective of the outcome of the decision by the EC on their proposal. Their continued collaboration will always be indebted to the USAID grant for the

experience gained and equipment purchased. [We have just received notice from the EC informing us that the proposal was turned down. We intend to revise the proposal in accordance with the referees' comments and submit it, once again, to an appropriate future call for proposals.]

The co-operation between the Israeli and Hungarian groups has resulted in the enhancement of the S&T bases of both partners and contributed significantly to the creation of new scientific and personal contacts and friendships between the two countries. Their high level of scientific achievement has been recognized by both of their governments by awarding them the above mentioned travel grant.

The two groups initiated a cooperative research program, which includes both Moslem and Christian Mediterranean countries, with the submission of the EC-Mediterranean Partner Programme proposal. This project, if implemented, can have a significant impact on the Mediterranean region and other rural areas of the world and its aims can be summarized as:

- The development of a DEMO plant demonstrating a clean and cost-efficient technology for fresh water production. The propagation of this technology will contribute to the sustainable development and the socio-economic modernization in many regions of the world.
- The propagation of this new technology will decrease the load on natural fresh water resources and thus, will lessen the political conflicts caused by the shortage of fresh water.
- The propagation of this technology will favor SMEs producing solar grade materials and SMEs fabricating and running solar desalination plant modules in the rural areas of the world.
- The scientific and technological cooperation between institutions and researchers from the partner countries will be strengthened.
- The balanced participation of the Mediterranean partner countries will aim to enhance the S&T base of the Euro-Mediterranean partnership and through the development of human contacts will aim to contribute to the lessening of both ethnic and religious tensions in the Mediterranean region.

10) LITERATURE CITED

- Aboabboud, M.M., Mink, G. and Karmazsin, É. (1993) Solar still of improved efficiency. In *Proc. ISES Solar World Congress, 22-27 August, Budapest, Hungary, Vol. 4*, 319-324.
- Aboabboud, M.M., Horváth, L., Szépvölgyi, J., Mink, G., Radhica, E. and Kudish, A.I. (1996) The use of thermal energy recycle in conjunction with a basin type solar still for enhanced productivity. *Energy* **23**, 83-91.
- Baumgartner, T., Jung, D., Kössinger, F., Schrag, H. and Sizmann, R (1992) Solarthermische Trinkwasser-bereitung. In: *Proc. 8. Intern. Sonnenforum, June 23-July 2, Berlin DGS, München*, pp. 432-347.
- Cooper, P.I. (1973) The maximum efficiency of a single effect solar still. *Solar Energy* **15**, 205-217.
- Delyannis, A. and Delyannis, E.E. (1980) *Seawater and Desalting*, Vol.1. Springer, Berlin, 188 pp.
- El-Bahi, A. and Inan, D. (1997) Analysis of a solar still built at Hacettepe University. In: *Proc. ISES Solar World Congress, 24-29 August, Taejon, Korea, Vol. 6*, pp. 193-202.

- El-Bahi, A. and Inan, D. (1999) Solar still with minimum inclination and coupled to an outside condenser. In: *Proc. ISES Solar World Congress*, 4-9 July, Jerusalem, Israel, in press.
- Fernandez, J.L. and Chargo, N. (1990) Multi-stage, indirectly heated solar still. *Solar Energy* **44**, 215-223.
- Harding, J. (1883) Apparatus for solar distillation. *Proc. Institute for Civil Engineering* **73**, 284.
- Kudish, A.I., Gale, J. and Zarmi, Y. (1982) A low cost design solar desalination unit. *Energy Conversion & Management* **22**, 269-274.
- Kudish, A.I. and Gale, J. (1986) Solar desalination in conjunction with controlled environment agriculture. *Energy Conservation & Management* **26**, 201-207.
- Kudish, A.I. (1991) Water Desalination. In: *Solar Energy in Agriculture-Energy in World Agriculture*, B.F. Parker (Ed), Vol. 4, pp. 255-294, Elsevier Science Publishers B.V., Amsterdam.
- Kudish, A.I., Mink, G. and Aboabboud, M.M. (1995) TLCC calculation on air-blown solar stills with heat recycle (personal communication).
- Kudish, A.I., Evseev, E.G., Horváth, L. and Mink, G. (1997) Heat transfer processes in an air-blown, multiple-effect solar still with thermal energy recycle. In: *Proc. ISES Solar World Congress*, 24-29 August, Taejon, Korea, **Vol. 6**, pp. 158-167.
- Kudish, A.I., Evseev, E.G., Horváth, L. and Mink, G. (1999) The performance and analysis of a multiple-effect solar still utilizing solar and/or waste energy. In: *Proc. ISES Solar World Congress*, 4-9 July, Jerusalem, Israel, in press.
- Lobo, P.C. and Araujo, S.R.D. (1977) Design of a simple multi-effect basin-type solar still. In: *Proc. ISES Solar World Congress*, New Delhi, India, p. 2026.
- Malik, M.A.S., Tiwari G.N., Kumar, A., and Sodha, M.S. (1982) *Solar Distillation*, Pergamon Press, Oxford, 175 pp.
- Mink, G., Jakabos, D. and Székely, T. (1988) Hungarian Patent 201,714.
- Mink, G., Aboabboud, M.M., Horvath, L., Evseev, E.G. and Kudish, A.I. (1997) Design and performance of an air-blown, multiple-effect solar still with thermal energy recycle. In: *Proc. ISES Solar World Congress*, 24-29 August, Taejon, Korea, **Vol. 6**, pp. 135-144.
- Mink, G., Aboabboud, M.M. and Karmazsin, É. (1998) Air-blown solar still with heat recycling. *Solar Energy* **62**, 309-317.
- Mink, G., Horváth, L., Evseev, E.G. and Kudish, A.I. (1998) Design parameters, performance testing and analysis of a double-glazed, air-blown solar still with thermal energy recycle. *Solar Energy* **62**, 309-317.
- Mink, G., Horváth, L., Evseev, E.G. and Kudish, A.I. (1999) Performance and analysis of a multiple-effect solar still utilizing an internal multi-tubular heat exchanger for thermal energy recycle. In: *Proc. ISES Solar World Congress*, 4-9 July, Jerusalem, Israel, in press.
- Müller-Holst, H., Kessling, W., Engelhardt, M. and Schölkopf, W. (1997) Solar thermal desalination with 24 hour thermal storage. In: *Proc. ISES Solar World Congress*, 24-29 August, Taejon, Korea, **Vol. 6**, pp. 168-176.
- Müller-Holst, H., Engelhardt, M. and Schölkopf, W. (1999) Small-scale thermal seawater desalination simulation and optimization of system design. *Desalination* **122**, 255-262.
- Sodha, M.S., Nayak, J.K., Tiwari, G.N. and Kumar A. (1980) Double-basin solar still. *Energy Conversion & Management* **20**, 23-32.
- Talbert, S.G., Eibling J.A., and Löf G.O.G. (1970) Manual on solar distillation of saline water. R. & D. Progress Report No. 546, US Department of Interior, 263 pp.
- Telkes M (1955) Solar stills. In: *Proceedings of the World Symposium on Applied Solar Energy*, Phoenix, AZ, p. 73.

- Tiwari, G.N. (1985) Enhancement of daily yield in a double solar still. *Energy Conversion & Management* **25**, 49-50.
- Tiwari, G.N. and Sharma S.B. (1991) Analytical study of double-effect distillation under active mode of operation. *Energy* **16**, 951-958.

APPENDIX



DESIGN PARAMETERS, PERFORMANCE TESTING AND ANALYSIS OF A DOUBLE-GLAZED, AIR-BLOWN SOLAR STILL WITH THERMAL ENERGY RECYCLE

G. MINK*, L. HORVÁTH*, E. G. EVSEEV** and A. I. KUDISH**,†

*Research Laboratory for Inorganic Chemistry, Hungarian Academy of Sciences, 1518 Budapest Pf 132, Hungary

**Solar Energy Laboratory, Department of Chemical Engineering, Ben-Gurion University of the Negev, Beer Sheva 84105, Israel

Received 6 November 1997; revised version accepted 23 June 1998

Communicated by ERNANI SARTORI

Abstract—An air-blown, multiple-effect solar still with thermal energy recycle consisting of an upper evaporation chamber and lower condensation chamber, has been recently proposed. The principle of operation of such a still, the main design parameters and the results of solar still performance tests are presented in this paper. The present discussion is restricted to the performance testing of a solar still with a nominal still area of 1 m^2 , utilizing a solar simulator providing a constant radiation intensity of $630 \pm 39 \text{ W m}^{-2}$. The solar still performance was monitored under the conditions: of a constant feedstock flow-rate, $8.22 \times 10^{-4} \text{ kg m}^{-2} \text{ s}^{-1}$, and varying air flow-rate, ranging from 0.89×10^{-4} to $12.53 \times 10^{-4} \text{ kg m}^{-2} \text{ s}^{-1}$. It was observed, under these conditions, that the thermal energy recycle began to be effective after about 30 min and that the still achieved steady-state after approximately 1 h of operation. The steady-state distillation rate exhibits an optimum (of the order of $3.06 \times 10^{-4} \text{ kg m}^{-2} \text{ s}^{-1}$) at air flow-rate in the range from 2.8 to $3.44 \times 10^{-4} \text{ kg m}^{-2} \text{ s}^{-1}$. The experimental results indicate that the still performance can be enhanced further by increasing the linear air stream velocity in the lower chamber by decreasing its cross-sectional flow area. © 1998 Elsevier Science Ltd. All rights reserved.

1. INTRODUCTION

Today there exists an estimated two billion people who go without fresh water on a daily basis. The consumption of water unfit for drinking, due to pathogens and salinity, is a major health hazard world-wide. In addition, the growth of the world's population and the consequent food shortage, requires the expansion of agriculture into arid zones, i.e., the greening of the desert. The famine in the Sahal region (viz., the Sahara Desert) and other less publicized regions on the globe provide ample evidence for the necessity of solving this problem by concerted efforts, both national and international. Arid and semi-arid zones constitute approximately 40% of the earth's land area and they are, in general, characterized by high levels of solar radiation and shortages of fresh water. Such regions often possess reservoirs of either brackish or saline water that may be used for both drinking and irrigation after suitable treatment. Solar desalination systems may be an ideal source

of fresh water for both drinking and agriculture in arid zones. This is especially true in that both the demand for fresh water and the intensity of solar radiation are, in general, cyclical in nature and in phase with each other.

The utilization of solar energy for the distillation of brackish or saline water has been practiced for a very long time. Various types of solar stills and solar-assisted desalination units have been designed and investigated. A number of papers have been published on this subject, for example, see Talbert *et al.* (1970); Malik *et al.* (1982); Kudish (1991).

Present day state-of-the-art single-effect solar stills exhibit annual productivities of the order of $1 \text{ m}^3 \text{ m}^{-2}$. The major drawback in the design of such single-effect solar stills is the dumping of a large fraction of the thermal energy input to the system to the ambient via condensation of the water vapour on the relatively cooler inner surface of the glazing. The underlying reason for the limited use of solar desalination plants constructed from such solar stills is their relatively low productivity per unit area (Delyannis and Delyannis (1980)), viz., they require the availabil-

†

†Author to whom correspondence should be addressed. E-mail: akudish@bgumail.bgu.ac.il

ity of large land areas and the fixed capital investment is directly proportional to the size (basin area) of the plant, though economics of scale may be involved with the peripheral equipment (mainly pumps and storage vessels, which, in general, contribute a small percentage to the total fixed capital investment) and operation and maintenance costs.

The multiple-effect solar still systems are designed to recover/recycle some fraction of the latent heat of condensation to preheat the feedstock either prior to entering or within the solar still basin and thereby enhance the system efficiency. This may be accomplished, in the former case, by condensing the water vapour on the surface of a heat exchanger through which the feedstock flows as the heat exchange medium. For example, the still may be constructed with a double glazing and by flowing the feedstock through the space between the glazing (i.e., essentially a simple liquid in glass condenser) prior to entering the still basin. Such a design, obviously, necessitates operating the still as a flow system (i.e., a continuous feed input) rather than a batch system. It also requires leakproof sealing of the double glazing. This may be facilitated by using an internally sealed doubled glazing such as that available for double glazed windows (i.e., 'storm windows') but at a much greater cost than single glazings.

An example of the recovery/recycle of the latent heat of condensation within the solar still system is that analyzed by Sodha *et al.* (1980). It is designated as a double basin solar still and is a simplified version of a multiple level solar still originally proposed by Dunkle (1961) and studied by Lobo and Araujo (1977). It is designed to utilize the latent heat of condensation from the lower basin (viz., the condensation of the water vapour on the underside of the transparent base supporting the upper basin) to heat the water in the upper still basin. This requires the use of a transparent base (e.g., glass) for the upper still. The practical application of such a design is questionable due to the many technical problems involved, such as the load on the transparent base of the upper still.

The two still designs described above are classified as double-effect solar stills, a single recovery/recycle of the latent heat of condensation. It is possible to envision the design of multiple-effect solar stills (e.g., adding on more basins with transparent bases, one top of the other, to achieve a multiple-effect) similar in concept to multiple-effect conventional desalina-

tion techniques. Needless to say, the cost of the solar still construction increases with complexity of the design and any additional costs must be weighed against the potential for increased productivity/efficiency.

Another example of such recycle systems is that described by Kössinger *et al.* (1993), i.e., a highly efficient solar desalination unit utilizing the latent heat of condensation to preheat the feedstock prior to entering the still. Müller-Holst *et al.* (1997) presented a total life cycle cost analysis for this system under different modes of operation.

The rationale behind the design of our air-blown, multiple-effect solar still was to overcome the inherent disadvantage in the operation of single-effect solar stills, viz., their efficiency, notwithstanding intensive research and development efforts, has remained stalled in the 30–40% range. Our goal being, enhanced productivity while incurring minimal incremental costs. This air-blown, multiple-effect solar still is designed to recycle the thermal energy (i.e., the latent heat of condensation) to heat or preheat the feedstock to the solar still. The mode of operation of this solar still will be described together with experimental results in the following sections.

The significance of this research project is obvious in that potable water is a commodity that is becoming scarce and has been a source of conflict between nations throughout history. If the latter part of the 20th Century can be characterized as one that the scarcity of oil was a *casus belli* than it is reasonable to state that the *casus belli* in the 21st Century will be the scarcity of potable water. In fact, the success of the peace treaties now in effect and in the making in the Middle East will depend to a significant degree on the availability of water for all countries concerned. Solar desalination can be an important source for water in this region, which is primarily composed of arid and semi-arid lands and has an abundance of solar radiation.

2. SOLAR STILL DESCRIPTION

A schematic diagram of the air-blown, multiple-effect solar still is presented in Fig. 1. It is essentially of the tilted-wick genre in the form of a thin rectangular box divided into two chambers (upper evaporator and lower condenser) by a central metal sheet. The central metal sheet does not extend across the full length of the still but leaves a slot of 10 mm between its top end and the still's upper extremity. The metal sheet also

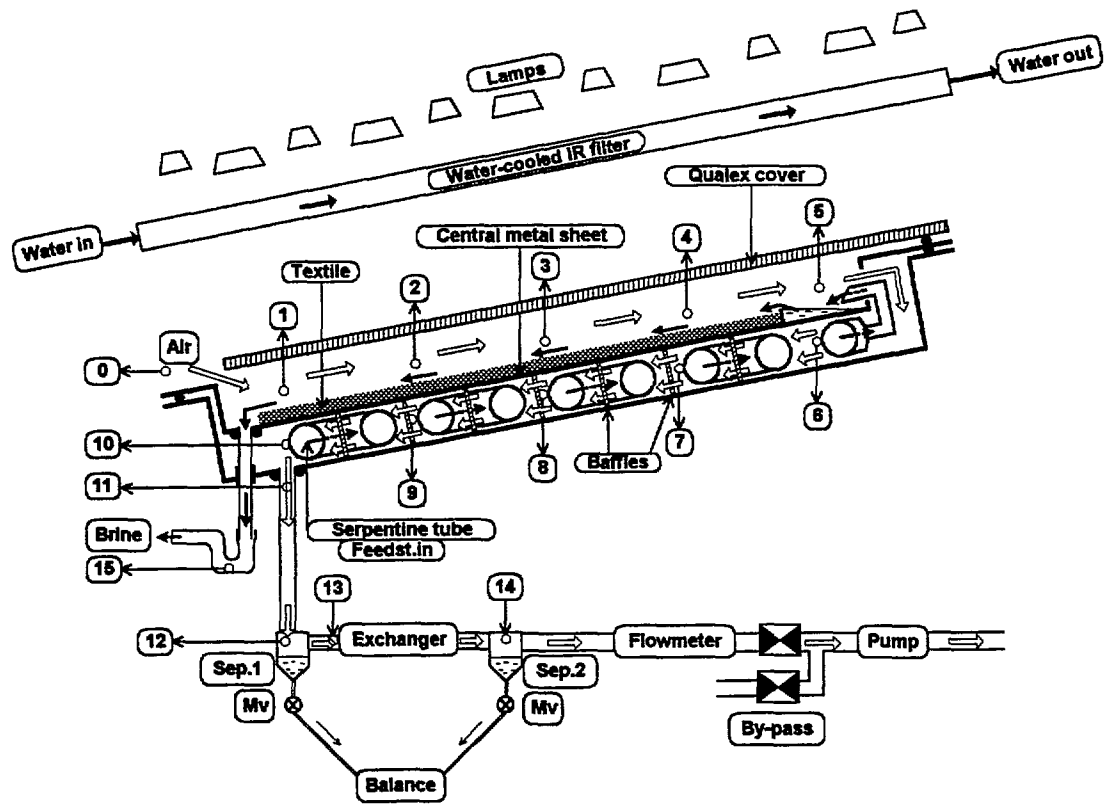


Fig. 1. A schematic diagram, longitudinal cross-section, of the experimental solar still set-up. The location of the 16 temperature probes are indicated by numbers 0 to 15.

functions as (i) the support for the wick (a black porous material) which covers it on the upper chamber side; (ii) the surface to which a serpentine tube, in the lower chamber side, for transporting the feedstock to the upper chamber, is in contact. This serpentine tube also functions as a heat exchanger for preheating the feedstock prior to entering the upper chamber. The spacing between the central metal plate and the upper chamber still glazing and the lower chamber backside are both 12 mm.

The mode of operation of the solar still is as follows: (1) ambient air is pumped into the upper chamber from the bottom of the tilted still and sweeps the water vapour evaporated from the tilted wick into the lower chamber via the slot at the top of the tilted still (maximum temperature of the air stream is measured at this point, above the slot, prior to entering to the lower chamber and serving as the hot fluid in what is essentially an air-liquid heat exchanger); (2) the major portion of the water vapour then condenses on the serpentine tube, which enters at the bottom of the lower chamber, transporting the feedstock to the upper chamber; or on the lower portion of the backside of the metal sheet supporting the wick; (3) the

feedstock, which enters the serpentine tube at a flow-rate in excess of the rate of evaporation from the wick, is preheated during its passage through the serpentine tube, exits the serpentine tube at the top edge of the central plate and passes over a weir and flows by gravity down the wick; (4) the distillate exits the lower chamber and is collected, whereas the humid air stream, also exiting the lower chamber, enters an external condenser, to further condense the water vapour remaining, prior to venting to the ambient.

In the upper chamber the air stream flows counter-current to the direction of feedstock flowing down the wick, whereas in the lower chamber the air stream flows both counter-current and perpendicular to the direction of the feedstock flowing through the serpentine tube. Due to the nature of this solar still, viz., that the upper chamber glazing does not serve as a condensation surface, it is possible and recommended to utilize a double glazing to reduce thermal energy losses via the glazing to the ambient. In fact, it is possible to use non-wetting polymeric glazings such as those used as transparent insulating material (TIMs), e.g., Qualex, a double-walled polycarbonate sheet, as the solar still glazing.

3. DESIGN PARAMETERS

3.1. System design parameters

(i) Feedstock and air flow-rates – Previous investigations by Mink *et al.* (1997, 1998) have shown that a feedstock flow-rate of $5.56 \times 10^{-4} \text{ kg m}^{-2} \text{ s}^{-1}$ is sufficient to completely wet the wick. They also found that increasing the feedstock flow-rate from 6.33×10^{-4} to $11.3 \times 10^{-4} \text{ kg m}^{-2} \text{ s}^{-1}$ had only a negligible effect on the still productivity. The present study utilized a solar still with a still area, of 1 m^2 tilted at an angle of 20° with a constant feedstock flow-rate of $8.22 \times 10^{-4} \text{ kg m}^{-2} \text{ s}^{-1}$. The previous investigations utilized double glazing consisting of 3-mm glass plates with a 20-mm gap, whereas the present study utilized a double-walled polycarbonate sheet with a 10-mm gap. The incident radiation intensity was $650 \pm 39 \text{ W m}^{-2}$, utilizing a solar simulator. Mink *et al.* (1997, 1998) found that the highest productivity was obtained for air flow-rates in the range between 5.00×10^{-4} and $9.72 \times 10^{-4} \text{ kg m}^{-2} \text{ s}^{-1}$ and in the present study the air flow-rates were varied between 0.89×10^{-4} and $12.53 \times 10^{-4} \text{ kg m}^{-2} \text{ s}^{-1}$.

(ii) Utilization of the vapour content of the air stream exiting the solar still – The primary distillate via condensation in the lower chamber was estimated to be approximately $1.94 \times 10^{-4} \text{ kg m}^{-2} \text{ s}^{-1}$. In view of the fact that the rate of evaporation in the upper chamber was found to be of the order of $3.05 \times 10^{-4} \text{ kg m}^{-2} \text{ s}^{-1}$, it is apparent that the humid air stream exiting the lower chamber is also a potential source of fresh water. This secondary distillate, of the order of $1.11 \times 10^{-4} \text{ kg m}^{-2} \text{ s}^{-1}$, can be recovered provided that the exiting air stream can be cooled by an external heat exchanger, viz., a condenser, to ambient temperature.

If $H_{1,\text{out}}$ denotes the enthalpy of the saturated air exiting the lower chamber in $\text{J kg}_{\text{BDA}}^{-1}$ and the mass flow-rate of the air stream, is expressed in units of $\text{kg m}^{-2} \text{ s}^{-1}$, the rate of thermal energy exiting with the air stream is given by:

$$q_{1,\text{out}} = m_a H_{1,\text{out}} \quad (1)$$

It is obvious that the temperatures within such a still are inverse functions of the mass flow-rate of the air stream. Consequently, it would be advantageous to operate the solar still at even lower air stream flow-rates, since higher exiting air stream enthalpy values translate into both higher temperatures and partial pressures of the water vapour (or vapour content) in the exiting air stream. Also, the overall heat transfer coefficient for condensa-

tion from the air stream decreases rapidly with decreasing temperature (see below). The lower air stream flow-rates will result in an increase in the air stream temperature in both chambers and an increase in the external condenser efficiency (i.e., the amount of secondary distillate) as a result of the greater temperature gradient. An increased condenser efficiency will allow a reduction in condenser size and/or cooling energy requirement and resultant decrease in construction and/or operating costs.

As mentioned previously, an optimum air stream flow-rate must exist in the range of relatively low flow-rates, since for this solar still design the productivity will be zero for an air flow-rate of zero. Mink *et al.* (1997, 1998) based upon their experimental results and analysis, suggested that the optimum air flow-rate was below the range they studied, viz., less than $5.00 \times 10^{-4} \text{ kg m}^{-2} \text{ s}^{-1}$. Consequently, in the present study the system was adapted to enable us to operate it under controllable and stable flow-rates below $5.00 \times 10^{-4} \text{ kg m}^{-2} \text{ s}^{-1}$.

(iii) Vapour/liquid separator, heat exchanger – In the performance testing of the solar still module in the laboratory, it was desired to measure the primary distillation/productivity rate within the module (i.e., the rate of condensation within the lower chamber, which is a direct measure of the efficiency of the thermal energy recycle process) and that obtained from the exiting air stream, secondary distillation. Therefore, the vapour/liquid mixture exiting the still module first entered vapour/liquid separator 1 (primary distillate), then the vapour stream was passed through a heat exchanger/condenser prior to entering vapour/liquid separator 2 (secondary distillate). In a scaled-up system it would be sufficient to have the outlet vapour/liquid mixture exiting the system to pass through a heat exchanger/condenser prior to entering a single vapour/liquid separator.

In the present study a simple water-cooled condenser functioned as the heat exchanger but it would be very advantageous to utilize the non-negligible thermal energy present in this stream to preheat the feedstock, viz., to utilize the feedstock as the cooling medium. In such a design the temperature of feedstock entering the still would approach $T_{1,\text{out}}$ and thereby further increase the still operating temperatures. This method of operation of the solar still is discussed in detail by Aboabboud *et al.* (1996).

(iv) Glazing – The amount of solar radiation absorbed within the still is the difference between

45

the incident solar radiation and the reflection losses from the still glazing and from the wet wick. The utilized solar energy is determined from the difference between the solar radiation absorbed and the thermal energy losses to the ambient through the glazing. Thus, the amount of utilized solar energy is given by:

$$Q_u = G_i - G_r - q_{\text{loss,amb}} \quad (2)$$

The air stream attains its maximum enthalpy, temperature and water vapour content at the top of the still, viz., in the vicinity of the slot connecting the upper and lower chambers, and thereby its maximum thermal energy, which is given by:

$$\begin{aligned} q_{\text{max}} &= m_a H_{\text{max}} \\ &= m_a H_{a,\text{in}} + Q_u + q_R + q_{\text{released}}, \end{aligned} \quad (3)$$

where $H_{a,\text{in}}$ is the enthalpy of the entering air plus vapour stream in $\text{J kg}_{\text{BDA}}^{-1}$. It is apparent from Eqs. (2) and (3) that for a given solar irradiance, the still performance is determined mainly by the top losses and the efficiency of the thermal energy recycle processes. Since the system is designed to operate at low mass flow-rates of air and at relatively high temperatures, the thermal energy losses to the ambient will increase with increasing temperature. To minimize these thermal energy losses the glazing should have good insulating properties. This was achieved by utilizing a double glazing. The disadvantage of a double glazing is the increased reflection losses but this is more than compensated for by the relatively higher temperature gradients, $\Delta T = T_w - T_a$, achieved. In addition, since the glazing does not function as a condensation surface it was possible to use a transparent insulating material such as Qualex, a transparent double-walled polycarbonate sheet which is non-wetting, as a glazing.

(v) Thermal energy recycle process and air velocity in the lower chamber. – The thermal energy recycle process occurs in the lower chamber via heat transfer from the humid air stream to the serpentine tube and to the lower portion of the central metal plate. The rate of condensation in the lower chamber and thereby the efficiency of the thermal energy recycle is directly related to these processes. The heat transfer processes include condensation and convective heat transfer from the air stream. The combined heat transfer coefficient, which strongly depends on the temperature (the vapour content of saturated air) and its fluid mechanical properties is approximated by:

$$h_{c,g} = 1 / [(1/h_c) + q_g / (qh_g)] \quad (4)$$

where the heat transfer coefficient for the condensed water film h_c is in the range of $5000\text{--}10\,000 \text{ W m}^{-2} \text{ K}^{-1}$; q_g is the heat transmitted by the gas (air + non-condensing vapour) and q is the total heat transmitted.

The overall heat transfer coefficient for thermal energy recycle process from the lower chamber to the upper surface of the wet wick, where the evaporation process is occurring, is given by:

$$\begin{aligned} U_{1w} &= 1 / [(1/h_{c,g}) + (\delta_m / \kappa_m) + (1/h_{sd}) + (1/h_f) \\ &\quad + (1/h_w)], \end{aligned} \quad (5)$$

where for a 1-mm thick copper sheet the value for κ_m / δ_m is $260\,000 \text{ W m}^{-2} \text{ K}^{-1}$; the heat transfer coefficient for scale deposit h_{sd} is approximately $5000 \text{ W m}^{-2} \text{ K}^{-1}$; the heat transfer coefficient for the feedstock/brine film above the plate h_f is about $3500 \text{ W m}^{-2} \text{ K}^{-1}$ and the heat transfer coefficient for a wet wick h_w , with a 1-mm thick water film, is about $660 \text{ W m}^{-2} \text{ K}^{-1}$. The heat transfer values for the scale deposit and feedstock/brine film are approximate (estimated from the data and equations given in Perry's Chemical Engineers' Handbook (1963)) but their effect on the overall heat transfer coefficient is marginal, since they offer minimal resistance to the thermal energy transfer.

The above equations for the heat transfer coefficients were solved by determining values for q_g / q from the Psychrometric tables for temperature intervals of 5°C and using the above values for the individual heat transfer coefficients. The following values for the heat transfer coefficient for the gas film h_g were considered, 80, 20, 10 and $5 \text{ W m}^{-2} \text{ K}^{-1}$. The results of this analysis are reported in Table 1. A value of $h_g = 80 \text{ W m}^{-2} \text{ K}^{-1}$ corresponds to turbulent flow with $\text{Re} < 10\,000$ and a gas velocity of 10 m s^{-1} or above, for the case of an equivalent diameter of approximately 0.02 m. Using the same value for the equivalent diameter, h_g values of 20, 10 and $5 \text{ W m}^{-2} \text{ K}^{-1}$ correspond to approximately 2, 1 and 0.5 m s^{-1} gas velocities, respectively.

It is obvious from the results of this analysis reported in Table 1 that the effectiveness of thermal energy recycle process and consequently the still performance depends mainly on U_{1w} . It is possible to increase, to a limited extent, the value of U_{1w} by decreasing the thickness of the porous wick, cf. Table 1.

The results of the analysis reported in Table 1 suggest that the still should be operated at high

Table 1. Overall heat transfer coefficient for thermal energy recycle as a function of temperature and gas film heat transfer coefficient for a wick thickness of 1 mm

$T, ^\circ\text{C}$	90	85	80	75	70	65	60	55	50	45	40	35
$h_g = 80 \text{ W m}^{-2} \text{ K}^{-1}$ $\dot{U}_{1w}^g (\text{W m}^{-2} \text{ K}^{-1})$	437	425	413	398	382	362	343	320	297	273	246	223
$h_g = 20 \text{ W m}^{-2} \text{ K}^{-1}$ $\dot{U}_{1w}^g (\text{W m}^{-2} \text{ K}^{-1})$	391 436 ^a	358 393 ^a	324 354 ^a	290 315 ^a	258 277 ^a	225 240 ^a	198 209 ^a	169 177 ^a	146 152 ^a	124 128 ^a	104 107 ^a	88 90 ^a
$h_g = 10 \text{ W m}^{-2} \text{ K}^{-1}$ $\dot{U}_{1w}^g (\text{W m}^{-2} \text{ K}^{-1})$	342	292	251	213	180	150	126	104	87	72	59	49
$h_g = 5 \text{ W m}^{-2} \text{ K}^{-1}$ $\dot{U}_{1w}^g (\text{W m}^{-2} \text{ K}^{-1})$	275	215	173	139	113	90	73	59	48	39	31	26

^a For a wick thickness of 0.5 mm.

temperatures and with high gas film heat transfer coefficient h_g values. Such high temperatures can be achieved only if sufficiently low mass flow-rates are applied, since at constant energy input the enthalpy gain of the air stream is inversely proportional to its mass flow-rate. On the other hand, high linear air stream velocities are necessary in the lower chamber in order to achieve a high heat transfer coefficient. This goal can be achieved by decreasing the height of the lower chamber (*viz.*, decreasing its cross sectional flow area) and/or by accelerating the air stream velocity with the help of baffles, since the air mass flow-rate must be low.

In the present solar still module the feedstock is preheated in the lower chamber and the height of the lower chamber is determined by the outer diameter of the serpentine tube. Therefore, in the lower chamber the gas velocity was accelerated, by a factor of about three by means of baffles, which were concentrated in the lower temperature/section of the chamber (*cf.* Fig. 2).

(vi) Serpentine tube area vs. still area – The

ratio of the thermal energy transmitted to the serpentine tube to that directly recycled to the central plate is estimated to be in the range of 0.3 to 0.6, depending on the air stream flow-rate, the temperature of the entering feedstock and the maximum temperature within the still. Ideally, the ratio of the tube to plate surface area should be identical to the thermal energy recycle ratio, since the nature of the heat transfer process to the tube and the plate is essentially the same. Nevertheless, if it is assumed that the average temperature gradient between the central metal plate and tube is about 2 K, and considering that the overall heat transfer coefficient is in the range between 200–300 $\text{W m}^{-2} \text{ K}^{-1}$, *i.e.*, the still operates under nearly optimum condition, it is possible to reduce the tube to plate surface area ratio to about 0.2, in order to achieve cost savings. This would be more than efficient if the entering feedstock is preheated close to $T_{l,out}$ by utilizing the enthalpy present in the air stream exiting the solar still.

(vii) Pressure drop in the system. – A drawback in increasing the air stream velocity in the lower

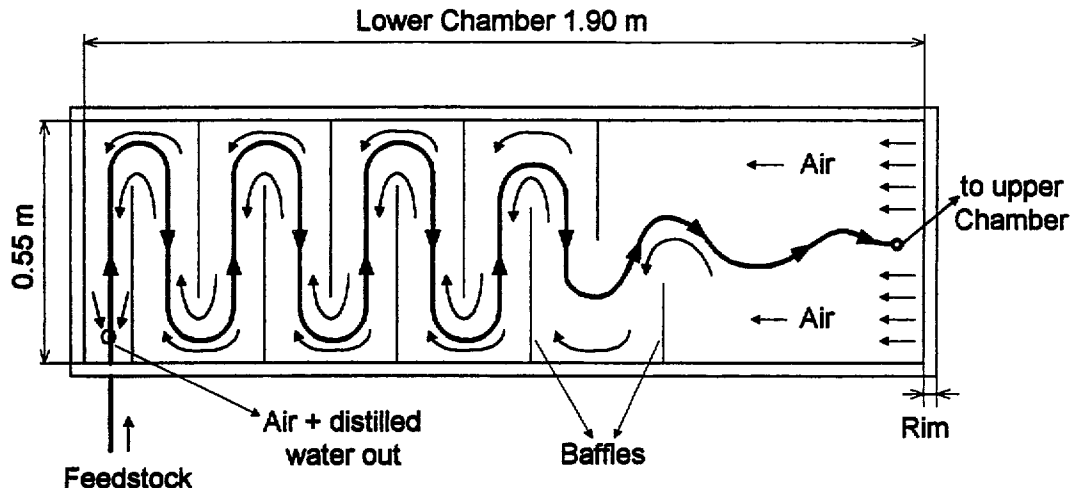


Fig. 2. A schematic diagram of the lower condenser chamber, top view, showing the serpentine tube through which the feedstock flows and the baffles.

chamber is that parasitic electric energy required to drive the air pump also increases. This may be a major problem in rural application where the electric energy may be supplied by PV panels. In addition, a system operating under high pressure drops requires sturdier and more expensive construction than that operating at nearly atmospheric pressure. The present solar still system was designed for very low (<100 Pa) pressure drops and may be considered to operate under atmospheric conditions. This low pressure drop was confirmed by measurements on the still during performance testing.

4. EXPERIMENTAL SET-UP AND PROCEDURE

4.1. Experimental set-up

The experimental set-up (cf. Fig. 1) consists of the following: solar still module, solar simulator, two vapour/liquid separators for collecting the product, heat exchanger, peristaltic pump to transport the feedstock, low pressure adjustable flow-rate air pump, gas flow meter; magnetic valves (Mv) to drain the separators periodically, electric balance to measure the amount of the drained distillate and temperature sensors. The effect of wind on still performance was simulated by a fan, not shown in Fig. 1, with an average wind velocity over the solar still surface of approximately 1 m s^{-1} . The system is connected on-line to a personal computer for data collection and analysis. The position of the air pump ensures that the system operates at a pressure somewhat below ambient. The pressure drop through the still was monitored by a U-tube attached to the outlet from the lower chamber, not shown in Fig. 1, and was found to be exceedingly small (<10 Pa).

4.2. Solar still module

The still consists of two shallow trays, supplied with perimeter rims, of slightly different dimen-

sion such that the upper tray can be inserted into the lower tray. Air tightness was ensured by inserting a rubber gasket tape between the rims and between the upper rim and glazing. The two trays and glazing were clamped together by screws. The upper and lower trays were constructed from a 1-mm thick copper sheet and the lower tray was insulated externally (i.e., its bottom and perimeter) with 50-mm thick polyurethane foam (not shown in Fig. 1). The two-tray design separates the solar still into two chambers connected by the slot in the upper chamber. The brine drain-off tube is soldered to the bottom of the upper tray (viz., in tilted position) and passes through the lower tray (via a stuffing box). The evaporation plate, i.e., the upper tray, is covered by a thin black porous fabric (wick). The serpentine tube carrying the feedstock in the lower chamber is attached to the bottom of the lower tray and the feedstock exits the serpentine tube onto the upper tray via its slot (cf. Figs. 1 and 2) and is evenly distributed over the width of the wick by means of an overflow weir near the top of the upper tray. The solar still module dimensions are listed in Table 2.

4.3. Solar simulator

The solar simulator consists of 16 halogen lamps (12×500 W and 4×300 W lamps), each fitted with a radiating screen of the same geometry which direct the radiation downward to the still. The simulator is positioned parallel to the solar still and the lamp arrangement was verified experimentally to provide an essentially homogeneous radiation intensity on the still outer glazing surface. A 10-mm thick double-walled polycarbonate sheet is positioned parallel between the simulator and still with a continuous stream of water flowing through it, in order to filter any radiation above $2.6 \mu\text{m}$ emitted by the solar simulator. The water absorbs the radiation in the 2.6- to $3\text{-}\mu\text{m}$ range; whereas the polycarbonate

Table 2. Dimension of solar still module

Double-glazing:	10-mm Thick double-walled polycarbonate sheet; $L=1.95$ m; $W=0.6$ m.
Upper chamber:	1-mm Thick copper; $L=1.87$ m; $W=0.545$ m; $H=12$ mm; rim width=30 mm Spacing between the two chambers=12 mm.
Wick:	0.3-mm Thick black porous fabric; $L=1.85$ m, $W=0.545$ m, $A=1 \text{ m}^2$; weir height=6 mm Spacing between textile and inner glazing=12 mm. It is assumed that the wick thickness is independent of water load.
Lower chamber:	1-mm Thick copper; $L=1.9$ m; $W=0.55$ m; $H=25$ mm; rim width=30 mm.
Serpentine tube:	Copper; $L=6$ m; $D_{\text{inner}}=10$ mm; $D_{\text{outer}}=12$ mm; $A=0.20 \text{ m}^2$.
Baffles:	Nine baffles soldered to the bottom of lower chamber; $H=12$ mm for all baffles; $L=0.44$ m for seven baffles; $L=0.36$ m and 0.28 m for each of the remaining two baffles.
Still casing:	Wood; $L=2.06$ m; $W=0.7$ m; $H=90$ mm; bottom thickness=10 mm; side thickness=15 mm.
Bottom and edge insulation:	50-mm Thick polyurethane foam; conductivity= $0.04 \text{ W m}^{-1} \text{ K}^{-1}$.

absorbs the radiation above 3 μm . The temperature of the filter, viz., the polycarbonate sheet, is 18°C at the lower end, water entrance, and 30°C at the upper end, water exit. Thus, its average temperature is below the average room temperature, 25 to 29°C. This set-up insures that the radiation incident on the solar still is in the range between 0.4 to 2.6 μm (the UV component of the lamp radiation is negligible, since the lamp filament temperature is approximately 2500 K).

4.4. External heat exchanger

The external heat exchanger was a standard laboratory glass condenser having a heat exchanger surface area of about 0.07 m^2 . The heat exchange medium was mains water, entering with a temperature in the range of 15–18°C and flowing counter-current to the air stream exiting from the solar still's lower chamber. It was sized for the estimated optimum operating conditions and therefore it was unable to cool the air stream to room temperature, about 26°C, for air mass flow-rates in excess of $2.78 \times 10^{-4} \text{ kg m}^{-2} \text{ s}^{-1}$.

4.5. Experimental conditions and procedure

The tilt angle of the solar still module and solar simulator was set at 20° throughout this study. The solar radiation intensity, provided by the solar simulator, incident on the outer glazing surface was $630 \pm 39 \text{ W m}^{-2}$. The differential and cumulative yields from separator 1 and 2 were measured automatically by a type PT 6 Satorius electric balance with an accuracy of $\pm 1 \text{ g}$. The temperatures were measured with an accuracy of $\pm 1^\circ\text{C}$ using calibrated temperature sensors of the silicon base type KTY 11-2A. The absolute humidity of air in the vicinity of the slot was calculated from the mass and energy balances on the still. A data acquisition system served to monitor and store the temperature data from the sixteen thermistors and to calculate differential and cumulative yields at variable time intervals. It

consisted of a PC with an A/D to D/A converter card, electronic measuring and magnetic valve control unit, temperature sensors and a digital balance with a RS232C serial interface. The data acquisition, control and analysis software were developed for the study.

The experimental procedure for the performance testing was as follows:

1. The air and feedstock flow-rates are defined and held constant;
2. The temperatures at the following locations are monitored:

Air stream – upper chamber: inlet, equally spaced probes in the direction of flow and above the slot;

lower chamber: below the slot, equally spaced probes in the direction of flow and at the outlet;

saturated air stream exiting the still to the external condenser;

Feedstock – lower chamber: inlet;

upper chamber: overflow weir and brine drain-off outlet;

3. The distillation rate is determined by measuring the cumulative distillate during a specified time interval.

5. RESULTS AND DISCUSSION

The solar still performance was tested as a function of the air flow-rate, which was varied in the range between 0.89×10^{-4} and $12.53 \times 10^{-4} \text{ kg m}^{-2} \text{ s}^{-1}$. The feedstock flow-rate was maintained constant at $8.22 \times 10^{-4} \text{ kg m}^{-2} \text{ s}^{-1}$. The solar still achieved steady-state, as evidenced by monitoring both air stream temperatures and the distillation rate, after approximately 1 h of operation. The maximum air stream temperature, in the range between 71.6 to 96.9 °C (inverse function of the air flow-rate), was measured at the upper end of the solar still, in the vicinity of the slot (cf. Table 3). It was determined that thermal energy

Table 3. The temperature profile of the solar still at steady-state as a function of air flow-rate for a constant feedstock flow-rate of $8.22 \times 10^{-4} \text{ kg m}^{-2} \text{ s}^{-1}$, cf. Fig. 1 for location of the 16 thermistors

Air flow-rate $\text{kg m}^{-2} \text{ s}^{-1}$ $\times 10^{-4}$	T_a T_0 °C	Upper chamber					Lower chamber					$T_{\text{L,out}}$ T_{11} °C	$T_{\text{Sep 1}}$ T_{12} °C	$T_{\text{X,in}}$ T_{13} °C	$T_{\text{X,out}}$ T_{14} °C	$T_{\text{Brine,drain}}$ T_{15} °C
		T_1 °C	T_2 °C	T_3 °C	T_4 °C	T_5 °C	T_6 °C	T_7 °C	T_8 °C	T_9 °C	T_{10} °C					
12.53	26.0	51.2	65.6	72.2	71.3	71.6	71.3	70.6	69.9	66.0	56.0	56.0	54.9	54.6	35.4	48.7
9.08	26.4	54.0	71.1	76.4	75.9	76.6	76.7	75.9	75.1	71.1	59.6	59.6	58.1	57.8	36.0	51.5
6.14	26.3	57.5	77.1	81.3	81.2	82.1	82.1	81.6	80.7	77.0	63.1	63.1	60.9	60.4	35.0	54.5
4.89	26.1	59.1	80.1	83.7	83.7	84.7	84.8	84.3	83.5	79.9	64.4	64.4	62.0	61.3	34.1	55.7
3.44	26.6	62.6	84.6	87.4	87.6	88.4	88.5	88.4	87.5	84.4	67.5	67.5	64.1	63.0	32.1	58.4
2.83	26.2	64.9	87.4	89.8	89.8	90.7	90.7	90.7	90.0	87.2	69.9	69.9	65.6	64.1	28.6	60.4
1.61	26.1	67.6	91.9	93.6	93.6	94.4	94.2	94.5	94.0	91.7	68.2	68.2	60.7	57.1	21.9	61.9
0.89	25.8	68.6	95.1	96.3	96.2	97.0	96.9	97.4	96.9	94.9	52.5	48.9	34.0	30.4	24.1	62.4

Table 4. Still productivity as a function of air flow-rate for a constant feedstock flow-rate of $8.22 \times 10^{-4} \text{ kg m}^{-2} \text{ s}^{-1}$

Air flow-rate $\text{kg m}^{-2} \text{ s}^{-1} \times 10^{-4}$	Primary distillate $\text{kg m}^{-2} \text{ s}^{-1} \times 10^{-4}$	Secondary distillate $\text{kg m}^{-2} \text{ s}^{-1} \times 10^{-4}$	Total distillate $\text{kg m}^{-2} \text{ s}^{-1} \times 10^{-4}$
12.53	1.81	0.89	2.69
9.08	2.08	0.81	2.86
6.14	2.33	0.75	3.08
4.89	2.42	0.56	2.97
3.44	2.67	0.42	3.08
2.83	2.69	0.36	3.06
1.61	2.58	0.11	2.69
0.89	1.89	0.03	1.92

recycle begins to take effect after about 30 min by comparing the continuously monitored air stream temperatures at the inlet to the upper chamber to that at the outlet from the lower chamber, viz., after about 30 min the latter exceeded the former. The steady-state distillation rate was found to be of the order of $2.78 \times 10^{-4} \text{ kg m}^{-2} \text{ s}^{-1}$, except for relatively low air flow-rate. It is of interest to note, that if the system was at steady-state and the air pump remained in operation after the solar simulator was shut-off, the still continued to produce distillate, albeit at a decreasing rate, for about another hour. In other words, in spite of the relatively low thermal mass of the solar still module, thermal energy recycling is still capable of enhancing the yield after 'sunset', i.e., after the solar simulator is shut-off.

The steady-state temperatures, as measured by the 16 thermistors (cf. Fig. 1 for thermistor locations) are reported in Table 3 as a function of air flow-rate. As expected, temperature measured at a specific location varies inversely with the air

flow-rate, viz., it increases with decreasing air flow-rate.

5.1. Productivity as a function of air flow-rate

The productivity is reported in Table 4 in terms of primary, secondary, and total distillation rate per hour. The primary distillation rate refers to that condensed within the lower chamber during the thermal energy recycle process, but in fact contains a marginal amount of secondary distillate $m'_{\text{SDR,T}}$ (which is non-negligible when performing precise mass and energy balance calculations) condensed within the tubing connecting the lower chamber outlet to the heat exchanger. The main secondary distillation rate $m'_{\text{SDR,X}}$ refers to that distillate condensed in the external heat exchanger and collected in separator 2. It is apparent from Table 4 that with regard to still productivity there exists an optimum range of air flow-rates for the system under consideration, approximately between 2.78×10^{-4} and $8.33 \times 10^{-4} \text{ kg m}^{-2} \text{ s}^{-1}$. It is also observed that the primary product decreases and the secondary increases with increasing air flow-rate (cf. Fig. 3). The reason for the optimum air flow-rate will be discussed in the following paragraphs.

Thermal energy analysis, utilizing mass and energy balances, of the solar still at steady-state as a function of air flow-rate, for a constant feedstock flow-rate, were performed in order to determine the sensitivity of a number of still parameters to changes in the rate of air flow. The results of these analyses, reported as hourly mass flow-rates, are reported in Table 5 and include the following: (a) the mass flow-rate of vapour

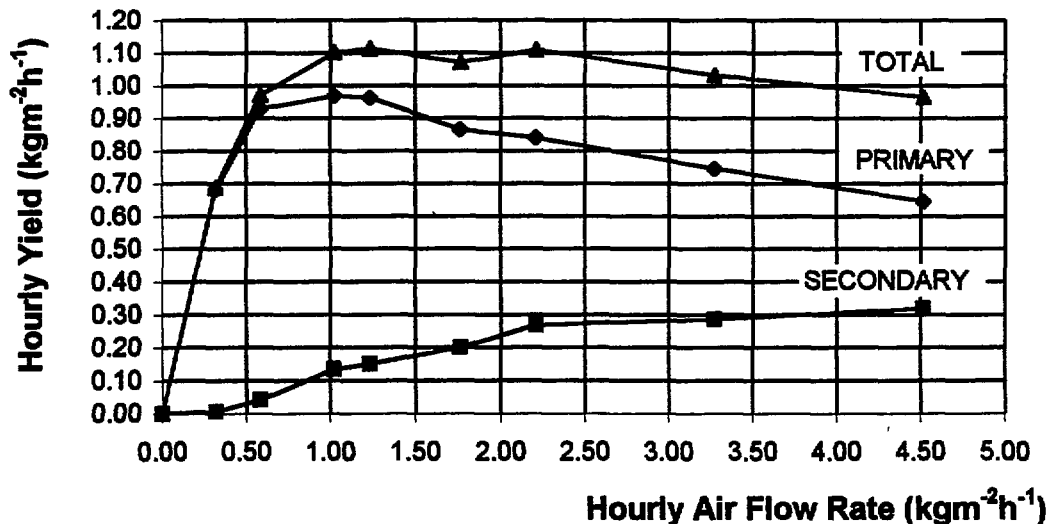


Fig. 3. Hourly still productivity as a function of air flow-rate for a feedstock flow-rate of $2.96 \text{ kg m}^{-2} \text{ h}^{-1}$.

50

Table 5. Mass and energy analysis of solar still at steady-state as a function of air flow-rate for a constant feedstock flow-rate of $8.22 \times 10^{-4} \text{ kg m}^{-2} \text{ s}^{-1}$

(a) Mass flow-rates of the water vapour through the solar still									
m_a $\text{kg m}^{-2} \text{ s}^{-1}$ $\times 10^{-4}$	Upper chamber			Lower chamber		Tubing		Heat exchanger	
	$m_{v,u,in}$ $\text{kg m}^{-2} \text{ s}^{-1}$ $\times 10^{-4}$	m_{evap} $\text{kg m}^{-2} \text{ s}^{-1}$ $\times 10^{-4}$	$m_{v,max}$ $\text{kg m}^{-2} \text{ s}^{-1}$ $\times 10^{-4}$	m_{PDR} $\text{kg m}^{-2} \text{ s}^{-1}$ $\times 10^{-4}$	$m_{v,l,out}$ $\text{kg m}^{-2} \text{ s}^{-1}$ $\times 10^{-4}$	$m'_{SDR,T}$ $\text{kg m}^{-2} \text{ s}^{-1}$ $\times 10^{-4}$	$m_{v,x,in}$ $\text{kg m}^{-2} \text{ s}^{-1}$ $\times 10^{-4}$	$m_{v,x,out}$ $\text{kg m}^{-2} \text{ s}^{-1}$ $\times 10^{-4}$	$m_{SDR,x}$ $\text{kg m}^{-2} \text{ s}^{-1}$ $\times 10^{-4}$
12.53	0.217	3.01	3.22	1.71	1.52	0.10	1.42	0.53	0.89
9.08	0.156	3.16	3.31	1.95	1.36	0.13	1.23	0.42	0.81
6.14	0.106	3.19	3.29	2.17	1.13	0.16	0.96	0.21	0.75
4.89	0.083	3.14	3.23	2.26	0.97	0.16	0.81	0.25	0.56
3.44	0.058	3.23	3.30	2.48	0.82	0.19	0.63	0.21	0.42
2.83	0.050	3.20	3.25	2.46	0.78	0.20	0.58	0.21	0.36
1.61	0.028	2.77	2.79	2.39	0.40	0.19	0.21	0.10	0.11
0.89	0.017	1.89	1.91	1.83	0.09	0.06	0.03	0.00	0.03

(b) Mass and heat flow-rates of feedstock/brine through the solar still									
m_a $\text{kg m}^{-2} \text{ s}^{-1}$ $\times 10^{-4}$	T_{max} $^{\circ}\text{C}$	Lower chamber				Upper chamber			
		$m_{f,in}$ $\text{kg m}^{-2} \text{ s}^{-1}$ $\times 10^{-4}$	$q_{f,l,in}$ at T_a	q_{PR} W m^{-2}	$q_{f,l,out}$ $^{\circ}\text{C}$	$T_{Brine,drain}$ $\text{kg m}^{-2} \text{ s}^{-1}$	$m_{Brine,drain}$ W m^{-2} $\times 10^{-4}$	$q_{Brine,drain}$ W m^{-2}	$q_{released}$
12.53	71.6	8.22	90	156	246	48.7	5.22	106	139
9.08	76.7	8.22	90	174	264	51.5	5.07	109	155
6.14	8.21	8.22	90	193	283	54.5	5.03	115	168
4.89	84.8	8.22	90	202	292	55.7	5.08	118	174
3.44	88.5	8.22	90	215	305	58.4	4.98	122	183
2.83	90.7	8.22	90	222	312	60.4	5.03	127	185
1.61	94.2	8.22	90	234	324	61.9	5.46	141	183
0.89	96.9	8.22	90	245	334	62.4	6.33	164	170

(c) Heat flows in upper evaporation chamber							
m_a $\text{kg m}^{-2} \text{ s}^{-1}$ $\times 10^{-4}$	$q_{a,u,in}$ W m^{-2}	q_R W m^{-2}	$q_{released}$ W m^{-2}	Q_U W m^{-2}	q_{max} $^{\circ}\text{C}$	T_{max} $^{\circ}\text{C}$	T_{dew}
12.53	110	215	139	471	935	71.6	68.7
9.08	80	256	155	451	942	76.7	74.2
6.14	54	285	168	415	922	82.1	79.8
4.89	43	296	174	383	896	84.8	82.3
3.44	30	330	183	363	906	88.5	86.4
2.83	25	316	185	363	889	90.7	88.5
1.61	14	283	183	294	760	94.2	91.7
0.89	9	123	170	227	520	96.9	93.0

(d) Heat flows in lower condenser chamber									
m_a $\text{kg m}^{-2} \text{ s}^{-1}$ $\times 10^{-4}$	T_{max} $^{\circ}\text{C}$	T_{dew} $^{\circ}\text{C}$	q_{max} W m^{-2}	$q_{l,out}$ W m^{-2}	$q_{Dist,out}$ W m^{-2}	$q_{B,loss}$ W m^{-2}	q_{RT} W m^{-2}	q_{PR} W m^{-2}	q_R W m^{-2}
12.53	71.6	68.7	935	491	40	33	371	156	215
9.08	76.7	74.2	942	426	50	36	430	174	256
6.14	82.1	79.8	922	345	58	41	478	193	285
4.89	84.8	82.3	896	294	61	43	498	202	296
3.44	88.5	86.4	906	245	70	46	545	215	330
2.83	90.7	88.5	889	231	72	48	538	222	316
1.61	94.2	91.7	760	119	74	50	517	234	283
0.89	96.9	93.0	520	60	42	50	368	245	123

through the system, (b) the mass and heat flow of both feedstock and brine drain-off, (c) heat flow in upper chamber and (d) heat flow in lower chamber. In this analysis the temperature of the entering air stream and feedstock were assumed to be $\approx 26^{\circ}\text{C}$, viz., room temperature, and an average value of 80% was assumed for the relative humidity of the entering air stream.

The measured primary distillation rate is a good

approximation of the rate of condensation in the lower chamber but as mentioned previously it also contains that quantity of distillate condensed in the tubing connecting the outlet from the lower chamber to the heat exchanger. To enhance the precision of the mass and energy balances the flow-rate of primary distillate exiting the lower chamber was determined as the difference between the measured primary distillation rate and

condensation rate of saturated air stream in the tubing between the lower chamber outlet and the heat exchanger. The latter is determined from the flow-rate of bone dry air in the following manner:

$$m'_{\text{PDR}} = m_{\text{PDR}} - m_{\text{BDA}}[M_v(\text{at } T_{1,\text{out}}) - M_v(\text{at } T_{x,\text{in}})], \quad (6)$$

where M_v is in units of (kg vapour/kg BDA). The maximum mass flow-rate of vapour carried by the air stream corresponds to that at maximum temperature and is given as:

$$m_{v,\text{max}} = m'_{\text{PDR}} + m_{\text{BDA}}[M_v(\text{at } T_{1,\text{out}})]. \quad (7)$$

The maximum rate of heat flow is also achieved at the maximum temperature and is given by:

$$q_{\text{max}} = c_a m_a T_{\text{max}} + m_{v,\text{max}} H_{v,\text{max}}, \quad (8)$$

where $H_{v,\text{max}}$ is the enthalpy of the vapour at T_{max} .

It is apparent from Table 4 that the optimum performance of the solar still module is obtained for air flow-rates in the range of 2.78×10^{-4} to $6.11 \times 10^{-4} \text{ kg m}^{-2} \text{ s}^{-1}$, which correspond to a total productivity rate of about $3.06 \times 10^{-4} \text{ kg m}^{-2} \text{ s}^{-1}$. In addition, it is observed from Table 5 (c) that the amount of solar energy utilized decreases with decreasing air flow-rate, in agreement with the increasing trend observed for the average temperatures within the upper chamber, cf. Table 3. It is also observed from Table 5 that despite the decrease in the amount of solar energy utilized with decreasing air flow-rate, maximum values for primary distillation rate, total thermal energy recycle, sum of thermal energy recycled directly to the upper chamber and thermal energy released from the feedstock to the air stream in the upper chamber are observed to occur for air flow-rates of 2.83×10^{-4} and $3.44 \times 10^{-4} \text{ kg m}^{-2} \text{ s}^{-1}$. At these air flow-rates the thermal energy recycle more than compensates for the decrease in solar energy efficiency, i.e., the first effect or direct solar to thermal energy conversion.

As a consequence of the above, it follows that in the range of 2.78×10^{-4} to $6.11 \times 10^{-4} \text{ kg m}^{-2} \text{ s}^{-1}$ air flow-rates, the mass flow-rate of water vapour exiting the lower chamber will be a minimum for air flow-rates between 2.83×10^{-4} and $3.44 \times 10^{-4} \text{ kg m}^{-2} \text{ s}^{-1}$ and the air stream temperature, $T_{1,\text{out}}$, will be a maximum. As a result, the cooling load for the external heat exchanger will be a minimum in this range of air flow-rates.

To demonstrate the heat flow processes occurring in the solar still module in this range of optimum performance, a thermal energy flow diagram is presented in Fig. 4 for an air flow-rate of $3.44 \times 10^{-4} \text{ kg m}^{-2} \text{ s}^{-1}$. It is seen from this diagram that the main heat transfer processes determining the solar still performance are Q_u , q_R and q_{PR} .

The decrease in the solar still performance for air flow-rates below $2.78 \times 10^{-4} \text{ kg m}^{-2} \text{ s}^{-1}$ is the result of two factors: (1) the increase in thermal energy losses from the upper chamber to the ambient and (2) the overall heat transfer coefficient for thermal energy recycle decreases rapidly with decreasing heat transfer coefficient for the gas film. The latter is approximately proportional to the linear velocity of air stream (i.e., the air and non-condensing water vapour) in the lower chamber. Consequently, a possible design change to enhance the solar still performance would be to attain higher linear air velocities in the lower chamber by decreasing its cross-sectional area. The down-side of such a design change would be an increase in the pressure drop of the still system and a subsequent increase in parasitic energy consumption. Since the present solar still design has a very low pressure drop there appears to be sufficient leeway for further reduction in the lower chamber cross-sectional area and we plan to study this effect in the future.

It should be noted that the condensation process in the lower chamber, upon the backside of the central metal plate and on the serpentine tube, occurs mainly on the lower portion of the chamber, mostly within a distance of 0.50 m from the bottom edge of the solar still.

Consequently, the condensation area is much smaller than that for evaporation and is a limiting factor in achieving higher thermal energy recycle efficiencies. We plan to investigate solutions for overcoming this limitation.

Further development in the solar still design will be related to problems of scale-up, with the goal of arriving at a still design which is economically viable with regard to construction, operation and maintenance.

6. CONCLUSIONS

The design and performance testing of a double glazed, air-blown, multiple-effect solar still with thermal energy recycle consisting of two chambers, upper evaporator and lower condenser, operating under steady-state conditions has been presented. A considerable fraction of the latent

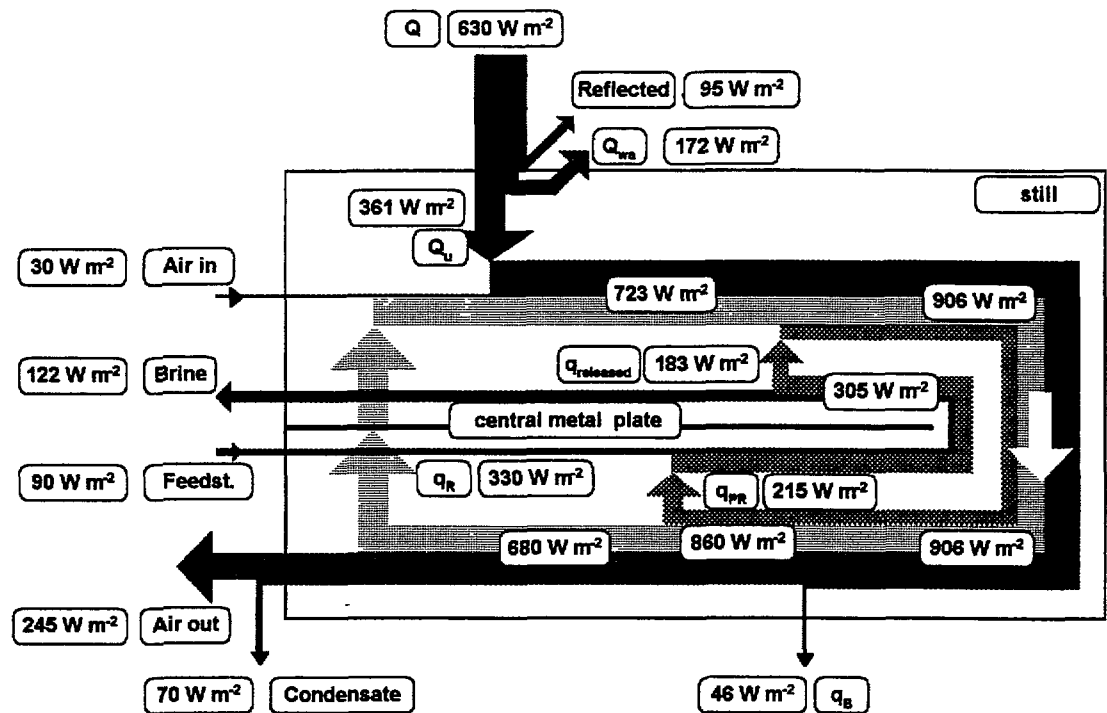


Fig. 4. Thermal energy flow diagram calculated by means of the mass and energy balances on the solar still for air and feedstock flow-rates of $1.24 \text{ kg m}^{-2} \text{ h}^{-1}$ and $2.96 \text{ kg m}^{-2} \text{ h}^{-1}$, respectively.

heat of condensation is recycled for preheating the feedstock and directly heating the evaporation plate, thereby enhancing the rate of the evaporation process.

The heat transfer processes are based upon film condensation from a saturated air stream, which is characterized by a relatively high heat transfer coefficient, especially when operating at relatively high temperatures. These high temperatures are achieved by operating the solar still system at low air mass flow-rates. In addition, the heat transfer process is further enhanced by increasing the air stream velocities in the lower (condensation) chamber.

The optimum feedstock flow-rate was found, based upon experimental results obtained utilizing a solar simulator with a constant radiation intensity of $630 \pm 39 \text{ W m}^{-2}$, to be in the range of $8.33 \times 10^{-4} \text{ kg m}^{-2} \text{ s}^{-1}$. This feedstock flow-rate is sufficient to maintain the wick in the upper evaporation chamber completely wetted at even higher incident radiation intensities and thereby, higher evaporation rates.

It was observed that the solar still performance was mainly a function of the flow-rate of the entering air stream. In this study, solar still

operating under a constant feedstock flow-rate and radiation intensity, the optimum air flow-rate was found to be in the range of $2.83 \times 10^{-4} - 3.44 \times 10^{-4} \text{ kg m}^{-2} \text{ s}^{-1}$, which corresponds to a maximum total productivity of $3.05 \times 10^{-4} \text{ kg m}^{-2} \text{ s}^{-1}$. The total productivity consists of about $2.50 \times 10^{-4} \text{ kg m}^{-2} \text{ s}^{-1}$ primary distillate (condensed within the lower chamber) and the remainder secondary distillate produced within the external condenser.

The solar still system operates under a very low pressure drop, of the order of several Pa per m^2 of still area, for low (viz., optimum range) air flow-rates. This is a distinct advantage with regard to both still construction and parasitic energy requirements for air blowers, especially for large scale systems.

The experimental results suggest that the solar still performance can be further enhanced by either decreasing the cross sectional flow area in the lower chamber and/or increasing the path length within the lower chamber of the still by the addition of baffles in order to achieve higher linear air velocities.

In the next generation of this solar still design, we will consider a number of modifications to simplify the still construction. In addition, we

plan to utilize the feedstock as the heat exchange medium (cooling stream) for the external condenser.

NOMENCLATURE

A	Still area (m^2)
c	Heat capacity ($\text{J kg}^{-1} \text{K}^{-1}$)
G	Solar radiation (W m^{-2})
H	Enthalpy (J kg^{-1})
h	Heat transfer coefficient ($\text{W m}^{-2} \text{K}^{-1}$)
M_v	Vapour content of air stream (kg vapour/kg BDA)
m	Mass flow-rate ($\text{kg m}^{-2} \text{s}^{-1}$)
$m_{\text{brine, drain}}$	Mass flow-rate of brine drain-off ($\text{kg m}^{-2} \text{s}^{-1}$)
m_{PDR}^r	Calculated primary distillation rate ($\text{kg m}^{-2} \text{s}^{-1}$)
$m_{\text{SDR, T}}^r$	Calculated secondary distillation rate in the tubing ($\text{kg m}^{-2} \text{s}^{-1}$)
$m_{\text{SDR, X}}^r$	Secondary distillation rate in the heat exchanger ($\text{kg m}^{-2} \text{s}^{-1}$)
Q_u	Solar energy utilized (W m^{-2})
q	Thermal energy (W m^{-2})
$q_{\text{B, loss}}$	Backside thermal energy losses (W m^{-2})
$q_{\text{brine, drain}}$	Thermal energy in brine drain-off (W m^{-2})
$q_{\text{loss, amb}}$	Thermal energy loss from upper chamber to ambient (W m^{-2})
q_{PR}	Thermal energy utilized to preheat the feedstock (W m^{-2})
q_{R}	Thermal energy recycled directly to upper chamber (W m^{-2})
q_{released}	Thermal energy released by the preheated feedstock to the air stream (W m^{-2})
q_{RT}	Total thermal energy recycled (W m^{-2})
T	temperature ($^{\circ}\text{C}$)
T_{dew}	Dew point temperature of air stream exiting upper chamber and entering lower chamber ($^{\circ}\text{C}$)
U_{lw}	Overall heat transfer coefficient from lower chamber to wick ($\text{W m}^{-2} \text{K}^{-1}$)

Greek letters

δ	Thickness (m)
κ	Thermal conductivity ($\text{W m}^{-1} \text{K}^{-1}$)

Subscripts

a	Air stream
abs	Absorbed
amb	Ambient
avg	Average value
BDA	Bone dry air
c	Condensed water film
c.g	Combined heat transfer coefficient
Dist, out	Distillate exiting lower chamber
evap	Evaporated
f	Feedstock
g	Gas film
i	Incident
in	Stream entering chamber
l	Lower chamber
m	Central metal plate
max	Maximum value
out	Stream exiting chamber

PDR	Primary distillation rate
r	Reflected
sd	Scale deposit
SDR	Secondary distillation rate
sep	Vapour/liquid separator
t	Serpentine tube
u	Upper chamber
v	Water vapour
w	Wick
X	External heat exchanger/condenser

Acknowledgements—This research was supported under Grant No. TA-MOU-95-C15-050, US-Israel Cooperative Development Research Program, Office of Agriculture and Food Security, Center for Economic Growth, Bureau for Global Programs, Field Support and Research, USAID.

REFERENCES

- Aboabboud M. M., Horvath L., Szepevolgyi J., Mink G., Radhica E. and Kudish A. I. (1996) The use of a thermal energy recycle unit in conjunction with a basin-type solar still for enhanced productivity. *Energy* **23**, 83–91.
- Delyannis A. and Delyannis E. E. (1980) *Seawater and Desalting*, Vol. 1., pp. 67–70, Springer-Verlag, Berlin.
- Dunkle R. V. (1961) Solar water distillation: The roof-type still and a multiple-effect diffusion still. In *International Developments in Heat Transfer, ASME, Proceedings International Heat Transfer*, Part 5, pp. 895–902, University of Colorado, USA.
- Kossinger F., Jung D. and Sizeman R. (1993) *Autonomous Solar Desalination Plants with Internal Free Convection*, Zold A. (Ed.), Vol. 4, pp. 331–336, Budapest, Hungary.
- Kudish A. I. (1991) Water desalination. In *Solar Energy in Agriculture – Energy in World Agriculture*, Parker B.F. (Ed), Vol. 4, pp. 255–294, Elsevier Science Publishers B.V., Amsterdam.
- Lobo P. C. and Araujo S. R. D. (1977) Design of a simple multi-effect basin-type solar still. In *Proceedings of ISES Solar World Congress*, p. 2026, New Delhi, India.
- Malik M. A. S., Tiwari G. N., Kumar A. and Sodha M. S. (1982) *Solar Distillation*, Pergamon Press, Oxford, 175 pp.
- Mink G., Aboabboud M. M., Horvath L., Evseev E. and Kudish A. I. (1997) Design and performance of an air-blown, multiple-effect solar still with thermal energy recycle. In *Proceedings of ISES Solar World Congress*, Vol. 6, pp. 135–144, Taejon, Korea.
- Mink G., Aboabboud M. M. and Karmazsin E. (1998) Air-blown solar still with heat recycling. *Solar Energy* **62**, 309–317.
- Müller-Holst H., Kessling W., Engelhardt M., Herve M. and Schölkopf W. (1997) Solar thermal sea-water desalination with 24-hour thermal storage. In *Proceedings of ISES Solar World Congress*, Vol. 6, pp. 168–176, Taejon, Korea.
- Sodha M. S., Nayak J. K., Tiwari G. N. and Kumar A. (1980) Double-basin solar still. *Energy Conversion and Management* **20**, 23–31.
- Talbert S. G., Eibling J. A. and Lof G. O. G. (1970) *Manual on Solar Distillation of Saline Water*, R&D Progress Report No. 546, US Department of Interior, 263 pp.

PERFORMANCE STUDIES ON AN AIR-BLOWN, MULTIPLE-EFFECT SOLAR STILL OPERATING ON SOLAR AND/OR WASTE ENERGY

A.I. KUDISH^{*}, E.G. EVSEEV^{*}, L. HORVÁTH^{**} and G. MINK^{**}

^{*}Solar Energy Laboratory, Department of Chemical Engineering, Ben-Gurion University of the Negev, Beer Sheva 84105, ISRAEL;

Tel: +972 7 6461488, Fax: +972 7 6472916, E-mail: akudish@bgumail.bgu.ac.il

^{**}Research Laboratory of Materials and Environmental Chemistry, Chemical Research Center, Hungarian Academy of Sciences, 1525 Budapest Pf 17, HUNGARY;

Tel: +36 1 325 5992, Fax: +36 1 335 7892, E-mail: mink@chemres.hu

Abstract: The performance of an air-blown, multiple-effect solar still designed to recycle the thermal energy of condensation heat recycle has been studied while operating in three different modes, i.e., driving forces: (i) solar energy; (ii) both solar and waste thermal energy; and (iii) waste thermal energy, both with and without insulating the still glazing. The still had a double-walled, structured polycarbonate glazing, a transparent insulation material (TIM), and the still area was 1 m². The solar energy was provided by a solar simulator, at a constant intensity of 650 W m⁻², this facilitated the inter-comparison of the system performance when operating in the three different modes. The waste thermal energy was simulated by a feedstock (water) reservoir maintained between 86 and 90 °C. The steady-state yields and temperatures were achieved within one hour, as a result of the low thermal mass of the still. Operating under constant energy input, the performance of the still was determined mainly by the flow rate of air, which functions both as a mass and energy carrier. The optimum range of the air flow rates, under all modes of operation, has been determined experimentally. In addition, mass and heat balances utilizing experimental results and referring to optimum operating conditions have been performed.

Key words: Solar energy, Waste energy, Distillation, Energy recycle.

1. INTRODUCTION

The utilization of solar energy for the distillation of brackish or saline water has been practiced for a very long time. Various types of solar stills and solar-assisted desalination units have been designed and investigated. A number of manuscripts have been published on this subject: a classic one by Talbert et al.¹, Malik et al.² and Kudish³

In arid zones, solar distillation can be an ideal source to produce fresh water from saline water, both for drinking and agriculture. The main disadvantage of the present day solar stills is that their productivity per unit area is low. Since the fixed capital investment cost of a solar desalination plant is roughly proportional to the still area, increasing the productivity by recycling the heat of condensation of the distillate is of paramount importance.

SS

The performance of an air-blown, multiple-effect solar still consisting of an upper evaporation chamber and a lower condensation chamber has been analyzed in detail^{4,6}. The analysis of the above system suggested that it is possible to utilize low grade waste energy, when available at the site, as the driving force in the distillation process. Thus, the still can operate 24 hours a day by utilizing solar energy, when available, and/or waste thermal energy in the daytime and waste thermal energy during the night, i.e., nocturnal distillation.

In the present paper we shall report on the experimental results obtained when operating the still under three different modes, i.e., driving forces: (i.) only solar energy; (ii.) both solar and waste thermal energy; and (iii.) only waste thermal energy.

2. EXPERIMENTAL

Experimental setup

The solar still under investigation is shown schematically in Fig. 1. It is essentially of the tilted-wick genre in the form of a thin rectangular box divided into two chambers (upper evaporator and lower condenser) by a central metal sheet. The central metal sheet does not extend across the full length of the still but leaves a slot of 10 mm between its top end and the still's upper extremity. The metal sheet also functions as (i) a support for the wick (a black porous material) which covers it on the upper chamber side; (ii) a surface to which a serpentine tube, in the lower chamber side, for transporting the feedstock to the upper chamber, is in contact. This serpentine tube also functions as a heat exchanger for preheating the feedstock prior to entering the upper chamber. The spacing between the central metal plate and the upper chamber still glazing and the lower chamber backside are both 12 mm

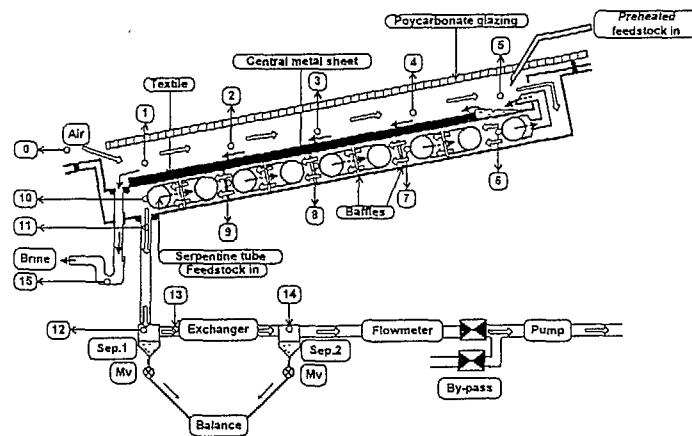


Fig. 1. Schematic diagram of the experimental unit. The location of the temperature probes are indicated by numbers 0 to 15

The mode of operation of the solar still is as follows: (1) ambient air is pumped into the upper chamber from the bottom of the tilted still and sweeps the water vapour evaporated from the tilted wick into the lower chamber via the slot at the top of the tilted still (maximum temperature of the air stream is measured at this point, above the slot, prior to entering the lower chamber and serving as the hot fluid in what is essentially an air-liquid heat exchanger); (2) the major portion of the water vapour then condenses on the serpentine tube, which enters at the bottom of the lower chamber, transporting the feedstock to the upper chamber; or on the lower portion of the reverse side of the metal sheet supporting the wick; (3) the feedstock, which enters the serpentine tube at a flow rate in excess of the rate of evaporation from the wick, is preheated during its passage through the serpentine tube, exits the serpentine tube at the top edge of the central plate and passes over a weir and flows by gravity down the wick; (4) the distillate exits the lower chamber and is collected, whereas the humid air stream, also exiting the lower chamber, enters an external condenser, to further condense the water vapour remaining prior to venting to the ambient.

In the upper chamber, the air stream flows countercurrently to the direction of feedstock flowing down the wick, whereas in the lower chamber the air stream flows both countercurrently and perpendicular to the direction of the feedstock flowing through the serpentine tube. Due to the nature of this solar still, viz., that the upper chamber glazing does not serve as a condensation surface, it is possible and recommended that a double glazing be utilized to reduce thermal energy losses via the glazing to the ambient. In fact, in our case, non-wetting polymeric transparent insulating material (TIM), e.g., a solar grade, double-walled, 10 mm thick polycarbonate sheet was used as solar still glazing. In this still, a large fraction of the heat of condensation of the distillate is successfully recycled to both preheat the feedstock and heat the reverse side of the evaporation plate, which separates the two chambers. Consequently, a two- to three-fold increase in distillate yield was achieved relative to that of conventional type solar stills^{4,6}.

Mode of operation when using solar energy and/or waste thermal energy

Waste thermal energy was simulated by means of a conventional heater that maintained the feedstock (water) reservoir at a temperature between 86 and 90 °C. In this mode of operation, the preheated feedstock entered the still at the upper part of the evaporation chamber (cf., Fig. 1), and consequently, the thermal energy recycle from the lower chamber to the upper chamber proceeded only via condensation on the reverse side of the central metal plate.

Experimental conditions and procedure

The tilt angle of the solar still module was set at 20° throughout this study. Similarly, the solar simulator provided a constant radiation intensity of 650±10 Wm⁻² and its tilt angle was also 20°. The differential and cumulative yields from Separator I and II were measured automatically by a type PT 6 Satorius electric balance with an accuracy of ±1 g. The temperatures were measured at 16 strategically positioned locations, cf., Fig. 1, with an accuracy of ±1 °C using calibrated temperature sensors of the silicon base type KTY 11-2A. The absolute humidity of air in the vicinity of the slot was calculated from the material and energy balances on the still. A data acquisition system served to monitor and store the temperature data from the sixteen thermistors and to calculate differential and cumulative yields at variable time intervals. It consisted of a PC with an A/D-D/A converter card, electronic measuring and magnetic valve control unit, temperature sensors and a digital balance with a RS232C serial interface. The data acquisition, control and analysis software were developed specifically for this study. The operational variables were the feedstock and the air flow rates.

3. RESULTS AND DISCUSSION

The steady-state yields and temperatures were achieved within one hour, in all experimental runs, as a result of the low thermal mass of the solar still. All the results reported in this study refer to steady-state conditions and the mass and energy flows are normalized to a 1 m² still area

Solar energy operation mode; 650 010 Wm⁻² radiation intensity

The temperature profile for the still at different air flow rates expressed in kg bone dry air per m² still area per hour is given in Table 1

Table 1 The temperature profile of the solar still at steady-state as a function of air flow rate for a constant feedstock flow rate of 2.96 kgm⁻²h⁻¹. The position of the 16 thermistors are shown in Fig. 1 (numbered 0 to 16) Irradiation = 650010 Wm⁻²

Air kgm ⁻² h ⁻¹	T _a °C	UPPER CHAMBER					LOWER CHAMBER					T _{Loat} °C	T _{Sep} °C	T _{X,in} °C	T _{X,out} °C	T _{brine} °C
		T0 °C	T1 °C	T2 °C	T3 °C	T4 °C	T5 °C	T6 °C	T7 °C	T8 °C	T9 °C					
4.51	26.0	51.2	65.6	72.2	71.3	71.6	71.3	70.6	69.9	66.0	56.0	56.0	54.9	54.6	35.4	48.7
3.27	26.4	54.0	71.1	76.4	75.9	76.6	76.7	75.9	75.1	71.1	59.6	59.6	58.1	57.8	36.0	51.5
2.21	26.3	57.5	77.1	81.3	81.2	82.1	82.1	81.6	80.7	77.0	63.1	63.1	60.9	60.4	35.0	54.5
1.76	26.1	59.1	80.1	83.7	83.7	84.7	84.8	84.3	83.5	79.9	64.4	64.4	62.0	61.3	34.1	55.7
1.24	26.6	62.6	84.6	87.4	87.6	88.4	88.5	88.4	87.5	84.4	67.5	67.5	64.1	63.0	32.1	58.4
1.02	26.2	64.9	87.4	89.8	89.8	90.7	90.7	90.7	90.0	87.2	69.9	69.9	65.6	64.1	28.6	60.4
0.58	26.1	67.6	91.9	93.6	93.6	94.4	94.2	94.5	94.0	91.7	68.2	68.2	60.7	57.1	21.9	61.9
0.32	25.8	68.6	95.1	96.3	96.2	97.0	96.9	97.4	96.9	94.9	52.5	48.9	34.0	30.4	24.1	62.4

The still productivity, as a function of air flow rates in the range from 0.32 to 4.51 kgm⁻²h⁻¹ is reported in Table 2 and in Fig. 2 in terms of primary (I), secondary (II), and total (Σ). The primary distillation rate refers to that condensed within the lower chamber during the thermal energy recycle process. The secondary distillation rate is that obtained by passing the saturated air stream exiting the solar still through an external condenser prior to venting to the ambient. It is apparent from Table 2 that with regard to still productivity there exists an optimum range for the air flow rate, approximately between 1 and 3 kgm⁻²h⁻¹, for the system under consideration. It is also observed that the ratio of secondary to primary product rises with an increasing flow rate, i.e., the primary decreases and the secondary rises with an increasing air flow rate (cf., Fig.2). The reason for the observed optimum air flow rate range was discussed in our previous papers^{4,6}.

BEST AVAILABLE COPY

Table 2 Still productivity (I- primary; II- secondary; Σ- total distillate) as a function of air flow rate. Feedstock flow rate = 2.96 kgm⁻²h⁻¹, Irradiation = 650010 Wm⁻².

Air Flow Rate (kgm ⁻² h ⁻¹)	I (kgm ⁻² h ⁻¹)	II (kgm ⁻² h ⁻¹)	Σ (kgm ⁻² h ⁻¹)
4.51	0.65	0.32	0.97
3.27	0.75	0.29	1.03
2.21	0.84	0.27	1.11
1.76	0.87	0.20	1.07
1.24	0.96	0.15	1.11
1.02	0.97	0.13	1.10
0.58	0.93	0.04	0.97
0.32	0.68	0.01	0.69

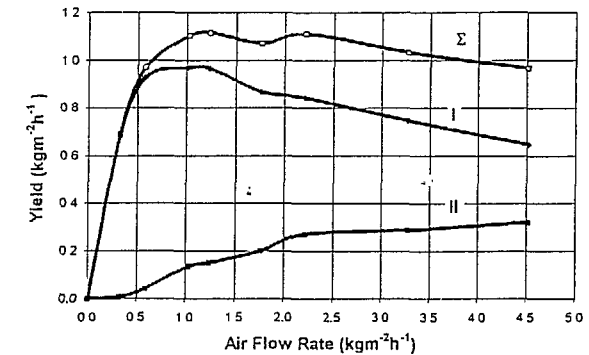


Fig 2 Productivity (yield) vs. air flow rate for a constant feedstock flow rate = 2.96 kgm⁻²h⁻¹. I is the primary distillate, II is the secondary distillate and Σ is the total distillate. Irradiation = 650010 Wm⁻²

Waste thermal energy operation mode without insulation placed on still glazing

In these experiments, the feedstock flow rate was kept constant at 9.3 kgm⁻²h⁻¹ and the feedstock was preheated to between 86 and 90 °C by a heat exchanger, in order to simulate the use of an external source of waste thermal energy. The preheated feedstock entered directly the top of the central metal plate, as shown in Fig. 1. The results of these experiments are summarized in Fig. 3 and in Tables 3 and 4

The utilized waste thermal energy, q_{waste} , which is defined as the heat released, $q_{released}$, by the preheated feedstock in the upper chamber is reported in Table 4. This term is defined as the difference between the thermal energy contained by the feedstock entering the upper chamber $q_{f,in}$ and that of brine exiting the upper chamber $q_{brine\ drain}$.

$$Q_{Waste} = Q_{Released} = Q_{L,in} - Q_{B,Brnc} = C_w m_f T_{L,in} - C_w m_{B,Brnc} T_{B,Brnc} \quad (1)$$

where $m_{B,Brnc}$ is determined from a material balance, viz., as a difference of the feedstock flow rate and the rate of evaporation in the upper chamber

Table 3. Temperature profiles at steady-state as a function of air flow rate utilizing only waste thermal energy for preheating the feedstock. Feedstock flow rate = 9.3 kgm⁻²h⁻¹, feedstock inlet temperature in the range of 86 to 90 °C

Air Flow Rate kgm ⁻² h ⁻¹	T _a °C	UPPER CHAMBER					LOWER CHAMBER					T _{1,out} °C	T _{sep,l} °C	T _{X,in} °C	T _{X,out} °C	T _{Brnc} °C
		T ₀ °C	T ₁ °C	T ₂ °C	T ₃ °C	T ₄ °C	T ₅ °C	T ₆ °C	T ₇ °C	T ₈ °C	T ₉ °C					
1.20	25.9	49.7	65.7	69.0	73.7	84.7	80.0	74.9	70.2	65.0	55.9	57.5	51.9	49.8	28.3	54.5
1.56	25.6	44.6	64.5	67.4	71.8	83.3	77.9	73.2	68.8	63.8	54.5	56.4	52.4	50.9	28.9	52.6
2.02	26.0	42.4	62.9	65.7	69.9	82.3	76.2	71.6	62.7	62.6	53.6	56.0	52.7	51.2	27.8	51.5
3.12	24.6	37.0	58.3	61.2	65.7	80.7	72.6	67.5	58.6	50.1	52.2	50.3	25.0	29.5	46.7	
4.11	24.9	35.0	54.6	57.8	62.3	78.3	70.2	64.3	56.1	48.7	50.7	49.1	25.5	30.6	45.3	
4.90	25.2	34.4	53.5	56.5	60.9	78.1	69.0	62.9	54.8	48.1	50.0	48.6	47.9	30.7	43.3	
7.07	23.6	31.1	49.1	51.9	56.7	77.7	66.3	59.0	50.9	45.7	46.6	45.5	44.9	31.0	41.4	

It is observed that increasing the air flow rate results in an increased productivity and also, an increase of the utilized waste energy, q_{Waste} . At reasonable air flow rates (i.e., around 3 kg h⁻¹, where the parasitic energy requirement of the air pump is still low) a total productivity rate of about 0.7 kg h⁻¹ could be obtained.

Table 4. Productivity rates at steady-state as a function of air flow rate utilizing only waste thermal energy. Feedstock flow rate = 9.3 kgm⁻²h⁻¹; feedstock inlet temperature in the range of 86 to 90 °C. The calculated waste thermal energy input, q_{Waste} , is also reported

Air Flow Rate (kg m ⁻² h ⁻¹)	Irradiation (W m ⁻²)	q_{Waste} (W m ⁻²)	I (kg m ⁻² h ⁻¹)	II (kg m ⁻² h ⁻¹)	S (kg m ⁻² h ⁻¹)
1.20	0	356	0.34	0.05	0.39
1.56	0	380	0.39	0.08	0.48
2.02	0	395	0.41	0.12	0.53
3.12	0	452	0.52	0.17	0.69
4.11	0	468	0.53	0.19	0.72
4.90	0	490	0.55	0.22	0.77
7.07	0	512	0.58	0.25	0.82

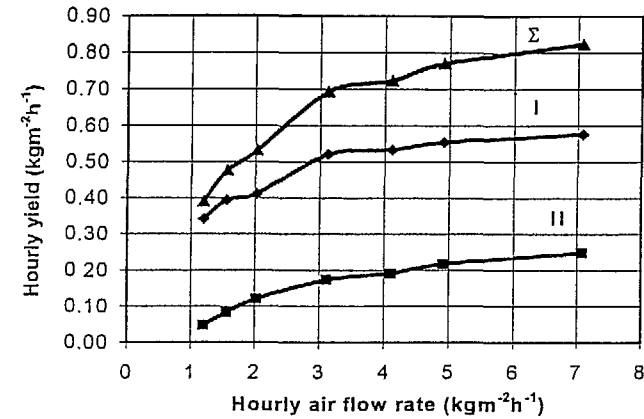


Fig. 3. Productivity vs. air flow rate when utilizing only waste energy. Feedstock flow rate = 9.3 kgm⁻²h⁻¹; feedstock inlet temperature in the range of 86 to 90 °C. I is the primary distillate, II is the secondary distillate and Σ is the total distillate.

Waste thermal energy operation mode with insulation placed on still glazing

Since thermal energy losses via the still glazing comprise the major portion of the thermal energy losses of a still even if it is double glazed, for nocturnal distillation it seemed to be reasonable to reduce the top losses by placing an insulating cover above the glazing. In our experiments a 5 mm thick polyurethane foam with a reflective aluminum foil on one side was placed upon the still glazing. The results of these experiments are presented in Fig. 3 and in Tables 5 and 6.

Table 5. Temperature profiles at steady-state as a function of air flow rate utilizing only waste thermal energy for preheating the feedstock and insulating the cover placed above the still glazing. Feedstock flow rate = 9.3 kgm⁻²h⁻¹; feedstock inlet temperature in the range of 86 to 90 °C.

Air Flow Rate kgm ⁻² h ⁻¹	T _a °C	UPPER CHAMBER					LOWER CHAMBER					T _{1,out} °C	T _{sep,l} °C	T _{X,in} °C	T _{X,out} °C	T _{Brnc} °C
		T ₀ °C	T ₁ °C	T ₂ °C	T ₃ °C	T ₄ °C	T ₅ °C	T ₆ °C	T ₇ °C	T ₈ °C	T ₉ °C					
1.05	25.9	56.3	71.9	74.2	77.6	85.0	81.4	78.3	29.6	70.7	61.0	63.4	58.0	55.8	25.5	59.3
1.55	25.7	48.6	69.8	72.4	75.5	84.3	79.4	76.3	73.2	68.7	58.6	60.8	57.1	55.7	30.0	56.2
2.00	25.9	45.7	67.6	70.3	73.5	83.1	77.7	74.5	26.4	66.8	57.5	59.8	57.0	55.6	30.2	54.4
3.15	24.0	38.4	61.8	64.8	68.5	81.1	74.3	70.0	21.9	61.7	53.0	55.2	53.2	24.9	30.6	48.4
4.11	24.7	37.2	57.9	61.4	65.3	79.4	72.0	66.9	19.5	59.3	51.7	53.9	52.3	25.8	32.9	47.8
4.58	25.1	36.7	56.8	60.1	64.1	78.6	71.2	65.8	18.3	58.0	51.3	53.0	51.7	51.0	32.8	45.7
6.99	23.7	32.0	50.6	53.9	58.2	77.3	67.0	60.3	12.8	52.7	47.4	48.5	47.4	46.7	33.2	42.7

It is observed that the use of this additional insulation on the still glazing resulted in both higher operational temperatures and productivity rates at comparable air flow rates, however, the increase in the total productivity was only in the range of $0.1 \text{ kg m}^{-2} \text{ h}^{-1}$.

Table 6 Productivity rates at steady-state as a function of air flow rate utilizing only waste thermal energy and insulating the cover placed above the still glazing. Feedstock flow rate = $9.3 \text{ kg m}^{-2} \text{ h}^{-1}$, feedstock inlet temperature in the range of 86 to $90 \text{ }^\circ\text{C}$. The calculated waste energy input, q_{waste} , is also reported.

Air Flow Rate ($\text{kg m}^{-2} \text{ h}^{-1}$)	Irradiation (W m^{-2})	q_{waste} (W m^{-2})	I ($\text{kg m}^{-2} \text{ h}^{-1}$)	II ($\text{kg m}^{-2} \text{ h}^{-1}$)	S ($\text{kg m}^{-2} \text{ h}^{-1}$)
1.05	0	308	0.36	0.07	0.43
1.55	0	348	0.46	0.13	0.55
2.00	0	375	0.51	0.16	0.67
3.15	0	442	0.64	0.17	0.81
4.11	0	451	0.61	0.24	0.85
4.58	0	463	0.60	0.26	0.87
6.99	0	504	0.64	0.27	0.91

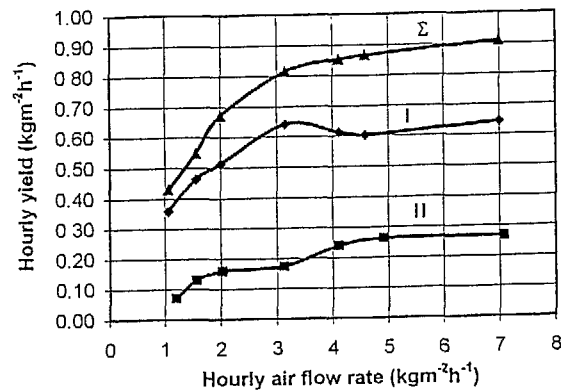


Fig. 4. Productivity vs. air flow rate when utilizing only waste thermal energy and an insulating cover placed above the still glazing. Feedstock flow rate = $9.3 \text{ kg m}^{-2} \text{ h}^{-1}$, feedstock inlet temperature is in the range of 86 to $90 \text{ }^\circ\text{C}$. I, II and Σ are as defined previously.

Hybrid mode of operation with simultaneous use of both solar and waste thermal energy

In these experiments a constant feedstock flow rate of $5.7 \text{ kg m}^{-2} \text{ h}^{-1}$ was used and the feedstock was preheated in the range of 86 to $90 \text{ }^\circ\text{C}$ by external simulated waste thermal energy prior to it entering the top of the central metal plate. The results are summarized in Tables 7 and 8 and in Fig. 5. It is observed that in this mode of operation, for an air flow rate

in the range of $2-3 \text{ kg m}^{-2} \text{ h}^{-1}$, total productivity rates as high as $1.57 \text{ kg m}^{-2} \text{ h}^{-1}$ could be achieved. These productivity rates are more than 40% higher than those obtained in the solar only operation mode (cf., Tables 2 and 8). This difference is due mainly to the fact that in hybrid operation mode the temperature and the vapour content of the air stream that exits the lower chamber is much higher and, consequently, the amount of distillate condensed in the external condenser (Yield II) is enhanced significantly. It is also observed that in this hybrid mode of operation the temperature and, therefore, the water vapour content of the saturated air stream that exits the condenser and is vented to the ambient is relatively high. The external condenser used in this study was incapable of recovering a major fraction of the water vapour content of the exiting air stream prior to venting to the ambient, viz., it is not efficient enough when the system operates in the hybrid mode.

Table 7 Temperature profiles at steady-state as a function of air flow rate utilizing both solar and waste thermal energy, hybrid mode. Feedstock flow rate = $5.7 \text{ kg m}^{-2} \text{ h}^{-1}$, feedstock inlet temperature in the range of 86 to $90 \text{ }^\circ\text{C}$, irradiation = $650 \text{ } 10 \text{ W m}^{-2}$

Air Flow Rate ($\text{kg m}^{-2} \text{ h}^{-1}$)	T_1	UPPER CHAMBER					LOWER CHAMBER					$T_{1\text{out}}$	$T_{\text{sep}1}$	$T_{\text{X.in}}$	$T_{\text{X.out}}$	T_{Bnn}
	T_0	T_1	T_2	T_3	T_4	T_5	T_6	T_7	T_8	T_9	T_{10}	T_{11}	T_{12}	T_{13}	T_{14}	T_{15}
1.33	31.8	72.2	95.6	97.6	97.5	99.0	97.4	97.1	48.5	94.1	84.7	87.6	86.1	84.9	51.5	73.4
2.03	34.4	62.5	88.5	91.7	91.6	94.3	92.1	91.2	42.4	87.1	78.2	80.5	79.3	78.3	49.3	67.4
3.52	28.4	56.9	80.8	85.5	85.4	89.5	86.7	84.8	36.3	80.1	73.3	74.2	72.9	71.6	48.9	60.6
4.02	30.9	56.6	79.4	83.8	83.8	90.9	86.3	83.4	34.9	78.5	72.5	73.3	72.3	71.1	51.2	60.7

Table 8. Productivity rates at steady-state as a function of air flow rate utilizing both solar and waste thermal energy, hybrid mode. Feedstock flow rate = $5.7 \text{ kg m}^{-2} \text{ h}^{-1}$, feedstock inlet temperature in the range of 86 to $90 \text{ }^\circ\text{C}$, irradiation = $650 \text{ } 10 \text{ W m}^{-2}$. The calculated waste energy input, q_{waste} , is also reported.

Air Flow Rate ($\text{kg m}^{-2} \text{ h}^{-1}$)	Irradiation (W m^{-2})	q_{waste} (W m^{-2})	I ($\text{kg m}^{-2} \text{ h}^{-1}$)	II ($\text{kg m}^{-2} \text{ h}^{-1}$)	S ($\text{kg m}^{-2} \text{ h}^{-1}$)
1.33	650	251	0.95	0.53	1.48
2.03	650	290	0.98	0.60	1.57
3.52	650	330	0.93	0.63	1.57
4.02	650	331	0.87	0.64	1.51

BEST AVAILABLE COPY

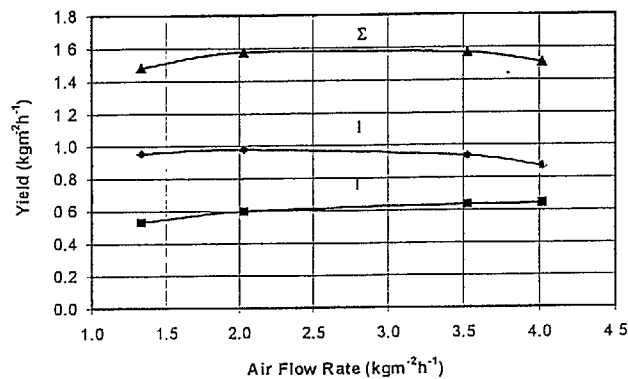


Fig 5 Productivity v.s air flow rate when utilizing both solar and waste thermal energy, hybrid mode. Feedstock flow rate = $5.7 \text{ kgm}^{-2}\text{h}^{-1}$; feedstock inlet temperature = 90°C . I II and Σ are as defined previously.

Evaluation of the results

The results of this experimental study are summarized with respect to the total distillate rate as a function of the air flow rate in Fig. 6. The operation of the solar still at relatively high air flow rates is not recommended due to the increase in the parasitic electric energy required to drive the air pump. The optimum air flow rate for both the hybrid operation mode, which utilizes both solar and waste thermal energy during the daytime and for nocturnal distillation mode, utilizing only waste thermal energy during nighttime, is observed to be in the range of $2\text{-}3 \text{ kg m}^{-2}\text{h}^{-1}$. We believe that operating the still in arid zones under these conditions, i.e., hybrid operation mode with nocturnal distillation, a productivity in excess of $20 \text{ kgm}^{-2}\text{day}^{-1}$ can be achieved. The analysis of the results of this study suggest that even higher productivity rates may be achieved in such a mode of operation if the feedstock is preheated in the lower chamber (viz., in the serpentine tube) as done in solar only operation mode and then heated further by the external waste thermal energy source prior to entering the upper chamber at the top of the evaporation plate.

BEST AVAILABLE COPY

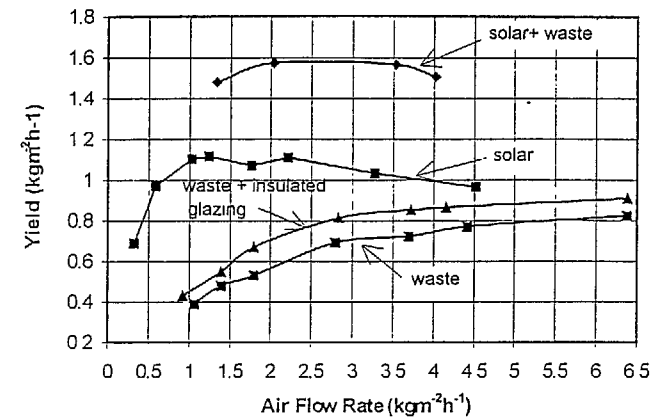


Fig. 6 The total productivity, Σ , as a function of the air flow rate for the four modes of operation. Experimental conditions for each mode of operation are defined in the text.

4. CONCLUSIONS

The performance of an air-blown, multiple-effect solar still consisting of an upper evaporation chamber and a lower condensation chamber has been analyzed in three modes of operation: (i) the still driving force is solar energy; (ii) the still driving force is both solar and waste thermal energy, viz., a hybrid mode of operation in the daytime; and (iii) the still driving force is waste thermal energy, viz., a nocturnal distillation mode of operation.

The still had a structured, double-walled, 10 mm thick polycarbonate glazing, a transparent insulation material (TIM) and the still area was 1 m^2 . The solar energy was provided by a solar simulator, at a constant intensity of $650 \pm 10 \text{ Wm}^{-2}$, this facilitated the inter-comparison of the system performance when operating in the three different modes. The waste thermal energy was simulated by a feedstock (water) reservoir maintained between 86 and 90°C . The steady-state yields and temperatures were achieved within one hour, as a result of the low thermal mass of the still.

In all operation modes, the performance of the still was determined mainly by the flow rate of the entering air stream and the optimum range of the air flow rates were determined experimentally. The optimum air flow rate for both the hybrid mode of operation in the daytime and the nocturnal distillation mode of operation in the nighttime is in the range of $2\text{-}3 \text{ kgm}^{-2}\text{h}^{-1}$. It is anticipated, that operating this still in arid zones under these conditions, i.e., hybrid operation mode with nocturnal distillation, a productivity in excess of $20 \text{ kgm}^{-2}\text{day}^{-1}$ may be achieved.

The analysis of the results suggests that preheating the feedstock in the lower chamber and then heating it further with an external waste thermal energy source, hybrid mode of operation, prior to entering the upper chamber at the top of the evaporation plate, will further enhance still performance and thereby decrease the need for cooling energy in the external heat exchanger.

NOMENCLATURE

c	heat capacity ($\text{Jkg}^{-1}\text{K}^{-1}$)
m	mass flow rate (in $\text{kgm}^{-2}\text{s}^{-1}$)
q	thermal energy normalized to unit still area (Wm^{-2})
q_{Waste}	waste energy input = q_{Released} normalized to unit still area (Wm^{-2})
q_{Released}	thermal energy released by the preheated feedstock in the upper chamber (Wm^{-2})
T	temperature ($^{\circ}\text{C}$)

Subscripts

a	ambient
Brine	brine drain-off
f	feedstock
I	primary distillate
II	secondary distillate
in	stream entering chamber
out	stream exiting chamber
sep	vapor/liquid separator
u	upper chamber
w	water
X	external heat exchanger/condenser

Acknowledgement- This research was supported under Grant No. TA-MOU-95-C15-050 US-Israel Cooperative Development Research Program. Office of Agriculture & Food Security Center for Economic Growth. Bureau for Global Programs. Field Support and Research. USAID One of the authors L. Horvath acknowledges also the support of the Hungarian OTKA Fund, project No F-025 342.

REFERENCES

- [1] Malik, M.A.S., Tiwari, G.N., Kumar, A. and Sodha, M.S.. *Solar Distillation*. Pergamon Press, Oxford, 1982.
- [2] Talbert, S.G., Eibling, J.A. and Lof, G.O.G. *Manual on Solar Distillation of Saline Water* R&D Progress Report No 546 US Department of Interior, 1970.
- [3] Kudish, A.I.: *Water Desalination*. In *Solar Energy in Agriculture-Energy in World Agriculture*. Parker B.F. (Ed), Vol. 4 pp. 255-294. Elsevier Science Publishers B.V.: Amsterdam, 1991
- [4] Mink, G., Aboabboud, M.M., Horvath, L., Evseev, E.G. and Kudish, A.I. *Design and performance of an air-blown solar still with thermal energy recycle*. Proceedings of the ISES Solar World Congress, Vol. 6 Taejon Korea, 1997. pp 135-144

BEST AVAILABLE COPY

- [5] Kudish, A.I., Evseev, E.G., Aboabboud, M.M., Horvath, L. and Mink, G. *Heat transfer processes in an air-blown, multiple-effect solar still with thermal energy recycle*. Proceedings of the ISES Solar World Congress, Vol. 6 Taejon, Korea, 1997 pp 158-167
- [6] Mink, G., Horvath, L., Evseev, E.G. and Kudish, A.I. *Design parameters, performance testing and analysis of a double-glazed, air-blown solar still with thermal energy recycle*. Solar Energy in press.

ISPITIVANJE ISKORISTIVOSTI ZRAKOM PROPULANOG, VIŠESTRUKO UČINKOVITOG SOLARNOG DESTILACIJSKOG UREĐAJA KOJI RADI NA SUNČEVU I/ILI ENERGIJU OTPADA

Sažetak: Iskoristivost zrakom propuhanoga, višestruko učinkovitog solarnog destilacijskog uređaja, konstruiranog za ponovno korištenje topline kondenzacije, proučavana je prilikom rada na tri različita načina, tj. korištenjem tri različite pogonske sile: (i) sunčeva energija; (ii) sunčeva energija i otpadna toplina te (iii) otpadna toplinska energija, sa i bez izolacije staklenoga pokriva destilacijskoga uređaja.

Destilacijski je uređaj imao dvoslojno ostakljenje od strukturiranoga polikarbonata, transparentnu izolaciju, a površina je bila 1 m^2 . Sunčeva energija dobavljena je pomoću sunčevog simulatora, uz konstantni intenzitet od $650 \pm 10 \text{ Wm}^{-2}$, što je pojednostavilo usporedbu iskoristivosti sustava prilikom rada na tri različita načina. Čišćenje toplinska energija simulirana je pomoću ogrjevnog (vodenog) spremnika održavanog između 86 i 90°C . Stacionarni dobici i temperature postignuti su unutar jednoga sata, kao rezultat male toplinske mase destilacijskog uređaja. Radeći uz konstantno dovođenje energije, iskoristivost destilacijskog uređaja najčešće je određivana pomoću količine protoka zraka, koji je nositelj i mase i energije. Optimalni raspon količina protoka zraka, prilikom sva tri navedena načina rada, određen je eksperimentalno. Također, postavljene su bilance mase i topline, upotrebljavajući eksperimentalne rezultate, u odnosu na optimalne uvjete rada.

Ključne riječi: sunčeva energija, otpadna energija, destilacija, ponovno korištenje energije

PERFORMANCE OF AN AIR-BLOWN SOLAR STILL WITH
INTERNAL MULTITUBULAR HEAT EXCHANGER FOR
CONDENSATION HEAT RECYCLE

G. MINK^{*}, M.M. ABOABBOUD^{*}, L. HORVÁTH^{*}, E.G. EVSEEV^{**}, A.I. KUDISH^{**}
^{*}Research Laboratory of Materials and Environmental Chemistry, Chemical Research
Center, Hungarian Academy of Sciences, 1525 Budapest Pf 17, HUNGARY;
Tel: +36 1 325 5992, Fax: +36 1 335 7892, E-mail: mink@chemres.hu
^{**}Solar Energy Laboratory, Department of Chemical Engineering, Ben-Gurion
University of the Negev, Beer Sheva 84105, ISRAEL.;
Tel: +972 7 6461488, Fax: +972 7 6472916, E-mail: akudish@bgumail.bgu.ac.il

Abstract: A detailed description of an innovative, air-blown, multitubular solar still fabricated from corrosion resistant materials (double-walled, solar grade polycarbonate glazing, plastic evaporation tray, plastic serpentine tube to preheat the feedstock and glass tubes for thermal energy recycle) is presented. The solar radiation intensity, provided by a solar simulator, was constant at a value of $650 \pm 10 \text{ Wm}^{-2}$. The solar still performance as a function of the air flow rate, under a constant feedstock flow rate, has been studied and the optimum operation parameters determined. The optimum productivity was determined to be $0.97 \text{ kgm}^{-2}\text{h}^{-1}$ for an air flow rate of $1.28 \text{ kgm}^{-3}\text{h}^{-1}$. The results of heat and mass balance calculations are also presented.

Key words: Solar distillation, Heat recycle; Simple construction, Corrosion resistant materials.

1. INTRODUCTION

The consumption of water unfit for drinking is a major health hazard in rural areas. To supply these rural people with salinity and/or pathogen free water is an urgent task to be solved. Solar distillation could be an ideal source of fresh water production, however, the crucial problem is that the productivity per unit area of the traditional solar stills is low. In addition, the fixed capital investment cost of a solar desalination plant is roughly proportional to the still area. Consequently, there are two possible approaches to overcome these limitations, to either increase solar still productivity per unit area and/or decrease the fixed capital investment per unit area.

In our previous papers¹⁻³ the performance of an air-blown, multiple-effect solar still that offers a significant increase of the still productivity per unit area at marginal incremental costs has been presented and analyzed, viz., the first approach. In this still, consisting of an upper evaporation chamber and lower condensation chamber, a large fraction of the heat of condensation of the distillate is successfully recycled both to the evaporation plate and to preheat the feedstock.

BEST AVAILABLE COPY

62

The aim of the present work was not to enhance the productivity of the above still but to simplify its construction and thereby make it a more economically viable alternative, viz., the second approach, reducing the fixed capital investment cost per unit area. This was achieved by utilizing relatively inexpensive and corrosion resistant materials in the construction of the solar still. This modified solar still design, though significantly different in appearance from the original, utilizes the same heat transfer processes to obtain the final distillate product.

2. DESIGN OF SOLAR STILL

This new solar still module, shown schematically in Figures 1A. and 1B, consists of a bottom and edge insulated thin, rectangular plastic tray, 40 glass tubes covered with a black wick and a plastic serpentine tube in which the feedstock is preheated. The still glazing is a transparent insulation material (TIM), i.e., a solar grade polycarbonate double-walled sheet. A low pressure, variable speed air pump was used for pumping the air and a peristaltic pump for the feedstock. The solar still operates in the following manner: (i.) air enters at the lower extremity of the tilted still, (ii.) evaporation occurs from the wick, which also wets the external surface of the glass tubes; (iii.) the air stream achieves both its highest temperature and vapour content at the upper extremity of the still; (iv.) the air stream is directed into the longitudinal glass tubes at the top of the still and then flows downwards, i.e., it reverses direction, and most of its vapour content condenses on the inner surface of the glass tubes, (v) the enthalpy of air stream that exits the lower chamber is utilized to preheat the feedstock. In the evaporation chamber, the feedstock is heated further in a plastic serpentine tube, and the preheated feedstock enters the black wick in the uppermost part of the evaporation chamber. The present paper gives a detailed description of this new, multitubular solar still. The solar still performance and its optimum operation parameters will also be discussed.

3. EXPERIMENTAL

Experimental setup, experimental conditions and procedure

The schematic diagram of the solar still is shown in Figs. 1A. and 1B. The tilt angle of the solar still module was set at 20° . The solar radiation intensity provided by the solar simulator was $650 \pm 10 \text{ Wm}^{-2}$ and its tilt angle was also 20° . The edge and bottom of the still were insulated with a 50 mm thick polyurethane foam. The differential and cumulative yields from Separator I and II were measured automatically by a type PT 6 Satorius electric balance with an accuracy of $\pm 1 \text{ g}$. The temperatures were measured at 11 locations with an accuracy of $\pm 1^\circ \text{C}$ using calibrated temperature sensors of the silicon base type KTY 11-2A. The absolute humidity of air in the vicinity of the slot was calculated from material and energy balances on the still. A data acquisition system served both to monitor and store the temperature data from the eleven thermistors and to calculate differential and cumulative yields at variable time intervals. It consisted of a PC with an A/D-D/A converter card, electronic measuring and magnetic valve control unit, temperature sensors and a digital balance with a RS232C serial interface. The data acquisition, control and analysis software were developed for the study. The feedstock was pumped into the still at ambient temperature, which varied between 23 and 27°C . The feedstock flow rate was kept constant at $2.5 \text{ kgm}^{-2}\text{h}^{-1}$ throughout the experiments and the still performance was investigated in an air flow range between $0.36 - 5.29 \text{ kgm}^{-2}\text{h}^{-1}$.

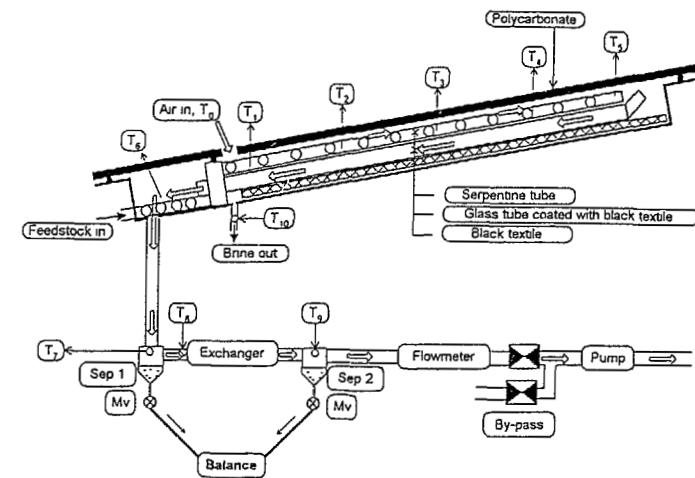


Fig. 1A. Schematic diagram of the multitubular solar still and the experimental setup. The location of the temperature probes are indicated by numbers 0 to 10.

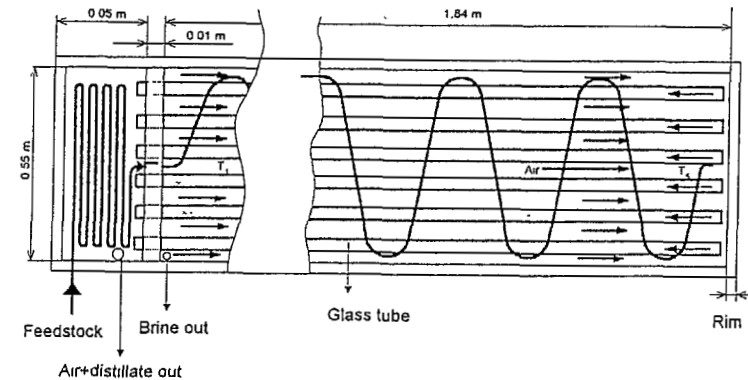


Fig. 1B. Simplified scheme of the top view of the multitubular solar still. The number of glass tubes is 40.

4. RESULTS AND DISCUSSION

Due to the low thermal mass of the still, the steady-state yields and temperatures have been achieved within one hour in all experiments. The results to be presented here refer to steady-state conditions and the mass and energy flows are normalized to a 1 m² still area.

Table 1. Temperature profile of the multitubular solar still at steady-state as a function of air flow rate for a constant feedstock flow rate of 2.5 kgm⁻²h⁻¹. The position of the 11 thermistors are as indicated in Fig. 1A (numbered 0 to 10). Irradiation = 650±10 Wm⁻².

Air Flow Rate (kgm ⁻² h ⁻¹)	T _a	CHAMBER					T _{preheater}	T _{sep1}	T _{X,in}	T _{X,out}
	T0	T1	T2	T3	T4	T5	T6	T7	T8	T9
0.34	23.5	80.3	97.1	99.1	97.8	98.3	80.1	57.7	51.9	25.8
1.28	24.7	76.2	91.1	93.6	90.2	92.8	73.6	58.9	63.6	27.3
2.53	25.0	65.5	75.7	82.3	84.0	84.6	65.6	57.8	56.3	26.8
5.29	27.1	57.2	62.3	70.9	73.4	75.2	60.1	53.3	52.8	28.8

Table 2. Still productivity (I- primary; II- secondary; Σ- total distillate) as a function of air flow rate. Feedstock flow rate = 2.5 kgm⁻²h⁻¹, Irradiation = 650±10 Wm⁻².

Air Flow Rate (kgm ⁻² h ⁻¹)	I (kgm ⁻² h ⁻¹)	II (kgm ⁻² h ⁻¹)	Σ (kgm ⁻² h ⁻¹)
0.34	0.56	0.05	0.61
1.28	0.82	0.16	0.97
2.53	0.68	0.19	0.87
5.29	0.66	0.29	0.95

The temperature profile of the still at different air flow rates expressed in kg bone dry air per m² still area per hour is given in Table 1. In Table 1, T_a is the ambient temperature; T_{preheater} is the preheater temperature; T_{sep1} is the temperature of the first separator; and T_{X,in} and T_{X,out} are the air temperatures entering and exiting the exchanger, respectively.

The still productivity, as a function of air flow rates in the range from 0.34 to 5.29 kgm⁻²h⁻¹ is reported both in Table 2 and in Fig. 2 in terms of primary (I), secondary (II), and total (Σ). The primary distillation rate refers to that condensed within the glass tubes and in the feedstock preheating compartment of the still. The secondary distillation rate is that obtained by passing the saturated air stream exiting the solar still through an external condenser prior to venting to the ambient. It is observed that with regard to the primary distillate rate, which is a direct measure of the thermal energy recycle, there exists an optimum range of air flow rates in the close vicinity of 1.3 kgm⁻²h⁻¹. It is also observed that the ratio of secondary to primary product increases with increasing flow rate, i.e., the primary decreases and the secondary increases with increasing air flow rate (cf. Fig.2). The reason for optimum air flow rate have been discussed in our previous papers^{2,4}.

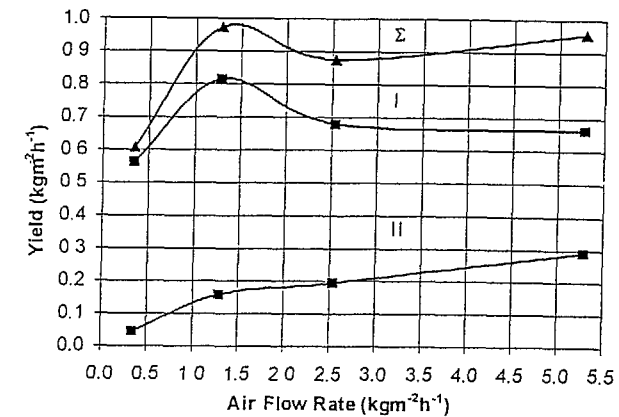


Fig 2. Productivity (yield) vs air flow rate for a constant feedstock flow rate = 2.96 kgm⁻²h⁻¹. I is the primary distillate, II is the secondary distillate and Σ is the total distillate. Irradiation = 650±10 Wm⁻².

Some results of the mass and energy balance on the still are presented in Table 3.

Table 3. The mass flow of vapor at steady-state as a function of air flow rate for a constant feedstock flow rate of 2.5 kgm⁻²h⁻¹.

Air Flow Rate (kgm ⁻² h ⁻¹)	T _{max} (T5) (°C)	T _{DEW} ^A (°C)	m _{v,in} ^B (kgm ⁻² h ⁻¹)	m _{vap} ^C (kgm ⁻² h ⁻¹)	m _{v,max} ^D (kgm ⁻² h ⁻¹)	m _{v,X,in} ^E (kgm ⁻² h ⁻¹)	m _{v,X,out} ^F (kgm ⁻² h ⁻¹)
0.34	98.3	91.9	0.003	0.614	0.617	0.057	0.007
1.28	92.8	84.3	0.013	0.987	1.000	0.180	0.030
2.53	84.6	74.2	0.026	0.901	0.927	0.247	0.057
5.29	74.2	65.0	0.062	1.022	1.084	0.414	0.134

- ^A - the calculated dew point of air stream turning into the glass tubes at T_{max};
^B - the mass flow of vapor carried by the entering air stream at T_a;
^C - evaporation rate in the evaporation chamber;
^D - the mass flow of vapor at T_{max};
^E - the mass flow of vapor entering the exchanger at T_{X,in};
^F - the mass flow of vapor exiting the exchanger at T_{X,out} and vented to the ambient.

The following comments are based upon the above analysis:

1. The calculated dew point temperatures are below the observed fluid temperature T_{max}, suggesting that the mass transport between the wet wick and the flowing air is not intense enough.
2. The operational optimum is in the vicinity of 1.28 kgm⁻²h⁻¹ air flow rate since

- (i) the total productivity is high ($0.97 \text{ kgm}^{-2}\text{h}^{-1}$);
 - (ii) the load on the external exchanger is moderate ($0.18 \text{ kgm}^{-2}\text{h}^{-1}$ vapour at relatively high fluid temperature (63.6°C);
 - (iii) the amount of vapour vented to the ambient is marginal ($0.03 \text{ kgm}^{-2}\text{h}^{-1}$)
- 3 Increasing air flow rate results in a higher evaporation rate but lower condenser efficiency and thereby, a greater thermal energy loss which is vented to the ambient

5. CONCLUSIONS

The description and performance analysis of an innovative, air-blown, multitubular solar still fabricated from corrosion resistant materials has been presented.

In the performance study, utilizing a solar simulator providing a constant radiation intensity of $650 \pm 10 \text{ W m}^{-2}$, the optimum conditions with respect to the still productivity and the need for external cooling energy have been determined.

Operating under a constant feedstock flow rate of $2.5 \text{ kgm}^{-2}\text{h}^{-1}$, the highest productivity, $0.97 \text{ kgm}^{-2}\text{h}^{-1}$, has been obtained in the vicinity of an air flow rate of $1.28 \text{ kgm}^{-2}\text{h}^{-1}$. Under these conditions the thermal load on the external condenser is low and the loss of productivity, i.e., the amount of vapor vented to the ambient is marginal.

The results of heat and mass balance calculations suggest that the still performance could be further enhanced by a more intense mass transfer between the wet wick and the air flow in the evaporative chamber.

Acknowledgement- This research was supported under Grant No. TA-MOU-95-C15-050, US-Israel Cooperative Development Research Program, Office of Agriculture & Food Security, Center for Economic Growth, Bureau for Global Programs, Field Support and Research, USAID.

One of the authors Mr. L. Horvath, acknowledges also the support of the Hungarian OTKA Fund, Project No F-025 342.

REFERENCES

- [1] Aboabboud, M.M. and Mink, G.: *Energy Recycle in solar distillation*. Proceedings of International Congress on Energy and Environment, Vol. I., Opatija, Croatia, 1996, pp 95-102.
- [2] Kudish, A.I., Evseev, E.G., Aboabboud, M.M., Horváth, L. and Mink, G.: *Heat transfer processes in an air-blown, multiple-effect solar still with thermal energy recycle*. Proceedings of the ISES Solar World Congress, Vol. 6, Taejon, Korea, 1997, pp 158-167.
- [3] Mink, G., Horváth, L., Evseev, E.G. and Kudish, A.I.: *Design parameters, performance testing and analysis of a double-glazed, air-blown solar still with thermal energy recycle*. Solar Energy, in press.
- [4] Mink, G., Aboabboud, M.M., Horváth, L., Evseev, E.G. and Kudish, A.I.: *Design and performance of an air-blown solar still with thermal energy recycle*. Proceedings of the ISES Solar World Congress, Vol. 6, Taejon, Korea, 1997, pp. 135-144.

ISKORISTIVOST ZRAKOM PROPULANOG SOLARNOG DESTILACIJSKOG UREĐAJA S UNUTARNJIM VIŠECIJEVNIM IZMJENJIVAČEM TOPLINE ZA PONOVO KORIŠTENJE TOPLINE KONDENZACIJE

Sažetak: U radu je prikazan detaljan opis novog, zrakom propuhanog, višecijevnog destilacijskog uređaja koji je izrađen od materijala otpornih na koroziju (dvoslojno, polikarbonatno ostakljenje, plastična podloga za isparivanje, plastična zavojita cijev za predgrijavanje ogrjevnog fluida i staklene cijevi za ponovno korištenje topline). Intenzitet sunčevog zračenja, dobivenog sunčevim simulatorom, konstantne je vrijednosti u iznosu od $650 \pm 10 \text{ Wm}^{-2}$. Proučavana je iskoristivost destilacijskog uređaja u funkciji protoka zraka, kod konstantnog protoka ogrjevnog fluida, te su određeni optimalni radni parametri. Određena je optimalna produktivnost u iznosu od $0,97 \text{ kgm}^{-2}\text{h}^{-1}$ za protok zraka od $1,28 \text{ kgm}^{-2}\text{h}^{-1}$. Također, predstavljeni su i rezultati proračuna bilanci topline i mase.

Ključne riječi: solarna destilacija, ponovno korištenje topline, jednostavna izvedba, materijali otporni na koroziju

PERFORMANCE AND ANALYSIS OF A MULTIPLE-EFFECT SOLAR STILL UTILIZING AN INTERNAL MULTI-TUBULAR HEAT EXCHANGER FOR THERMAL ENERGY RECYCLE

G. MINK*, L. HORVÁTH*, E.G. EVSEEV** and A.I. KUDISH**

*Research Laboratory of Materials and Environmental Chemistry, Chemical Research Center, Hungarian Academy of Sciences, 1525 Budapest Pf 17, HUNGARY; Tel: +36 1 325 5992, Fax: +36 1 335 7892, E-mail: mink@chemres.hu

**Solar Energy Laboratory, Institutes for Applied Research, Ben-Gurion University of the Negev, Beer Sheva 84105, ISRAEL.; Tel: +972 7 6461488, Fax: +972 7 6472916, E-mail: akudish@bgumail.bgu.ac.il

Abstract - To achieve a relatively high productivity at reduced investment costs, an innovative, air-blown, multi-tubular solar still module was fabricated from readily available, corrosion resistant materials. Performance studies were made as a function of the air flow rate (in the range of 0.36 - 5.29 kgm⁻²h⁻¹) utilizing a solar simulator providing a constant irradiation of 630±10 Wm⁻² and a constant feedstock flow rate of 2.5 kgm⁻²h⁻¹. A simulation model has also been developed to describe the heat and mass transfer processes occurring in this prototype solar still and it was validated by the experimental data. It has been found, both experimentally and by the simulation model, that the total amount of thermal energy recycled (to preheat the feedstock and to directly heat the evaporating surface) is a maximum at an air flow rate of ~ 1.28 kgm⁻²h⁻¹; corresponding to a maximum still productivity of 0.97 kgm⁻²h⁻¹.

1. INTRODUCTION

The consumption of water unfit for drinking is a major health hazard in rural areas. To supply these rural people with water free of salinity and/or pathogens is an urgent task to be solved. Solar distillation could be an ideal source of fresh water production, however, the crucial problem is that the productivity per unit area of the traditional solar stills is low. In addition, the fixed capital investment cost of a solar desalination plant is roughly proportional to the still area. Consequently, there are two possible approaches to overcome these limitations; to either increase solar still productivity per unit area and/or decrease the fixed capital investment per unit area.

In our previous papers¹⁻³ the performance of an air-blown, multiple-effect solar still that offers a significant increase of the still productivity per unit area at marginal incremental costs has been presented and analyzed, viz., the first approach. In this still, consisting of an upper evaporation chamber and lower condensation chamber, a large fraction of the heat of condensation of the distillate is successfully recycled both to the evaporation plate and to preheat the feedstock.

The aim of the present work was not to enhance the productivity of the above still but to simplify its construction and thereby make it a more economically viable alternative, viz., the second approach, reducing the fixed capital investment cost per unit area. This was achieved by utilizing relatively inexpensive and corrosion resistant materials in the construction of the solar still. The new solar still design, though significantly different in appearance from the original, utilizes the same heat transfer processes to obtain the final distillate product.

In spite of its simple construction, the heat and mass transfer processes occurring within the still are numerous and mutually interrelated. Another aim of this work was to develop a mathematical model, utilizing non-linear differential equations, which is capable of simulating still performance under both transitional and steady-state conditions.

2. SOLAR STILL DESIGN

The solar still module under investigation is shown schematically in Figs. 1.a and 1.b. It consists of a bottom and edge insulated, thin, rectangular plastic tray (L = 1.84 m; b = 0.54 m; H = 12 mm; area = 1 m²), 40 glass tubes (D_{out} = 7 mm; D_m = 5 mm; L = 1.8 m) covered with a black wick and a plastic serpentine tube (D_{out} = 4 mm; D_m = 3 mm; L = 20 m). The still glazing is a solar grade polycarbonate double-walled sheet (10 mm thick), a transparent insulation material (TIM). A low pressure variable speed air pump was used for the air, the mass and thermal energy carrier, and a peristaltic pump for the feedstock.

The still shown schematically in Fig. 1, operates in the following manner: (i.) ambient air at temperature T₀ enters at the lower extremity of the still; (ii.) evaporation occurs from the wick, which is also wets the external surface of the glass tubes; (iii.) the air stream achieves both its highest temperature and vapor content at the upper extremity of the still; (iv.) the air stream is directed into the longitudinal glass tubes at the top of the still and then flows downwards, i.e., it reverses direction, and most of its vapor content condenses on the inner surface of the glass tubes and the thermal energy of condensation is conducted via the tube wall to the wet wick to enhance the rate of evaporation from the wick; (v.) the enthalpy of air stream, at temperature T₆, entering the lower compartment, which unifies the air streams exiting the 40 glass tubes, is utilized to preheat the feedstock,

prior to its entering the evaporation chamber. The feedstock flows through a 5 m long black tube packed within this compartment to facilitate the heat exchange process. (vi.) in the evaporation chamber the feedstock is further heated as it flows through another 15 m of the black serpentine tube, positioned above the glass tubes, before exiting the serpentine tube onto the black still wick at the uppermost part of the evaporation chamber. (vii) the air stream and distillate exiting the solar still enter a gas-liquid separator (Sep. 1) to collect the primary distillate (I), in order to determine the amount of distillate which condenses within the still and is a measure of the efficiency of the thermal energy recycle process; (viii) the air stream exiting Sep. 1, still containing vapors, then enters an external heat exchanger and a second separator (Sep. 2), where the secondary distillate (II) is collected.

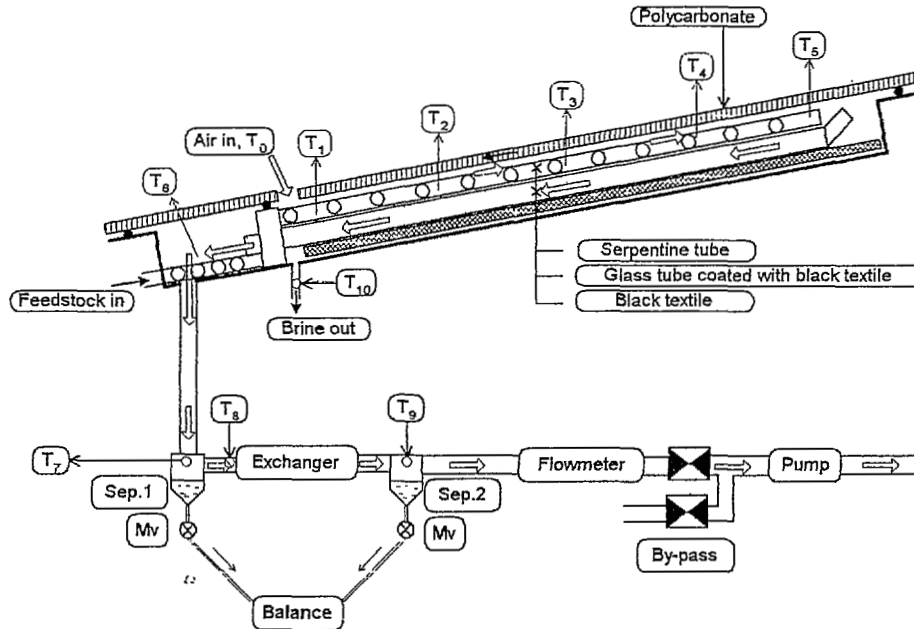


Fig. 1.a Schematic diagram of the multi-tubular solar still and the experimental setup. The location of the temperature probes are indicated by numbers 0 to 10.

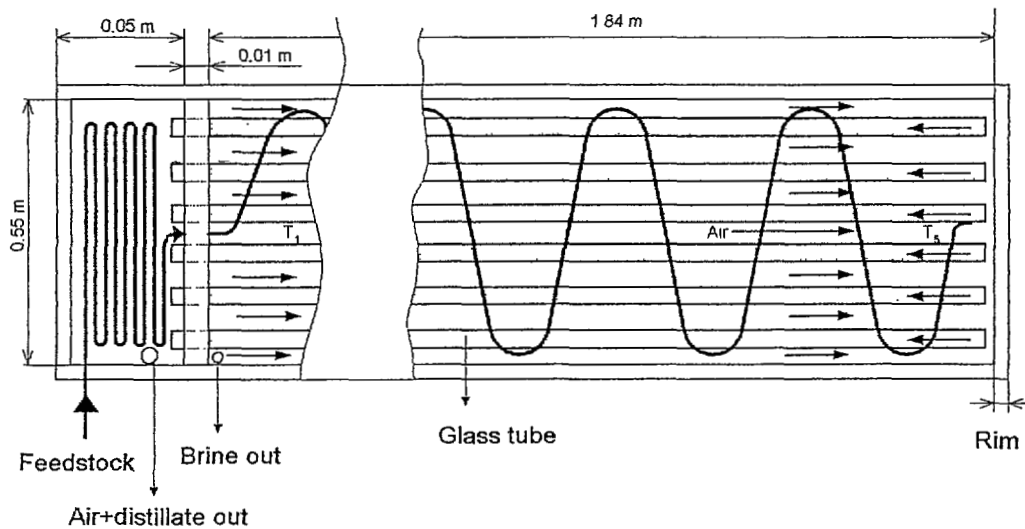


Fig. 1.b Simplified scheme of the top view of the multi-tubular solar still. The actual number of glass tubes is 40.

3. EXPERIMENTAL

The solar still was tilted at an angle of 20° . To facilitate the parametric sensitivity studies (viz., the dependence on air flow rate) a solar simulator, also tilted at 20° , was utilized. It provided a constant solar radiation intensity of $630 \pm 10 \text{ Wm}^{-2}$. A 50 mm thick polyurethane foam was used to insulate the edge and bottom of the solar still (not shown in Figs. 1.a and 1.b). The differential and cumulative yields from Separator 1 and 2 were measured automatically with a type PT 6 Satorius electric balance with an accuracy of $\pm 1 \text{ g}$. The temperatures were measured at 11 locations with an accuracy of $\pm 1^\circ \text{C}$ using calibrated temperature sensors of the silicon base type KTY 11-2A. The absolute humidity of air entering the glass tubes was calculated from material and energy balances on the still. The feedstock was pumped into the still at ambient temperature, which varied between 23 and 27°C . The feedstock flow rate was kept constant at $2.5 \text{ kgm}^{-2}\text{h}^{-1}$ throughout the experiments and the still performance was investigated in an air flow range between 0.36 and $5.29 \text{ kgm}^{-2}\text{h}^{-1}$.

A data acquisition system served both to monitor and store the temperature data from the eleven thermistors and to calculate differential and cumulative yields at variable time intervals. It consisted of a PC with an A/D-D/A converter card, electronic measuring and magnetic valve control unit, temperature sensors and a digital balance with a RS232C serial interface. The data acquisition, control and analysis software were developed for the study.

4. RESULTS AND DISCUSSION

Transitional stage of the distillation

All the mass and energy flows were normalized to a 1 m^2 still area. Due to the low thermal mass of the still, the steady-state yields and temperatures were achieved within one hour of start-up in all experiments. A set of experimental result, typical of those obtained, are shown Figs. 2 and 3. The transitional and steady-state temperatures corresponding to air temperatures T_1 , T_2 and T_5 in the evaporation chamber (cf., Fig. 1.a) are shown in Fig. 2.

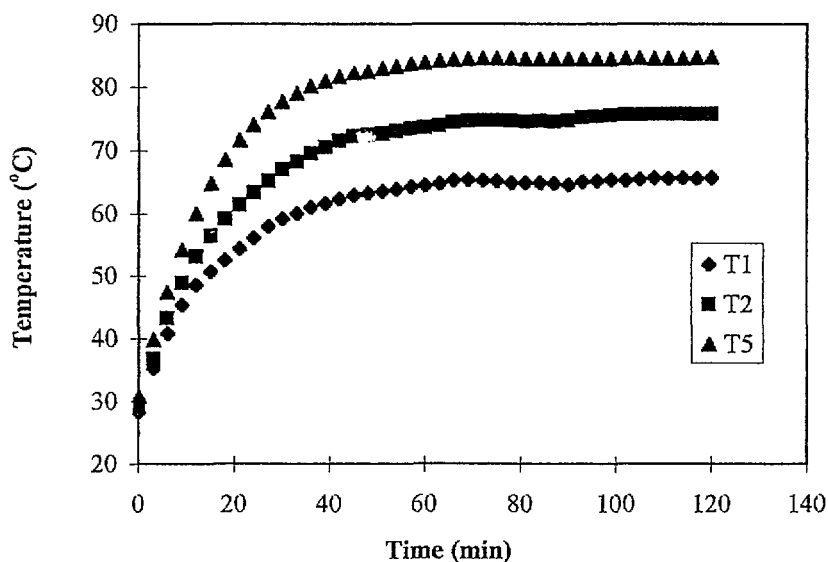


Fig.2. Variation of the air temperatures T_1 , T_2 and T_5 with the time of irradiation. Feedstock flow rate = $2.5 \text{ kgm}^{-2}\text{h}^{-1}$, irradiation = $630 \pm 10 \text{ Wm}^{-2}$.

The approach to steady-state distillation rates, primary (I), secondary (II) and total (Σ), as a function of the time lapse since start-up is presented in Fig. 3. The primary distillation rate refers to that condensed within the glass tubes and in the feedstock preheating compartment of the still. The secondary distillation rate is that obtained by passing the saturated air stream exiting the solar still through an external heat exchanger prior to venting to the ambient.

It is observed in Fig. 3 that there is a time delay of 27 minutes before the first breakout of distillate from the still. This is caused by the fact that when starting with a dry still, distillate first appears in the separator only after all the inside surfaces have been wetted and the small but not negligible dead volumes of the system are filled with the distillate. Once steady state is achieved, approximately after one hour, a random variation in the measured yields is observed. This is due to the high surface tension water which flows into separator 1 both continuously and periodically, in the form of rivulets. Therefore, steady state yields have been defined as an average of the data measured during at least one hour of operation under steady state conditions.

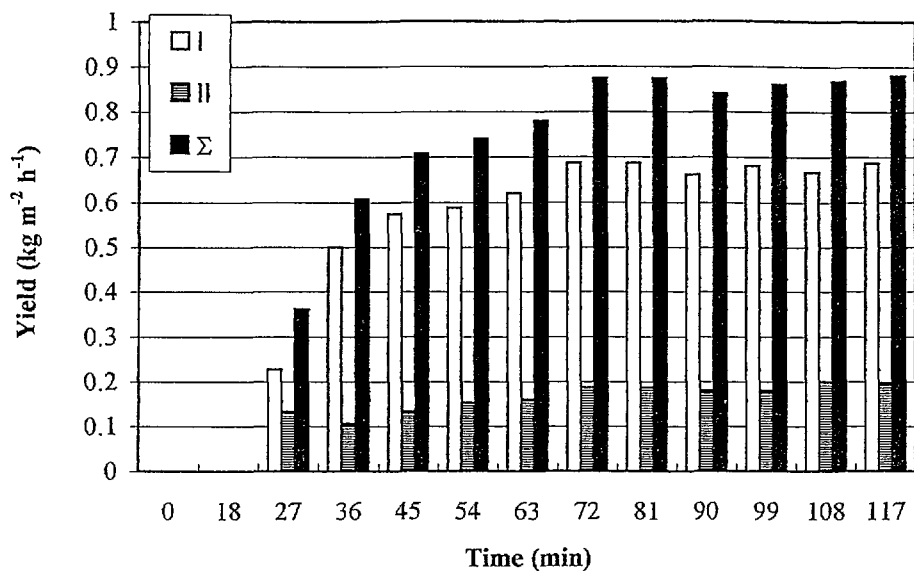


Fig. 3 Still productivity as function of time since start-up. Feedstock flow rate = $2.5 \text{ kgm}^{-2}\text{h}^{-1}$, irradiation = $630 \pm 10 \text{ Wm}^{-2}$.

Still performance under steady state conditions

The temperature profile of the still at different air flow rates expressed in kg bone dry air per m^2 still area per hour is reported in Table 1, where T_{amb} is the ambient temperature; T_{PREHEAT} the temperature of the preheating compartment; T_{SEPI} the temperature of the first separator; and $T_{X,\text{in}}$ and $T_{X,\text{out}}$ the air temperatures entering and exiting the external heat exchanger, respectively.

Table 1. Temperature profile of the multi-tubular solar still at steady-state as a function of air flow rate for a constant feedstock flow rate of $2.5 \text{ kgm}^{-2}\text{h}^{-1}$ and irradiation = $630 \pm 10 \text{ Wm}^{-2}$. The position of the thermistors are shown in Fig. 1.a.

Air Flow Rate ($\text{kgm}^{-2}\text{h}^{-1}$)	T_{amb}	CHAMBER					T_{PREHEAT}	T_{SEPI}	$T_{X,\text{in}}$	$T_{X,\text{out}}$
	T_0 ($^{\circ}\text{C}$)	T_1 ($^{\circ}\text{C}$)	T_2 ($^{\circ}\text{C}$)	T_3 ($^{\circ}\text{C}$)	T_4 ($^{\circ}\text{C}$)	T_5 ($^{\circ}\text{C}$)	T_6 ($^{\circ}\text{C}$)	T_7 ($^{\circ}\text{C}$)	T_8 ($^{\circ}\text{C}$)	T_9 ($^{\circ}\text{C}$)
0.34	23.5	80.3	97.1	99.1	97.8	98.3	80.1	57.7	51.9	25.8
1.28	24.7	76.2	91.1	93.6	90.2	92.8	73.6	65.9	63.6	27.3
2.53	25.0	65.5	75.7	82.3	84.0	84.6	65.6	57.8	56.3	26.8
5.29	27.1	57.2	62.3	70.9	73.4	75.2	60.1	53.3	52.8	28.8

The still productivity, as a function of air flow rates in the range from 0.34 to $5.29 \text{ kgm}^{-2}\text{h}^{-1}$ is reported both in Table 2 and in Fig. 4. It is observed that for the primary distillate rate, which is a direct measure of the thermal energy recycle efficiency, there exists an optimum range of air flow rates in the vicinity of $1.3 \text{ kgm}^{-2}\text{h}^{-1}$. It is also observed that the ratio of secondary to primary product increases with increasing flow rate, i.e., the primary decreases and the secondary increases with increasing air flow rate (cf., Fig. 4). The reason for an optimum air flow rate has been discussed in our previous papers²⁻⁴ and it will be also shown later in section 5 that the simulation model also predicts a maximum for the primary distillation at the same air flow rate.

The heat and mass balances on the still were calculated from the experimental data assuming that the air stream, after its temperature in the glass tubes dropped to the dew point of the air that enters into the glass tubes, was always saturated while passing through the glass tube to the ambient. Consequently, saturated air exits the glass tubes at temperature T_6 , enters separator 1 at T_7 , the external heat exchanger at T_8 , the separator 2 at T_9 and vented to the ambient also at T_9 . The dew point temperature of the air and the mass flow of vapor as calculated from the mass and energy balances on the still are reported in Table 3.

Table 2. Still productivity as a function of air flow rate. Feedstock flow rate = $2.5 \text{ kgm}^{-2}\text{h}^{-1}$; irradiation = $630 \pm 10 \text{ Wm}^{-2}$.

Air Flow Rate ($\text{kgm}^{-2}\text{h}^{-1}$)	I ($\text{kgm}^{-2}\text{h}^{-1}$)	II ($\text{kgm}^{-2}\text{h}^{-1}$)	Σ ($\text{kgm}^{-2}\text{h}^{-1}$)
0.34	0.56	0.05	0.61
1.28	0.82	0.16	0.97
2.53	0.68	0.19	0.87
5.29	0.66	0.29	0.95

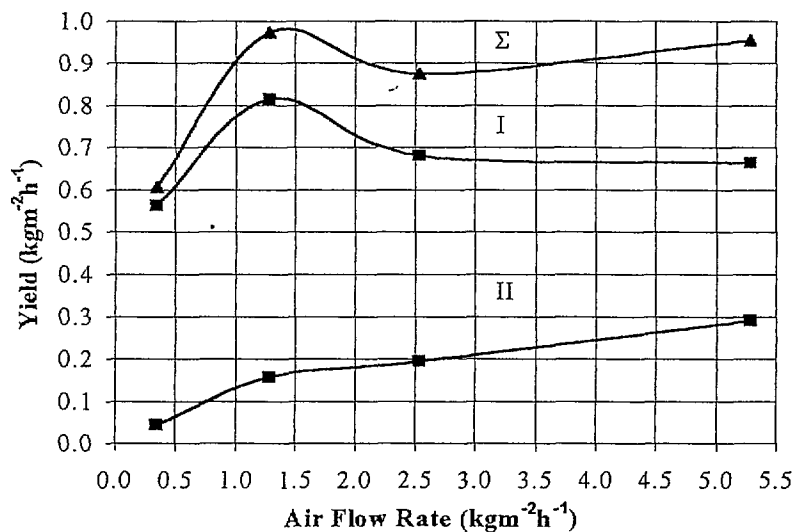


Fig. 4. Still productivity as a function of air flow. Feedstock flow rate = $2.5 \text{ kgm}^{-2}\text{h}^{-1}$, irradiation = $630 \pm 10 \text{ Wm}^{-2}$.

Table 3. The mass flow of vapor at steady-state as a function of air flow rate. Feedstock flow rate = $2.5 \text{ kgm}^{-2}\text{h}^{-1}$; irradiation = $630 \pm 10 \text{ Wm}^{-2}$.

Air Flow Rate ($\text{kgm}^{-2}\text{h}^{-1}$)	T_{max} (T_s) ($^{\circ}\text{C}$)	$T_{\text{DEW}}^{\text{A}}$ ($^{\circ}\text{C}$)	$m_{v,\text{in}}^{\text{B}}$ ($\text{kgm}^{-2}\text{h}^{-1}$)	m_{ev}^{C} ($\text{kgm}^{-2}\text{h}^{-1}$)	$m_{v,\text{max}}^{\text{D}}$ ($\text{kgm}^{-2}\text{h}^{-1}$)	$m_{v,X,\text{in}}^{\text{E}}$ ($\text{kgm}^{-2}\text{h}^{-1}$)	$m_{v,X,\text{out}}^{\text{F}}$ ($\text{kgm}^{-2}\text{h}^{-1}$)
0.34	98.3	91.9	0.003	0.614	0.617	0.057	0.007
1.28	92.8	84.3	0.013	0.987	1.000	0.180	0.030
2.53	84.6	74.2	0.026	0.901	0.927	0.247	0.057
5.29	74.2	65.0	0.062	1.022	1.084	0.414	0.134

- A - the calculated dew point of air stream turning into the glass tubes at T_{max} ;
 B - the mass flow of vapor carried by the entering air stream at T_a ;
 C - evaporation rate in the evaporation chamber;
 D - the mass flow of vapor at T_{max} ;
 E - the mass flow of vapor entering the exchanger at $T_{X,\text{in}}$;
 F - the mass flow of vapor exiting the exchanger at $T_{X,\text{out}}$ and vented to the ambient.

The following comments are based upon the above analysis presented in Table 3:

- The calculated dew point temperatures are below the observed fluid temperature T_{max} , which suggests that the mass transport between the wet wick and the air stream is not intense enough.
- The operational optimum is observed in the vicinity of an air flow rate of $1.28 \text{ kgm}^{-2}\text{h}^{-1}$ since (i) the total productivity is high ($0.97 \text{ kgm}^{-2}\text{h}^{-1}$); (ii) the load on the heat exchanger is moderate ($0.18 \text{ kgm}^{-2}\text{h}^{-1}$ vapor at a relatively high fluid temperature ($63.6 \text{ }^{\circ}\text{C}$); (iii) the amount of vapor vented to the ambient is marginal (0.03

kgm⁻²h⁻¹) and (iv) because the air flow rate is low, the parasitic electrical energy required to drive the air pump is marginal (≤ 1 W per m² still area), which in rural areas might be provided by PV panels.

3. Increasing air flow rate results in a higher evaporation rate but lower condenser efficiency and thereby, greater thermal energy and water vapor losses which are vented to the ambient. Additionally, at higher flow rates the parasitic electrical energy requirement increases.

5. SIMULATION MODEL OF THE MULTI-TUBULAR SOLAR STILL

A simulation model of the multi-tubular, air-blown solar still was developed. The temperatures of the air stream and feedstock at each node in the thermal analysis of the solar still system were modeled by the appropriate energy and mass balance relationships. This resulted in a model consisting of a set of nonlinear energy transfer equations. The model was solved numerically, using an explicit predictor-corrector difference scheme assuming "steady-state conditions" by using sufficiently small time intervals during which the feedstock flow rate and ambient temperature are assumed to be constant. The following assumptions have been made in this analysis:

1. The water film is replenished locally on a continuous basis, is stagnant and very thin; thus its thickness and temperature are assumed to be that of the wetted wick.
2. The system is considered to be uni-dimensional in the flow direction of the individual streams.
3. The Lewis number for the air-water mixtures in the operational temperature range is assumed to be equal to 1.0, yielding $h/h_m = C_s$.
4. In the evaporator, as well as in the internal heat exchanger in the lower compartment, a single-row serpentine geometry is assumed. Therefore, the moist air stream is assumed to pass in a cross-flow pattern over the feedstock tube.
5. In order to simplify the model by eliminating the j-th surface temperatures T_j ($j=g, t$ or w) and to preserve at the same time a reasonable accuracy for the long-wave radiative exchange processes (Duffie and Beckman, 1980), the net flux containing the above temperature is expressed by

$$Q_{r,j} = \epsilon_j \sigma \cdot (T^4 - T_j^4) \approx h_{r,j} \cdot (T - T_j), \quad (1)$$

where

$$h_{r,j} = 4\epsilon_j \sigma \cdot [(T_{j,in} + 2T + T_{j,out})/4]^3 \quad (1a)$$

and T is the corresponding air stream temperature, either above or below the surface node.

Mathematical model

The total thermal energy transferred through any j-th surface temperature T_j ($j=g, t$ or w) is given by

$$Q_{(j)} + U_{(j),in} \cdot (T_{in} - T_j) = A_{out}/A_{in} \cdot U_{(j),out} \cdot (T_j - T_{out}), \quad (2)$$

where $Q_{(j)}$ is the sensible thermal energy transfer due to either the condensation/evaporation process or the incident solar radiation heat flux.

The total temperature difference above and below any surface is given

$$\Delta T_{tot} \equiv T_{in} - T_{out} = \Delta T_{in} + \Delta T_{out}; \quad \Delta T_{in} = T_{in} - T_j, \quad \Delta T_{out} = T_j - T_{out}. \quad (3)$$

The differences from Eq. (3) may be calculated formally in term of ΔT_{tot} , by substituting for the corresponding surface temperature as

$$\Delta T_{in} = (U_{(j),in} + A_{out}/A_{in} \cdot U_{(j),out})^{-1} [A_{out}/A_{in} \cdot U_{(j),out} \Delta T_{tot} - Q_{(j)}], \quad (4)$$

$$\Delta T_{out} = (U_{(j),in} + A_{out}/A_{in} \cdot U_{(j),out})^{-1} [U_{(j),in} \Delta T_{tot} + Q_{(j)}]. \quad (5)$$

The glazing, tube wall and wetted absorber temperatures may be substituted from the corresponding mass and energy balances (Veza et al., 1993; Kudish et al., 1997). Consequently, the energy transfer equations in the evaporator are obtained as follows:

$$\begin{aligned} (\rho c \delta)_{a,2} \partial T_{a,2} / \partial t + m_a / b_{w,2} \cdot \partial ((c_a + W_2 c_s) T_{a,2}) / \partial x_2 &= Q_{ev,2} - Q_{con,t,2} - Q_{con,g} \\ &+ A_g / A_{w,2} \cdot U_2 (U_{amb} + U_2)^{-1} [U_{amb} (T_{amb} - T_{a,2}) + Q_{con,g} + G_g] \\ &+ U_2 (U_1 + D_{in,1}/D_{out,1} \cdot U_2)^{-1} \cdot [D_{in,1}/D_{out,1} \cdot U_1 (T_{a,1} - T_{a,2}) + Q_{ev,2} + D_{in,1}/D_{out,1} \cdot Q_{con,1} + G_w] \\ &+ A_t / A_{w,2} \cdot U_2 (U_2 + D_{in,t}/D_{out,t} \cdot U_f)^{-1} \cdot [D_{in,t}/D_{out,t} \cdot U_f (T_{f,2} - T_{a,2}) - Q_{con,t,2} - G_t], \end{aligned} \quad (6)$$

$$\begin{aligned} (\rho c D_{in,t} / 4 D_{out,t})_{f,2} \partial T_{f,2} / \partial t + m_f c_f / \pi D_{out,t} \cdot \partial T_{f,2} / \partial x_t &= Q_{con,t,2} + G_t \\ &+ U_f (D_{in,t}/D_{out,t} U_f + U_2)^{-1} [U_2 (T_2 - T_f) - Q_{con,t,2} - G_t], \end{aligned} \quad (7)$$

$$m_a \partial W_2 / \partial x_2 = h_{m,2} b_2 \cdot (W_{s,2} ((T_{a,2} + T_{amb})/2) - W_2). \quad (8)$$

Similarly, the energy transfer equations within the glass tube are given by the following, where $x_1 = -x_2$ to account for the reverse in flow direction:

$$(\rho c D_{in,1}^2 / 4D_{out,1})_{a,1} \partial T_{a,1} / \partial t + m_{a,1} / \pi D_{out,1} \cdot \partial((c_a + W_1 c_s) T_{a,1}) / \partial x_1$$

$$= -Q_{con,1} + U_1 (D_{in,1} / D_{out,1} U_1 + U_2)^{-1} [U_2 (T_{a,2} - T_{a,1}) + Q_{ev,2} + Q_{con,1} + G_w], \quad (9)$$

$$m_{a,1} \partial W_1 / \partial x_1 = h_{m,1} \cdot \pi D_{out,1} \cdot (W_{s,1} ((T_{a,1} + T_{amb}) / 2) - W_1). \quad (10)$$

The energy transfer equations for the air stream, feedstock and humidity in the internal heat exchanger are analogous to Eqs. (6) – (8) but with a view to being concise they are not detailed in this manuscript.

Equations (6)-(10) were solved by imposing the following initial and boundary conditions:

$$T_{a,1}(x,0) = T_{a,2}(x,0) = T_{amb}, \quad T_{f,2}(x,0) = T_{wat,0}, \quad W_2(x=0) = W_{amb}, \quad (11)$$

$$T_{a,2}|_{x=0} = T_{amb}, \quad T_{f,2}|_{x=0} = T_{wat,in}, \quad T_{a,1}|_{x=L} = T_{a,2}|_{x=L}, \quad W_1|_{x=L} = W_2|_{x=L}. \quad (12)$$

The definitions for the heat and mass flux and corresponding transfer coefficients applying to Eqs. (6)- (10) are:

$$Q_{ev} = \lambda (T_a) M_{ev}, \quad Q_{con} = \lambda (T_a) M_{con}, \quad (13)$$

$$U_2 = h_{c,2} + 0.9 \cdot \sigma \cdot 4 \cdot [(T_{a,1} + 3 \cdot T_{a,2}) / 4]^3, \quad (14)$$

$$U_{amb} = h_{amb} + 0.9 \cdot \sigma \cdot 4 \cdot [(3 \cdot T_{amb} + T_{a,2}) / 4]^3, \quad (15)$$

$$1/U_1 = 1/h_{c,1} + D_{in,1} \cdot \log(D_{out,1} / D_{in,1}) / 2\kappa_w + 1/h_{con,1}, \quad (16)$$

$$1/U_f = 1/h_f + D_{in,t} \cdot \log(D_{out,t} / D_{in,t}) / 2\kappa_w, \quad (17)$$

$$1/h_{amb} = 1/h_g + 1/h_a + 2 \cdot \delta_g / \kappa_g, \quad (18)$$

$$h_{wd} = 5.7 + 3.8 V_{amb}; \quad (19)$$

where h_g (cf., Eq. (18)) is determined from the Nusselt number correlation for natural convection between two parallel planes as proposed by Buchberg et al. (1976):

$$Nu_g = 1 + 1.446(1 - 1708/Ra^*), \quad \text{for } 1708 < Ra^* < 5900, \quad (20)$$

and

$$Ra^* = 2g\rho_a^2(T_{a,2} - T_{amb})\delta_a^3 \cos\theta \cdot Pr / (3T_{a,2} + T_{amb})\mu_a^2. \quad (21)$$

The heat transfer coefficient for forced convection in the laminar flow regime is determined from the following correlation (Heaton et al., 1964),

$$Nu_{c,j} = 5.4 + 0.0019[Re_j Pr D_{H,j} / L]^{1.71} / (1 + 0.00563[Re_j Pr D_{H,j} / L]^{1.17}), \quad j=1,2, \quad (22)$$

which is valid for $Re_j < 2.3 \cdot 10^3$. The values for $h_{c,j}$ determined by Eq. (22) were corrected for the effect of simultaneous heat and mass transfer by applying the Ackerman correction (Treybal, 1980). The forced convective heat transfer coefficient h_f for laminar flow is estimated from the Nusselt number (Kreith, 1976),

$$Nu_f = [3.65 + (0.0668 Re_f Pr D_{in,t} / L_t) / (1 + 0.04(Re_f Pr D_{in,t} / L_t)^{2/3})]^{1/4}. \quad (23)$$

The overall heat transfer coefficient through the bottom of the still to the ambient is given by

$$U_{loss} = 1 / (\delta_{ins} / \kappa_{ins} + \delta_b / \kappa_b). \quad (24)$$

The condensation heat transfer coefficient at low mass fluxes inside smooth horizontal tubes is given by Chato (1962) with the correlated coefficients proposed by Singh et al., (1996):

$$h_{con,1} = 0.0925 \cdot [\rho_w (\rho_w - \rho_s) g \lambda^* \kappa_w^3 / D_{in,1} \mu_w (T_{a,1} - T_{a,2})]^{1/4}, \quad (25)$$

$$\lambda^* = \lambda + 0.68 c_w (T_{a,1} - T_{a,2}). \quad (25a)$$

The heat transfer coefficient for condensation from the saturated air stream on the inner glazing surface is given by (Kreith, 1976) as

$$h_{con,2} = 0.725 [\rho_s (\rho_s - \rho_a) g \sin\theta \lambda \kappa_s^3 / 2L_2 \mu_s (T_{a,2} - T_{amb})]^{1/4}. \quad (26)$$

The heat transfer coefficient for condensation from the moist air stream onto the surface of the feedstock tubes is given by (Kreith, 1976) as

$$h_{con,t} = 0.943 [\rho_w (\rho_w - \rho_s) g \lambda \kappa_w^3 / 2L_1 \mu_w (T_{a,1} - T_{amb})]^{1/4}. \quad (27)$$

The mass transfer coefficient h_m is determined utilizing assumption 3. The rates of evaporation and condensation are calculated using the following relationships:

$$M_{con,g} = h_{m,con} [W_{a,2} - W_s (0.5(T_{a,2} + T_{amb}))], \quad (28)$$

$$M_{con,t,j} = h_{m,con} [W_{a,j} - W_s (0.5(T_{a,j} + T_{f,j}))], \quad j = 2,3, \quad (29)$$

$$M_{ev} = h_{m,ev} [W_s (0.5(T_{a,2} + T_{a,1})) - W_{a,2}], \quad (30)$$

where the value of W_s at the given temperature T_a is calculated from

The saturation pressure of the water vapor $P_s(T_a)$ is evaluated from an empirical formula which was derived by a least square analysis of the data taken from the steam tables (see Elsayed, 1983).

Numerical solution

We have used the "predictor-corrector" difference scheme (Marchuk, 1975) along each x-direction for the numerical solution of Eqs. (6) - (10), in the following format:

$$(T_i^{n+1/2} - T_i^n)/0.5\Delta t + f(W^n)(T_i^{n+1/2} - T_{i-1}^{n+1/2})/\Delta x = F(T_i^n), \quad (32)$$

$$0.5 \cdot (T_i^{n+1} - T_i^n + T_{i-1}^{n+1} - T_{i-1}^n)/\Delta t + f(W^{n+1/2})(T_i^{n+1/2} - T_{i-1}^{n+1/2})/\Delta x = F(T_i^{n+1/2}), \quad (33)$$

where $i=1, \dots, I$ and $I=L/N$ is the number of mesh points. At first, we utilize Eq. (32), a linear but strongly stable scheme, to obtain intermediate values of $T^{n+1/2}$ and apply Eq. (3) to refine the calculation by correcting for the whole step. Convergence was achieved for the initial air and fluid temperatures with various grid-steps. The results shown in Figs. (5) and (6) were obtained with grid-steps $\Delta x = 0.1m$ and $\Delta t = 0.3s$. The measured and calculated air temperature T_5 and T_6 as a function of air flow rate are shown in Fig. 5 and the dependence of the primary distillate on the air flow rate is shown in Fig. 6. In both cases, there is good agreement between the measured and calculated values. It is important to note, that the simulated primary distillate rate exhibits a maximum value, corresponding a maximum in the thermal energy recycle efficiency, at the same location as that measured.

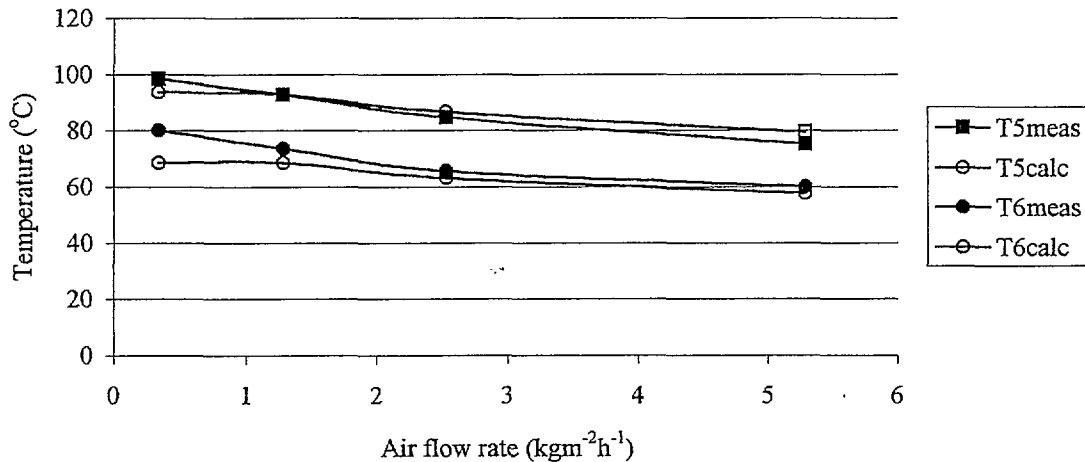


Fig. 5 Measured and simulated values for T_5 and T_6 as a function of air flow rate.

6. CONCLUSIONS

An innovative, air-blown, multi-tubular solar still fabricated from readily available, corrosion resistant materials has been studied experimentally and a simulation model describing it was developed and validated by the experimental data.

The performance testing was done using a constant feedstock flow rate of $2.5 \text{ kgm}^{-2}\text{h}^{-1}$ (sufficient to maintain the wick completely wetted). A maximum in the steady-state productivity ($0.97 \text{ kgm}^{-2}\text{h}^{-1}$) was observed as a function of the air flow rate at $1.28 \text{ kgm}^{-2}\text{h}^{-1}$, both experimentally and predicted by the simulation model. These optimum operating conditions correspond to the highest thermal energy recycle efficiency of the system, a relatively low thermal load on the external heat exchanger and relatively low parasitic electrical energy requirements to drive the air pump.

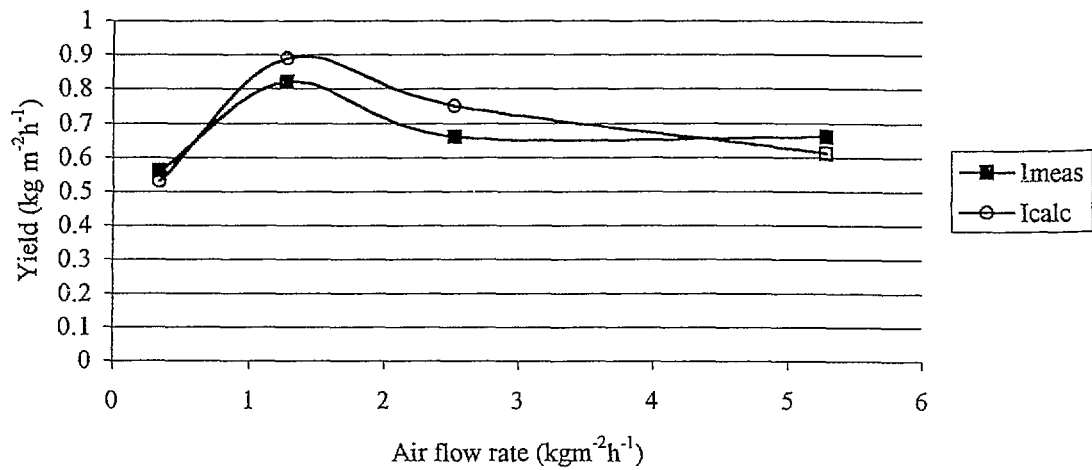


Fig. 6 Measured and simulated values of the primary distillate rate as a function of air flow rate.

NOMENCLATURE

A	surface area (m ²)
b	width (m)
c	heat capacity (Jkg ⁻¹ K ⁻¹)
D(D _H)	diameter (hydraulic diameter) (m)
G	solar radiation (Wm ⁻²)
g	gravitational constant (ms ⁻²)
H	height (m)
h	heat transfer coefficient (Wm ⁻² K ⁻¹)
h _m	mass transfer coefficient (kgs ⁻¹ m ⁻² K ⁻¹)
L	length (m)
M	mass flow rate (kg m ⁻² s ⁻¹)
m	air/water flow (kg s ⁻¹)
N	number of mesh points in the chamber
P	pressure (Nm ⁻²)
Q	thermal energy (Wm ⁻²)
T	temperature (K)
U	overall heat transfer coefficient (Wm ⁻² K ⁻¹)
V	linear velocity (ms ⁻¹)
W _s	saturated humidity for air at T (kg v·(kg dry air) ⁻¹)
W	air humidity (kg v·(kg dry air) ⁻¹)

Greek

δ	thickness (m)
θ	surface tilt angle
κ	thermal conductivity (Wm ⁻¹ K ⁻¹)
λ	latent heat of vaporization (Jkg ⁻¹)
μ	dynamic viscosity (kgm ⁻¹ s ⁻¹)
ρ	density (kgm ⁻³)
σ	Stefan-Boltzmann constant (Wm ⁻² K ⁻⁴)

Subscripts

a	air
amb	ambient
b	bottom
c	convection
con	condensation

ev	evaporation
f	feedstock
g	glazing
in	inlet/inside
ins	insulation
out	outlet/outside
r	radiation
s	saturated
t	tube
w	wick/water
wd	wind
1	internal heat exchanger
2	evaporator
3	external heat exchanger

Acknowledgment- This research was supported under Grant No. TA-MOU-95-C15-050, US-Israel Cooperative Development Research Program, Office of Agriculture & Food Security, Center for Economic Growth, Bureau for Global Programs, Field Support and Research, USAID. One of the authors Mr. L. Horváth acknowledges also the support of the Hungarian OTKA Fund, Project No. F-025 342.

REFERENCES

- Aboabboud, M.M. and Mink, G. (1993) Solar still of improved efficiency. *Proceedings of ISES solar World Congress, Vol. 4*, Budapest, Hungary, pp.319-324.
- Kudish, A.I., Evseev, E.G., Aboabboud, M.M., Horváth, L. and Mink, G.(1997) Heat transfer processes in an air-blown, multiple-effect solar still with thermal energy recycle. *Proceedings of the ISES Solar World Congress, Vol. 6*, Taejon, Korea, pp. 158-167.
- Mink, G., Horváth, L., Evseev, E.G. and Kudish, A.I. (1998) Design parameters, performance testing and analysis of a double-glazed, air-blown solar still with thermal energy recycle. *Solar Energy* 64, 265-277.
- Mink, G., Aboabboud, M.M., Horváth, L., Evseev, E.G. and Kudish, A.I. (1997) Design and performance of an air-blown solar still with thermal energy recycle. *Proceedings of the ISES Solar World Congress, Vol. 6*, Taejon, Korea, pp. 135-144.
- Buchberg, H., Catton, I. and Edwards, D.K. (1976) Natural convection in enclosed spaces: A review of application to solar energy collection. *Trans. of ASME, J. Heat Transfer* 98, 182-188.
- Duffie, J.A. and Beckman, W.A. (1980) *Solar Energy of Thermal Processes*, Wiley Interscience, New York, 762 pp.
- Veza, J.M.,and Ruiz., V. (1993) Solar distillation in forced convection. Simulation and experience. *Renewable Energy* 3, 691-699..
- Heaton, H.S., Reynolds, W.C. and Kays, W.M. (1964) Heat transfer in annular passages. Simultaneous development of velocity and temperature fields in laminar flow. *Int'l. J. Heat & Mass Transfer* 7, 763-781.
- Kreith, F. (1976) *Principles of Heat Transfer*, 3rd edn, Harper & Row, Publishers, New York, 656 pp.
- Marchuk, G.I.(1975) *Methods of Numerical Mathematics*, Springer-Verlag, New York, pp. 316.
- Treybal, R.W. (1980) *Mass Transfer Operations*, 2nd edn, McGraw-Hill, New York, 717 pp..
- Chato, J.C. (1962) Laminar condensation inside horizontal and inclined tubes. *ASHRAE Journal* 4, 52-60.
- Elsayed, M.M.(1983) Comparison of transient performance predictions of a solar-operated diffusion-type still with a roof-type still, *Journal of Solar Energy Engineering* 105, 23-28.
- Singh, A., Ohadi, M.M., and Dessiatoun, S.V., (1996) Empirical modeling of stratified-wavy flow condensation heat transfer in smooth horizontal tubes, *ASHRAE Transactions* 102, 596-603.

**THE PERFORMANCE AND ANALYSIS OF A MULTIPLE-EFFECT SOLAR STILL
UTILIZING SOLAR AND/OR WASTE THERMAL ENERGY**

A.I. KUDISH*, E.G. EVSEEV*, L. HORVÁTH** and G. MINK**

*Solar Energy Laboratory, Institutes for Applied Research, Ben-Gurion University of the Negev,
Beer Sheva 84105, ISRAEL; Tel: +972 7 6461488, Fax: +972 7 6472916, E-mail: akudish@bgumail.bgu.ac.il

**Research Laboratory of Materials and Environmental Chemistry, Chemical Research Center,
Hungarian Academy of Sciences, 1525 Budapest Pf 17, HUNGARY;
Tel: +36 1 325 5992, Fax: +36 1 335 7892, E-mail: mink@chemres.hu

Abstract - The performance of an air-blown, multiple-effect solar still designed to recycle the thermal energy of condensation has been studied in three operational modes, viz., driving forces, utilizing: (i) solar energy; (ii) waste thermal energy and (iii.) both solar and waste thermal energy. The still glazing was a double-walled polycarbonate sheet, a transparent insulation material (TIM) and the still area was 1 m². A solar simulator providing a constant irradiation intensity of 650±10 Wm⁻² was used, which facilitated the inter-comparison of the system performance under different conditions. The waste thermal energy was simulated using a feedstock reservoir maintained between 86 and 90°C. As a result of the low thermal mass of the still, steady-state temperatures and yields were achieved within one hour after start-up. The performance of the solar still, operating under constant energy input (i.e., a constant irradiation intensity) was determined mainly by the flow rate of the air stream, which functions both as a mass and energy carrier. The optimum range of the air flow rates, under all modes of operation, was determined experimentally. Mass and heat balances utilizing experimental results and referring to optimum operating conditions were also performed.

1. INTRODUCTION

The utilization of solar energy for the distillation of brackish or saline water has been practiced for a very long time. Various types of solar stills and solar-assisted desalination units have been designed and investigated. A number of manuscripts have been published on this subject, which include a classic one by Talbert, et al. (1970), Malik, et al. (1982) and Kudish (1990). In arid zones, solar distillation can be an ideal source to produce fresh water from saline water, for both human consumption and agriculture. The main disadvantage of the solar stills presently available is that their productivity per unit area is relatively low. The fixed capital investment cost of a solar desalination plant is roughly proportional to the still area; consequently, increasing the productivity per unit area by recycling the thermal energy of condensation of the distillate can be of paramount importance.

The performance of an air-blown, multiple-effect solar still consisting of an upper evaporation chamber and a lower condensation chamber has been analyzed and reported in detail by Kudish, et al (1997) and Mink, et al. (1997, 1998). These analyses suggested that it would be possible to utilize low grade waste thermal energy, when available at the site, as the driving force in the distillation process. This would allow the still to operate 24 hours a day by utilizing solar energy and/or waste thermal energy during the daytime and waste thermal energy during the night, i.e., nocturnal distillation.

In the present paper we shall report on the experimental results obtained when operating the still under three different operation modes, i.e., driving forces: (i.) only solar energy, (ii) waste thermal energy and (iii.) both solar and waste thermal energy.

2. EXPERIMENTAL

Experimental setup

The solar still prototype under investigation is shown schematically in Figs. 1.a and 1.b. It is essentially of the tilted-wick genre in the form of a thin rectangular box divided into two chambers (upper evaporator and lower condenser) by a central metal sheet. The central metal sheet does not extend across the full length of the still but leaves a slot of 10 mm between its top end and the still's upper extremity. The metal sheet also functions as (i) the support for the wick (a black porous material), which covers it on the upper chamber side; (ii) the surface to which a serpentine tube is in contact with in the lower chamber side. This serpentine tube serves as a conduit to transport the feedstock to the upper chamber and also functions as a heat exchanger for preheating the feedstock prior to entering the upper chamber. The spacing between both the upper chamber still glazing and lower chamber backside and the central metal plate is 12 mm.

Mode of operation when using solar energy

The mode of operation of the solar still is as follows: (1) ambient air is pumped into the upper chamber at the bottom of the tilted still and sweeps the water vapor evaporated from the tilted wick into the lower chamber via the slot at the top of the tilted still. The maximum temperature of the air stream is measured at this point, above the slot, prior to reversing direction and entering to the lower chamber. In the lower chamber it serves as the hot

In the upper chamber the air stream flows countercurrently to the feedstock flowing down the wick by gravity, whereas in the lower chamber it flows countercurrently to the direction of the feedstock flowing upward through the serpentine tube (cf., Fig. 1.b). Due to the nature of this solar still, viz., that the upper chamber glazing does not function as a condensation surface and, in fact, any such condensation is detrimental to still performance, a double glazing is used to reduce thermal energy losses via the glazing to the ambient. We have used a solar grade, double-walled, 10 mm thick polycarbonate sheet as the solar still glazing. It is a non-wetting polymeric transparent insulating material (TIM). It has been reported previously (Kudish, et al., (1997) and Mink, et al., (1997, 1998)), that a relatively large fraction of the thermal energy of condensation of the process was successfully recycled to both preheat the feedstock and heat the backside of the evaporation plate, which separates the two chambers. Consequently, a two- to three-fold increase in distillate yield was achieved relative to that reported for conventional type solar stills.

Mode of operation when using solar energy and/or waste thermal energy

The waste thermal energy was simulated by means of a conventional heater that maintained the feedstock reservoir at a temperature between 86 and 90°C. In this mode of operation, since the feedstock was preheated externally, it entered the still at the upper part of the evaporation chamber (cf., Fig. 1.a); i.e., the feedstock did not enter via the serpentine tube. Consequently, the thermal energy recycle from the lower chamber to the upper chamber is via a single process, viz., condensation on the backside of the central metal plate.

Experimental conditions and procedure

The tilt angle of the solar still module was set at 20° throughout this study. Similarly, the solar simulator provided a constant radiation intensity of $650 \pm 10 \text{ Wm}^{-2}$ and its tilt angle was also 20°. The differential and cumulative yields from Separator I and II were measured automatically by a type PT 6 Satorius electric balance with an accuracy of $\pm 1 \text{ g}$. The temperatures were measured at 16 strategically positioned locations, cf., Fig. 1.a, with an accuracy of $\pm 1 \text{ }^\circ\text{C}$ using calibrated temperature sensors of the silicon base type KTY 11-2A. The absolute humidity of air in the vicinity of the slot was calculated from the material and energy balances on the still. A data acquisition system served to monitor and store the temperature data from the sixteen thermistors and to calculate differential and cumulative yields at variable time intervals. It consisted of a PC with an A/D-D/A converter card, electronic measuring and magnetic valve control unit, temperature sensors and a digital balance with a RS232C serial interface. The data acquisition, control and analysis software was developed specifically for this study. The parameters under investigation were the feedstock and the air flow rates.

3. RESULTS AND DISCUSSION

Solar radiation driving force

As a result of the low thermal mass of the solar still, steady-state temperatures and yields were achieved within one hour of start-up in all experimental runs. All results reported in this study refer to steady-state operating conditions and the mass and energy flows were normalized to a 1 m^2 still area. The temperature profile for the still operating under a solar energy only driving force as a function of the air flow rates, expressed as kg bone dry air per m^2 still area per hour, is given in Table 1.

Table 1. The temperature profile of the solar still at steady-state as a function of air flow rate. The position of the thermistors are shown in Fig. 1.a (numbered 0 to 15). Feedstock flow rate = $2.96 \text{ kgm}^{-2}\text{h}^{-1}$; irradiation = $650 \pm 10 \text{ Wm}^{-2}$ and ambient temperature = $25.8 - 26.6 \text{ }^\circ\text{C}$.

Air Flow Rate ($\text{kgm}^{-2}\text{h}^{-1}$)	UPPER CHAMBER					LOWER CHAMBER					$T_{1,\text{out}}$	$T_{\text{sep,I}}$	$T_{X,\text{in}}$	$T_{X,\text{out}}$	T_{brne}
	T_1 ($^\circ\text{C}$)	T_2 ($^\circ\text{C}$)	T_3 ($^\circ\text{C}$)	T_4 ($^\circ\text{C}$)	T_5 ($^\circ\text{C}$)	T_6 ($^\circ\text{C}$)	T_7 ($^\circ\text{C}$)	T_8 ($^\circ\text{C}$)	T_9 ($^\circ\text{C}$)	T_{10} ($^\circ\text{C}$)	T_{11} ($^\circ\text{C}$)	T_{12} ($^\circ\text{C}$)	T_{13} ($^\circ\text{C}$)	T_{14} ($^\circ\text{C}$)	T_{15} ($^\circ\text{C}$)
0.32	68.6	95.1	96.3	96.2	97.0	96.9	97.4	96.9	94.9	52.5	48.9	34.0	30.4	24.1	62.4
0.58	67.6	91.9	93.6	93.6	94.4	94.2	94.5	94.0	91.7	68.2	68.2	60.7	57.1	21.9	61.9
1.02	64.9	87.4	89.8	89.8	90.7	90.7	90.7	90.0	87.2	69.9	69.9	65.6	64.1	28.6	60.4
1.24	62.6	84.6	87.4	87.6	88.4	88.5	88.4	87.5	84.4	67.5	67.5	64.1	63.0	32.1	58.4
1.76	59.1	80.1	83.7	83.7	84.7	84.8	84.3	83.5	79.9	64.4	64.4	62.0	61.3	34.1	55.7
2.21	57.5	77.1	81.3	81.2	82.1	82.1	81.6	80.7	77.0	63.1	63.1	60.9	60.4	35.0	54.5
3.27	54.0	71.1	76.4	75.9	76.6	76.7	75.9	75.1	71.1	59.6	59.6	58.1	57.8	36.0	51.5
4.51	51.2	65.6	72.2	71.3	71.6	71.3	70.6	69.9	66.0	56.0	56.0	54.9	54.6	35.4	48.7

The solar still productivity, as a function of air flow rate in the range from 0.32 to 4.51 $\text{kgm}^{-2}\text{h}^{-1}$ is reported both in Table 2 and in Fig. 2 in terms of the primary (I), secondary (II), and total (Σ) distillation rate. The primary distillation rate refers to that condensed within the lower chamber during the thermal energy recycle process. The secondary distillation rate is that obtained by passing the humid air stream exiting the solar still through an external heat exchanger prior to venting to the ambient. It is apparent from Table 2 that with regard to still productivity there exists an optimum range for the air flow rate, approximately between 1 and 3 $\text{kgm}^{-2}\text{h}^{-1}$, for the system under investigation. It is also observed that the ratio of secondary to primary product increases with increasing flow rate, i.e., the primary decreases and the secondary increases with increasing air flow rate (cf., Fig. 2). The reason for this optimum air flow rate range has been discussed in our previous papers (Kudish et al (1997) and Mink et al. (1997, 1998)).

Table 2. Still productivity (I- primary; II- secondary; Σ - total distillate) as a function of air flow rate. Feedstock flow rate = 2.96 $\text{kgm}^{-2}\text{h}^{-1}$; irradiation = 650±10 Wm^{-2} .

Air Flow Rate ($\text{kgm}^{-2}\text{h}^{-1}$)	I ($\text{kgm}^{-2}\text{h}^{-1}$)	II ($\text{kgm}^{-2}\text{h}^{-1}$)	Σ ($\text{kgm}^{-2}\text{h}^{-1}$)
0.32	0.68	0.01	0.69
0.58	0.93	0.04	0.97
1.02	0.97	0.13	1.10
1.24	0.96	0.15	1.11
1.76	0.87	0.20	1.07
2.21	0.84	0.27	1.11
3.27	0.75	0.29	1.03
4.51	0.65	0.32	0.97

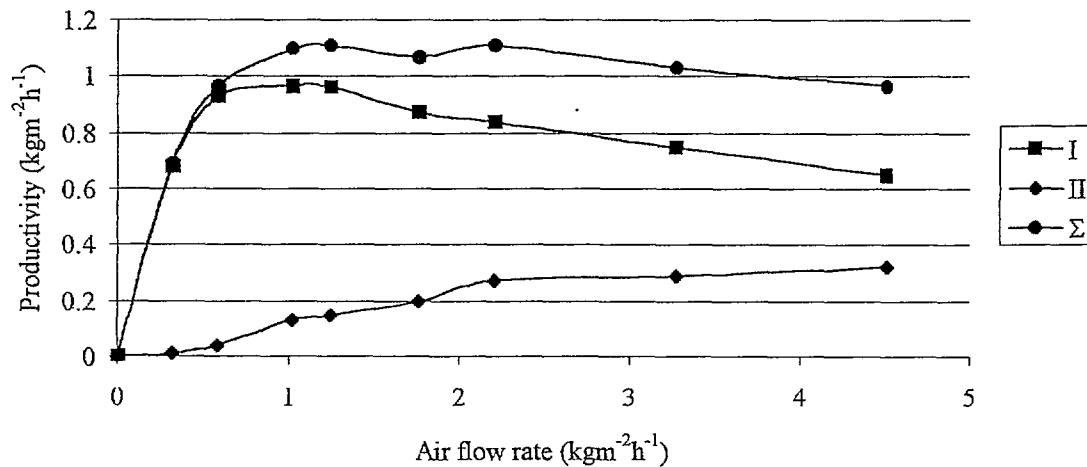


Fig. 2. Productivity in terms of primary, secondary and total distillation rate as a function of air flow rate. Feedstock flow rate = 2.96 $\text{kgm}^{-2}\text{h}^{-1}$; irradiation = 650±10 Wm^{-2} .

Waste thermal energy driving force-exposed glazing

In this mode of operation the feedstock flow rate was maintained at 9.3 $\text{kgm}^{-2}\text{h}^{-1}$. The feedstock was preheated between 86 and 90 °C by a heat exchanger, in order to simulate an external source of waste thermal energy. As mentioned previously, the preheated feedstock entered the upper chamber at the top of the central metal plate, cf., Fig. 1.a and did not pass through the serpentine tube. The experimental results are summarized in Fig. 3 and in Tables 3 and 4.

The waste thermal energy utilized, q_{waste} , which is defined as the heat released by the preheated feedstock in the upper chamber, q_{Released} , is reported in Table 4. This term is defined as the difference between the thermal energy contained by the feedstock entering the upper chamber $q_{f,\text{in}}$ and that of brine exiting the upper chamber q_{brine} ,

$$q_{\text{waste}} = q_{\text{Released}} = q_{f,\text{in}} - q_{\text{brine}} = c_w m_f T_{f,\text{in}} - c_w m_{\text{brine}} T_{\text{brine}}, \quad (1)$$

where m_{brine} was determined from a material balance, viz., as a difference of the feedstock flow rate and the rate of evaporation in the upper chamber.

It is observed that increasing the air flow rate results an increase in both productivity and utilized waste energy, q_{waste} . Also, it is apparent from the results that at a reasonable air flow rates (i.e., around $3 \text{ kgm}^{-2}\text{h}^{-1}$, where the parasitic energy requirement of the air pump is still relatively low) a total productivity rate of about 0.7 kg h^{-1} was obtained.

Table 3. Temperature profiles at steady-state as a function of air flow rate when utilizing only waste thermal energy for preheating the feedstock. Ambient temperature = $23.6 - 26.0^\circ\text{C}$; feedstock flow rate = $9.3 \text{ kgm}^{-2}\text{h}^{-1}$ and feedstock inlet temperature = $86 - 90^\circ\text{C}$.

Air Flow Rate ($\text{kgm}^{-2}\text{h}^{-1}$)	UPPER CHAMBER					LOWER CHAMBER					$T_{l,\text{out}}$	$T_{\text{sep},l}$	$T_{X,\text{in}}$	$T_{X,\text{out}}$	T_{brine}
	T_1 ($^\circ\text{C}$)	T_2 ($^\circ\text{C}$)	T_3 ($^\circ\text{C}$)	T_4 ($^\circ\text{C}$)	T_5 ($^\circ\text{C}$)	T_6 ($^\circ\text{C}$)	T_7 ($^\circ\text{C}$)	T_8 ($^\circ\text{C}$)	T_9 ($^\circ\text{C}$)	T_{10} ($^\circ\text{C}$)	T_{11} ($^\circ\text{C}$)	T_{12} ($^\circ\text{C}$)	T_{13} ($^\circ\text{C}$)	T_{14} ($^\circ\text{C}$)	T_{15} ($^\circ\text{C}$)
1.20	49.7	65.7	69.0	73.7	84.7	80.0	74.9	70.2	65.0	55.9	57.5	51.9	49.8	28.3	54.5
1.56	44.6	64.5	67.4	71.8	83.3	77.9	73.2	68.8	63.8	54.5	56.4	52.4	50.9	28.9	52.6
2.02	42.4	62.9	65.7	69.9	82.3	76.2	71.6	62.7	62.6	53.6	56.0	52.7	51.2	27.8	51.5
3.12	37.0	58.3	61.2	65.7	80.7	72.6	67.5	19.1	58.6	50.1	52.2	50.3	50.0	29.5	46.7
4.11	35.0	54.6	57.8	62.3	78.3	70.2	64.3	16.7	56.1	48.7	50.7	49.1	48.5	30.6	45.3
4.90	34.4	53.5	56.5	60.9	78.1	69.0	62.9	15.4	54.8	48.1	50.0	48.6	47.9	30.7	43.3
7.07	31.1	49.1	51.9	56.7	77.7	66.3	59.0	11.4	50.9	45.7	46.6	45.5	44.9	31.0	41.4

Table 4. Productivity rates and calculated waste thermal energy input, q_{waste} , at steady-state as a function of air flow rate when utilizing only waste thermal energy. Ambient temperature = $23.6 - 26.0^\circ\text{C}$; feedstock flow rate = $9.3 \text{ kgm}^{-2}\text{h}^{-1}$ and feedstock inlet temperature = $86 - 90^\circ\text{C}$.

Air Flow Rate ($\text{kgm}^{-2}\text{h}^{-1}$)	Irradiation (Wm^{-2})	q_{waste} (Wm^{-2})	I ($\text{kgm}^{-2}\text{h}^{-1}$)	II ($\text{kgm}^{-2}\text{h}^{-1}$)	Σ ($\text{kgm}^{-2}\text{h}^{-1}$)
1.20	0	356	0.34	0.05	0.39
1.56	0	380	0.39	0.08	0.48
2.02	0	395	0.41	0.12	0.53
3.12	0	452	0.52	0.17	0.69
4.11	0	468	0.53	0.19	0.72
4.90	0	490	0.55	0.22	0.77
7.07	0	512	0.58	0.25	0.82

Waste thermal energy driving force-insulated glazing

During the nocturnal distillation mode of operation, it seemed to be logical to further reduce the top losses via the double-glazing by covering it with an insulating material. A 5 mm thick polyurethane foam with a reflective aluminum foil on one side was placed upon the still glazing. The results of these experiments are reported in Fig. 4 and in Tables 5 and 6. It is observed that the use of this additional insulation on the still glazing resulted in both higher operating temperatures and productivity rates at comparable air flow rates. However, the increase in the total productivity was only in the range of $0.1 \text{ kgm}^{-2}\text{h}^{-1}$.

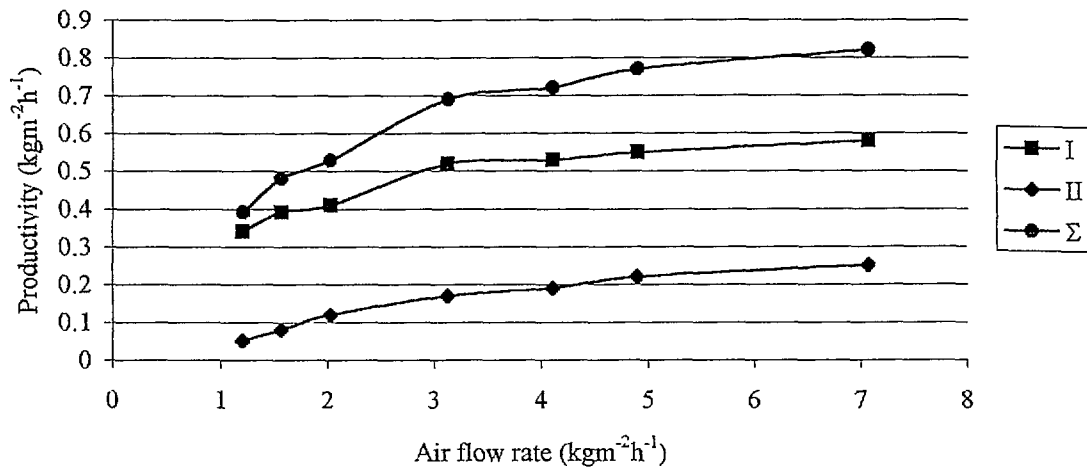


Fig. 3. Productivity as a function of air flow rate when utilizing only waste thermal energy. Ambient temperature = 23.6 - 26.0°C; feedstock flow rate = 9.3 kgm⁻²h⁻¹ and feedstock inlet temperature = 86 - 90°C.

Table 5. Temperature profiles at steady-state as a function of air flow rate when utilizing only waste thermal 23.7 - 25.9°C; feedstock flow rate = 9.3 kgm⁻²h⁻¹ and feedstock inlet temperature = 86 - 90°C.

Air Flow Rate (kgm ⁻² h ⁻¹)	UPPER CHAMBER					LOWER CHAMBER					T _{l,out}	T _{sep,l}	T _{X,in}	T _{X,out}	T _{brine}
	T ₁ (°C)	T ₂ (°C)	T ₃ (°C)	T ₄ (°C)	T ₅ (°C)	T ₆ (°C)	T ₇ (°C)	T ₈ (°C)	T ₉ (°C)	T ₁₀ (°C)	T ₁₁ (°C)	T ₁₂ (°C)	T ₁₃ (°C)	T ₁₄ (°C)	T ₁₅ (°C)
1.05	56.3	71.9	74.2	77.6	85.0	81.4	78.3	29.6	70.7	61.0	63.4	58.0	55.8	25.5	59.3
1.55	48.6	69.8	72.4	75.5	84.3	79.4	76.3	73.2	68.7	58.6	60.8	57.1	55.7	30.0	56.2
2.00	45.7	67.6	70.3	73.5	83.1	77.7	74.5	26.4	66.8	57.5	59.8	57.0	55.6	30.2	54.4
3.15	38.4	61.8	64.8	68.5	81.1	74.3	70.0	21.9	61.7	53.0	55.2	53.2	52.4	30.6	48.4
4.11	37.2	57.9	61.4	65.3	79.4	72.0	66.9	19.5	59.3	51.7	53.9	52.3	51.5	32.9	47.8
4.58	36.7	56.8	60.1	64.1	78.6	71.2	65.8	18.3	58.0	51.3	53.0	51.7	51.0	32.8	45.7
6.99	32.0	50.6	53.9	58.2	77.3	67.0	60.3	12.8	52.7	47.4	48.5	47.4	46.7	33.2	42.7

Hybrid mode of operation, simultaneous use of both solar and waste thermal energy as the driving forces

In these experiments a constant feedstock flow rate of 5.7 kgm⁻²h⁻¹ was used. The feedstock was preheated in the range of 86 to 90°C by the external heat exchanger to simulate the waste thermal energy prior to entering at the top of the central metal plate. The results are summarized in Tables 7 and 8 and in Fig. 5. It is observed that in this mode of operation, for an air flow rate in the range of 2 - 3 kgm⁻²h⁻¹, total productivity rates as high as 1.57 kgm⁻²h⁻¹ were achieved. These productivity rates are more than 40% higher than those obtained in the solar only operation mode (cf., Tables 2 and 8). This enhanced productivity is due mainly to the fact that in the hybrid operation mode the temperature and the vapor content of the air stream that exits the lower chamber is much higher and consequently, the amount of distillate condensed in the external condenser (II) is significantly enhanced. It is also observed that in this hybrid mode of operation that the temperature and therefore, the water vapor content of the saturated air stream that exits the condenser and vented to the ambient was relatively high. The external condenser used in this study was incapable of recovering a major fraction of the water vapor content of the exiting air stream prior to venting to the ambient, viz., it was not efficient enough for the system when operating in the hybrid mode.

Table 6. Productivity rates and calculated waste energy input, q_{waste} , at steady-state as a function of air flow rate when utilizing only waste thermal energy for preheating the feedstock and placing an insulating cover on the still glazing. Ambient temperature = 23.7 - 25.9°C; feedstock flow rate = 9.3 kgm⁻²h⁻¹ and feedstock inlet temperature = 86 - 90°C.

Air Flow Rate (kgm ⁻² h ⁻¹)	Irradiation (Wm ⁻²)	q_{waste} (Wm ⁻²)	I (kgm ⁻² h ⁻¹)	II (kgm ⁻² h ⁻¹)	Σ (kgm ⁻² h ⁻¹)
1.05	0	308	0.36	0.07	0.43
1.55	0	348	0.46	0.13	0.55
2.00	0	375	0.51	0.16	0.67
3.15	0	442	0.64	0.17	0.81
4.11	0	451	0.61	0.24	0.85
4.58	0	463	0.60	0.26	0.87
6.99	0	504	0.64	0.27	0.91

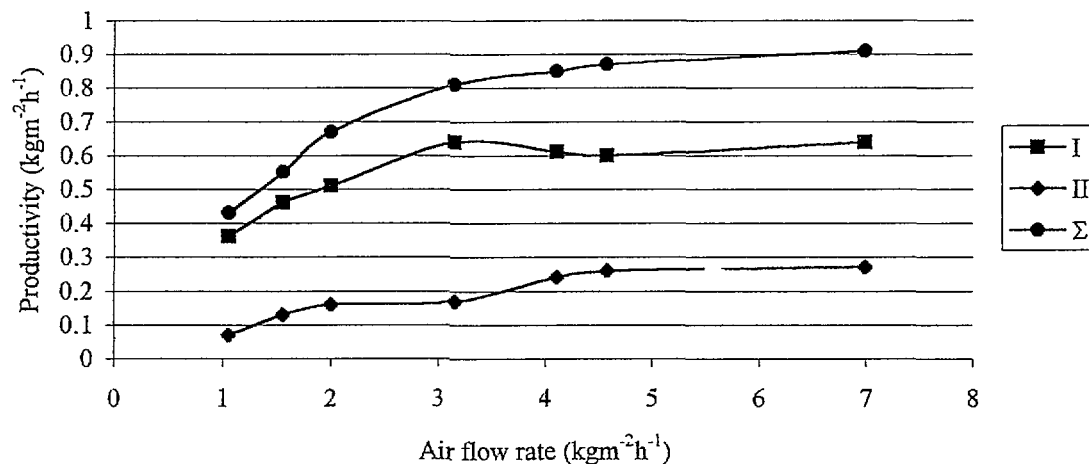


Fig. 4. Productivity as a function of air flow rate when utilizing only waste thermal energy and placing an insulating cover on the still glazing. Ambient temperature = 23.7 - 25.9°C; feedstock flow rate = 9.3 kgm⁻²h⁻¹ and feedstock inlet temperature = 86 - 90°C.

Table 7. Temperature profiles at steady-state as a function of air flow rate when operating in the hybrid mode. Ambient temperature = 28.4 - 34.4°C; feedstock flow rate = 5.7 kgm⁻²h⁻¹; feedstock inlet temperature = 86 - 90°C and irradiation = 650±10 Wm⁻².

Air Flow Rate (kgm ⁻² h ⁻¹)	UPPER CHAMBER					LOWER CHAMBER					T _{l,out}	T _{sep,I}	T _{X,in}	T _{X,out}	T _{brine}
	T1 (°C)	T2 (°C)	T3 (°C)	T4 (°C)	T5 (°C)	T6 (°C)	T7 (°C)	T8 (°C)	T9 (°C)	T10 (°C)	T11 (°C)	T12 (°C)	T13 (°C)	T14 (°C)	T15 (°C)
1.33	72.2	95.6	97.6	97.5	99.0	97.4	97.1	48.5	94.1	84.7	87.6	86.1	84.9	51.5	73.4
2.03	62.5	88.5	91.7	91.6	94.3	92.1	91.2	42.4	87.1	78.2	80.5	79.3	78.3	49.3	67.4
3.52	56.9	80.8	85.5	85.4	89.5	86.7	84.8	36.3	80.1	73.3	74.2	72.9	71.6	48.9	60.6
4.02	56.6	79.4	83.8	83.8	90.9	86.3	83.4	34.9	78.5	72.5	73.3	72.3	71.1	51.2	60.7

Table 8. Productivity rates and calculated waste energy input, q_{Waste} , at steady-state as a function of air flow rate when operating in the hybrid mode. Ambient temperature = 28.4 - 34.4°C; feedstock flow rate = 5.7 $\text{kgm}^{-2}\text{h}^{-1}$; feedstock inlet temperature = 86 - 90°C and irradiation = 650±10 Wm^{-2} .

Air Flow Rate ($\text{kgm}^{-2}\text{h}^{-1}$)	Irradiation (Wm^{-2})	q_{Waste} (Wm^{-2})	I ($\text{kgm}^{-2}\text{h}^{-1}$)	II ($\text{kgm}^{-2}\text{h}^{-1}$)	Σ ($\text{kgm}^{-2}\text{h}^{-1}$)
1.33	650	251	0.95	0.53	1.48
2.03	650	290	0.98	0.60	1.57
3.52	650	330	0.93	0.63	1.57
4.02	650	331	0.87	0.64	1.51

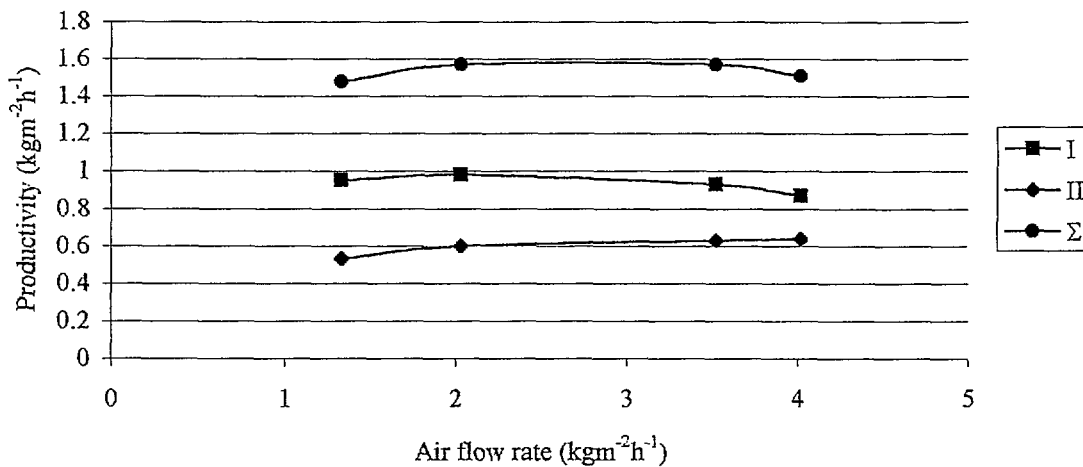


Fig. 5. Productivity as a function of air flow rate when operating in the hybrid mode. Ambient temperature = 28.4 - 34.4°C; feedstock flow rate = 5.7 $\text{kgm}^{-2}\text{h}^{-1}$; feedstock inlet temperature = 86 - 90°C and irradiation = 650±10 Wm^{-2} .

Inter-comparison of the modes of operation

The results of this experimental study are summarized in Fig. 6 with respect to the total distillate rate as a function of the air flow rate for all the modes of operation investigated. It is not recommended to operate this prototype solar still at relatively high air flow, since this will result in an increase in the parasitic electric energy required to drive the air pump. The optimum air flow rate for both the hybrid and the nocturnal distillation modes is observed to be in the range of 2 - 3 $\text{kgm}^{-2}\text{h}^{-1}$. We believe that a productivity in excess of 20 $\text{kgm}^{-2}\text{day}^{-1}$ may be achieved when operating the still in arid zones under these conditions, i.e., hybrid mode with nocturnal distillation. It may be possible to further enhance the productivity, based upon the results of this study, by preheating the feedstock in the lower chamber (i.e., flow through the serpentine tube) even in the hybrid mode of operation.

4. CONCLUSIONS

The performance of an air-blown multiple-effect solar still consisting of an upper evaporation chamber and a lower condensation chamber has been analyzed in three modes of operation, i.e., driving forces: (i) solar energy; (ii) waste thermal energy and (iii) hybrid, both solar and waste thermal energy.

In all modes of operation the performance of the still was determined as a function of the flow rate of the entering air stream and the optimum range of the air flow rates were determined experimentally. The optimum air flow rate for both the hybrid (during the daytime) and the nocturnal distillation modes was in the range of 2-3 $\text{kgm}^{-2}\text{h}^{-1}$. Based upon the experimental results of this study, a productivity in excess of 20 $\text{kgm}^{-2}\text{day}^{-1}$ may be achieved when operating the still in arid zones under these modes, i.e., hybrid mode with nocturnal distillation.

It may be possible to further enhance the productivity, based upon the results of this study, by preheating the feedstock in the lower chamber (i.e., flow through the serpentine tube) even in the hybrid mode of operation. Such a mode of operation will be studied in the future.

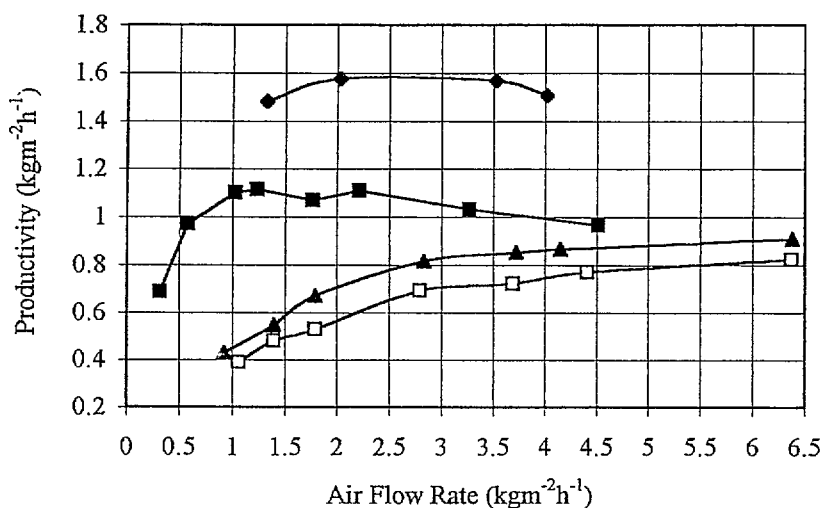


Fig. 6 Inter-comparison of the total productivity as a function of the air flow rate for all modes of operation investigated. The experimental conditions for each mode of operation are defined in the text.

NOMENCLATURE

c	heat capacity (Jkg ⁻¹ K ⁻¹)
m	mass flow rate (kgm ⁻² s ⁻¹)
q	thermal energy normalized to unit still area (Wm ⁻²)
Q _{Waste}	waste energy input = q _{Released} normalized to unit still area (Wm ⁻²)
Q _{Released}	thermal energy released by the preheated feedstock in the upper chamber (Wm ⁻²)
T	temperature (°C)

Subscripts

a	ambient
brine	brine drain-off
f	feedstock
I	primary distillate
II	secondary distillate
in	stream entering chamber
out	stream exiting chamber
sep	vapor/liquid separator
u	upper chamber
w	water
X	external heat exchanger/condenser

Acknowledgment- This research was supported under Grant No. TA-MOU-95-C15-050. US-Israel Cooperative Development Research Program. Office of Agriculture & Food Security. Center for Economic Growth. Bureau for Global Programs. Field Support and Research. USAID. One of the authors L. Horváth acknowledges also the support of the Hungarian OTKA Fund, project No F-025 342.

REFERENCES

- Kudish, A.I. (1990) Water Desalination. In *Solar Energy in Agriculture-Energy in World Agriculture*. Parker, B.F. (Ed). Vol. 4. pp. 255-294. Elsevier Science Publishers B.V. Amsterdam.
- Kudish, A.I., Evseev, E.G., Aboabboud, M.M., Horváth, L. and Mink, G. (1997) Heat transfer processes in an air-blown multiple-effect solar still with thermal energy recycle. *Proceedings of the ISES Solar World Congress, Vol. 6.*, Taejon, Korea, pp. 158-167.

- Malik, M.A.S., Tiwari, G.N., Kumar, A. and Sodha, M.S. (1982) *Solar Distillation*. Pergamon Press. Oxford, pp. 175.
- Mink, G., Aboabboud, M.M., Horváth, L., Evseev, E.G. and Kudish, A.I. (1997) Design and performance of an air-blown solar still with thermal energy recycle. *Proceedings of the ISES Solar World Congress, Vol. 6*, Taejon, Korea, pp. 135-144.
- Mink, G., Horváth, L., Evseev, E.G. and Kudish, A.I. (1998) Design parameters, performance testing and analysis of a double-glazed, air-blown solar still with thermal energy recycle. *Solar Energy* **64**, 265-277.
- Talbert, S.G., Eibling, J.A. and Löf, G.O.G. (1970) *Manual on Solar Distillation of Saline Water*. R&D Progress Report No. 546. US Department of Interior.